Recombination … electron - ions

Recombination

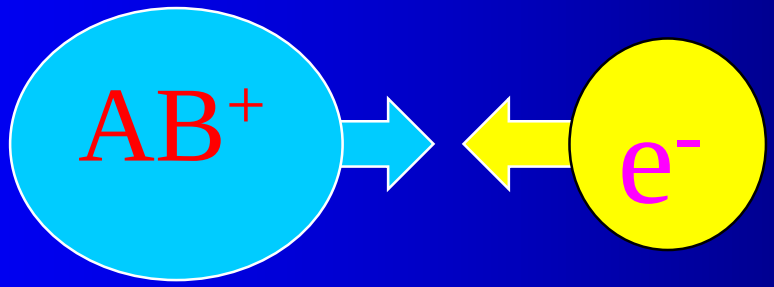

Radiative recombination

$Ar^+ + e^- \rightarrow Ar + h\nu$

Dissociative recombination

$AB^+ + e \rightarrow A + B$

$O_2^+ + e \rightarrow O + O$

Processes: at low impact energies

Elastic scattering

$AB + e \rightarrow AB + e$

Electronic excitation

$AB + e \rightarrow AB^* + e$

Vibrational excitation

$AB(v''=0) + e \rightarrow AB(v') + e$

Rotational excitation

$AB(N'') + e \rightarrow AB(N') + e$

Dissociative attachment

$AB + e \rightarrow A^- + B$

$\rightarrow A + B^-$

Impact dissociation

$AB + e \rightarrow A + B + e$

all go via $(AB^-....)^{**}$.

Dissociative recombination

$AB^+ + e \longrightarrow A + B$

Go via $(AB....)^{**}$.

Vibrational excitation, deexcitation and dissociation in H_2^+ - e^- collisions

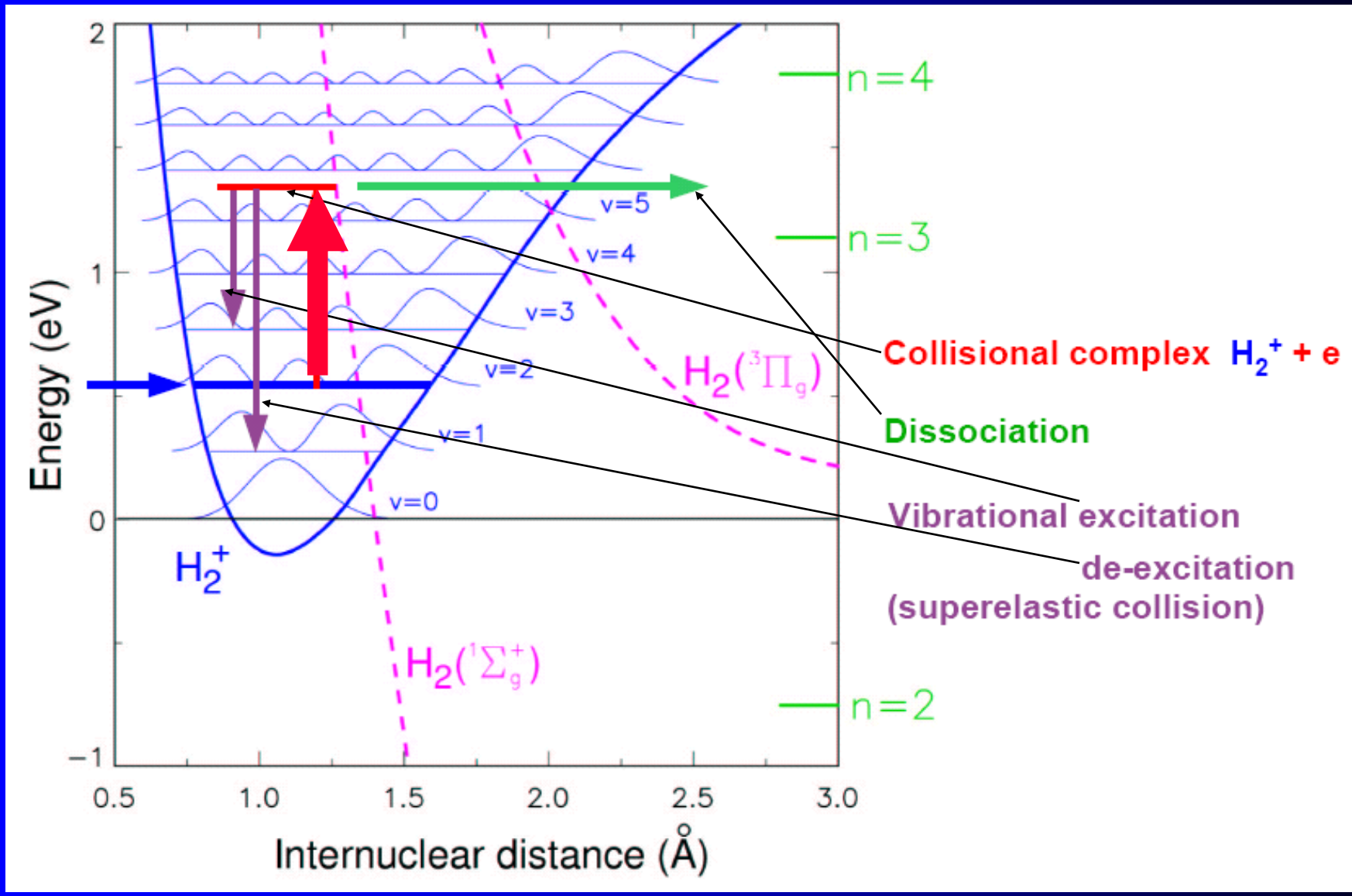

Electron –ion recombination

$H^+ + e^- \rightarrow$ products

$H_2^+ + e^- \rightarrow$ products

$H_3^+ + e^- \rightarrow$ products

$H_5^+ + e^- \rightarrow$ products

92.1% of nucleons in the universe are protons
7.8% are helium nuclei !

Recombination processes in plasma

Binary recombination

$\alpha\,[\mathrm{cm^3 s^{-1}}]$

$H^+ + e \rightarrow H + h\nu$ — RR — radiative recombination

$O_2^+ + e \rightarrow O + O$ — DR — dissociative recombination

$$\frac{dn_e}{dt} = \frac{d[O_2^+]}{dt} = -\alpha[O_2^+]n_e = -\alpha n_e^2$$

$Fe^{7+} + e \rightarrow Fe^{6+}$ — DiR — dielectronic recombination

Ternary electron assisted recombination

Recombination processes in plasma

Binary recombination

$\alpha\,[\mathrm{cm^3 s^{-1}}]$

$H^+ + e \rightarrow H + h\nu$ — RR — radiative recombination

$O_2^+ + e \rightarrow O + O$ — DR — dissociative recombination

$$\frac{dn_e}{dt} = \frac{d[O_2^+]}{dt} = -\alpha[O_2^+]n_e = -\alpha n_e^2$$

$Fe^{7+} + e \rightarrow Fe^{6+}$ — DiR — dielectronic recombination

Ternary electron assisted recombination

$Ar^+ + e + e \rightarrow Ar + e$

$$\frac{dn_e}{dt} = \frac{d[Ar^+]}{dt} = -K_e[Ar^+]n_e^2 = -\alpha_{eff}[Ar^+]n_e$$

Collisional Radiative Recombination

CRR

$K_{CRR}\,[\mathrm{cm^6 s^{-1}}]$

$\alpha_{eff} = K_e n_e$

Ternary neutral assisted recombination

$Ar^+ + e + He \rightarrow Ar + He$

$$\frac{dn_e}{dt} = \frac{d[Ar^+]}{dt} = -K_M[Ar^+]n_e[He] = -\alpha_{eff}[Ar^+]n_e$$

$K_M\,[\mathrm{cm^6 s^{-1}}]$

$\alpha_{eff} = K_M[He]$

Electron - Ion Collision

$H^+ + e^- \rightarrow$ ~ very slow recombination ☹

$H^+ + e^- \rightarrow H + h\nu$ RR

$H^+ + e^- + e^- \rightarrow H + e^-$ ternary CRR

$H_2^+ + e^- \rightarrow H + H,$

Dissociative Recombination - DR

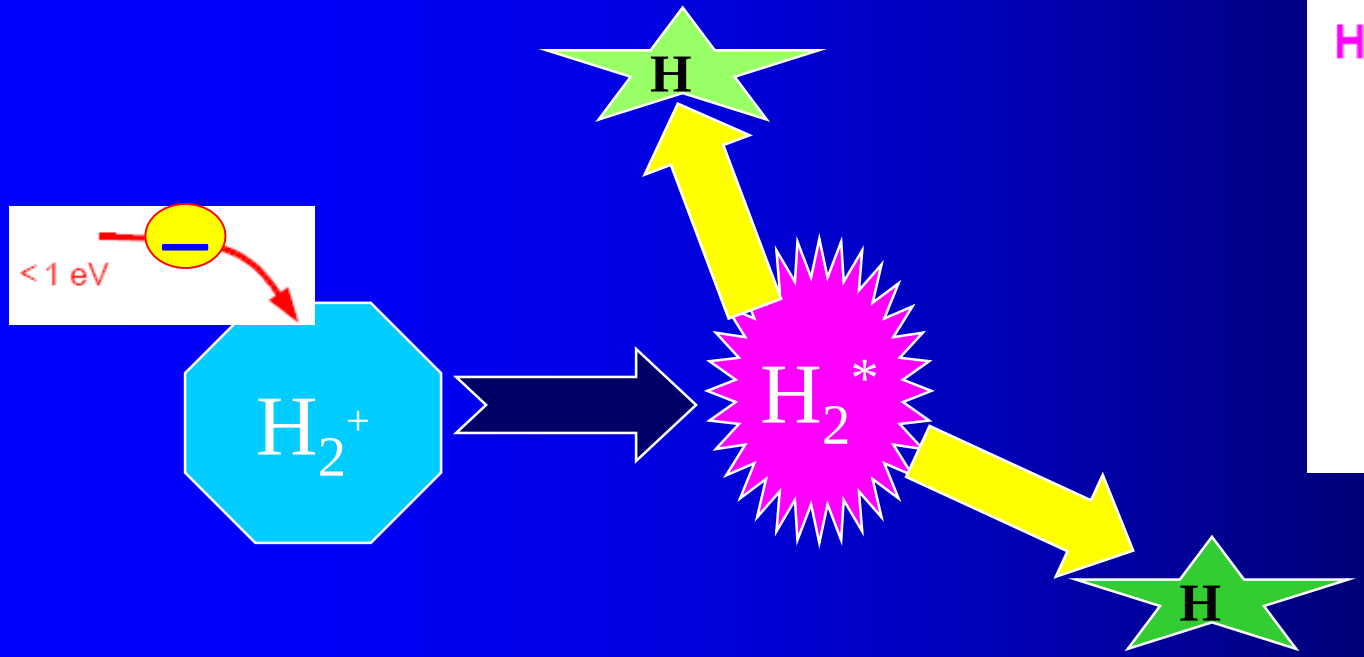

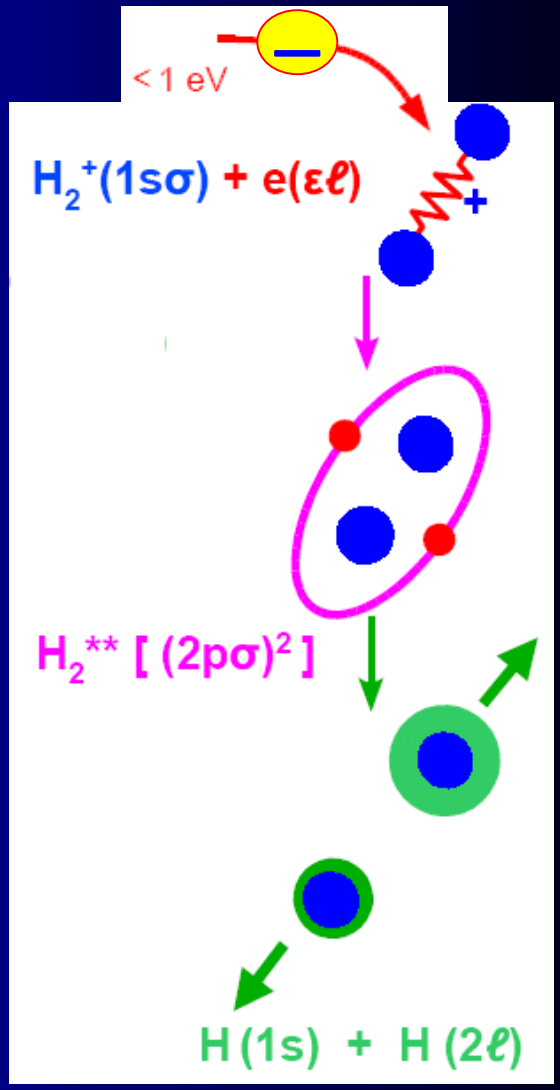

Electron collisions with H_2^+ - how to describe ????

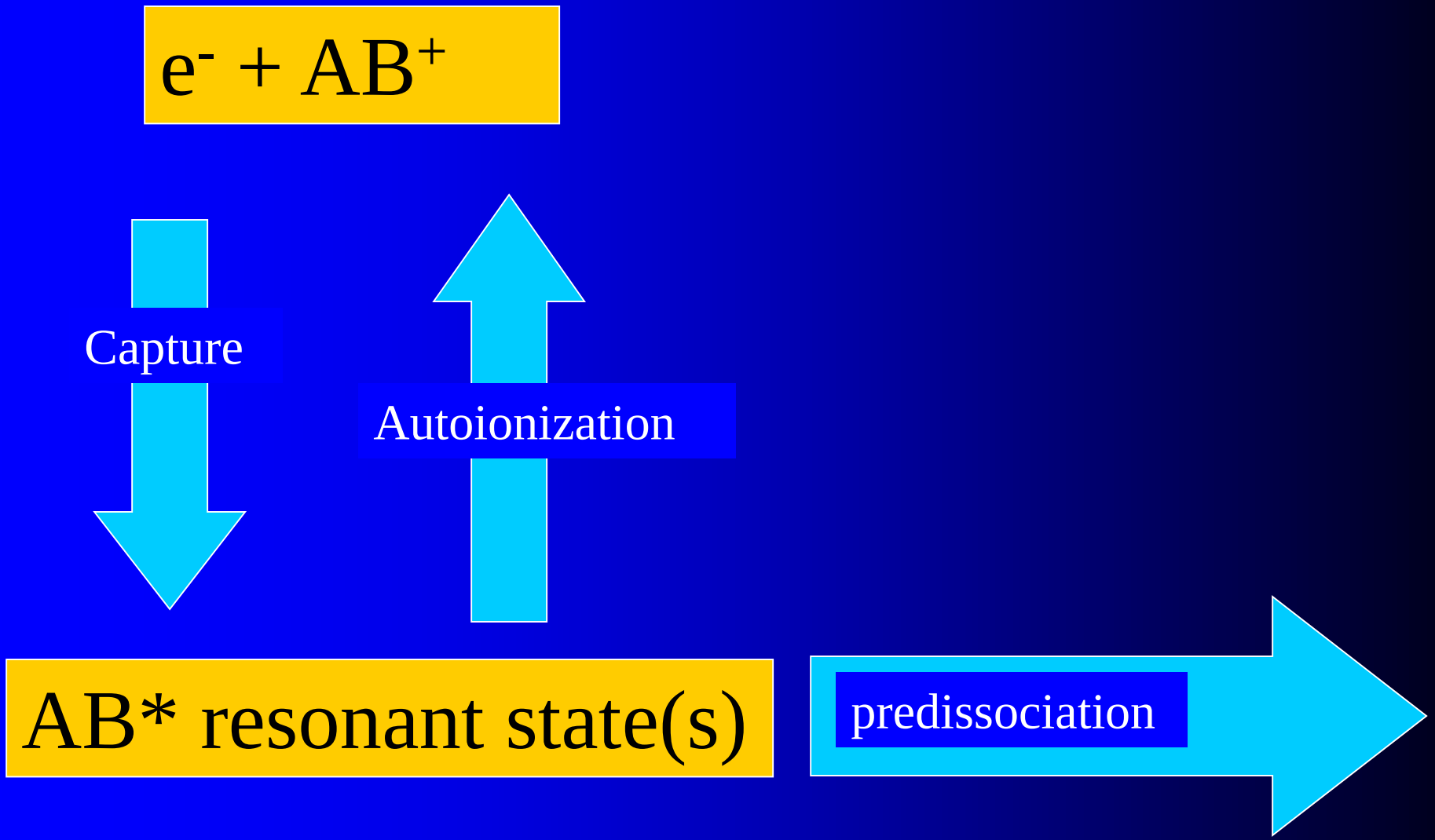

To get high recombination rate, we need

(a) efficient capture

(b) predissociation faster than auto-ionization

Electron-cold molecular ion reaction: Dissociative Recombination

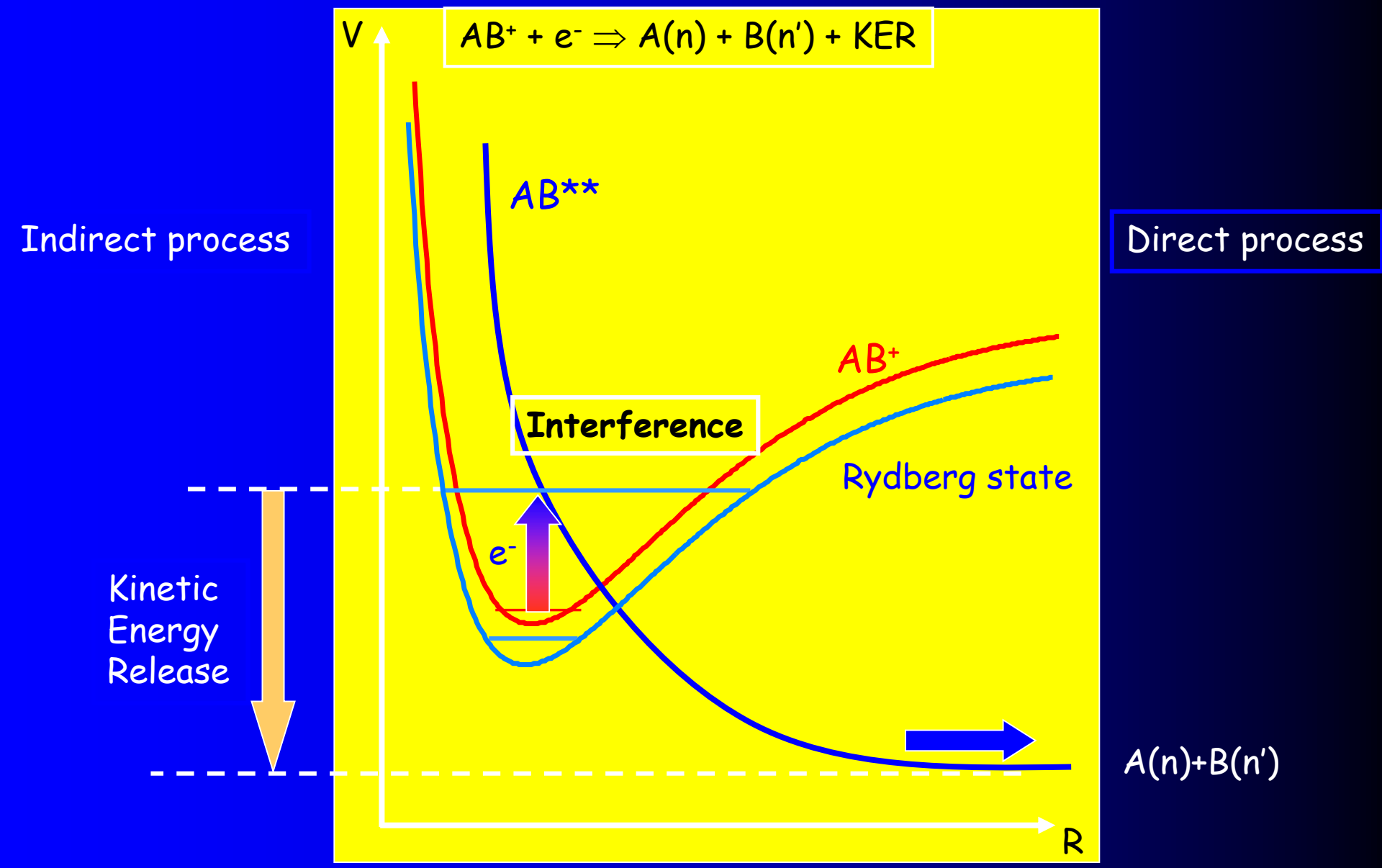

Recombination of H_3^+ : No ion-neutral crossing

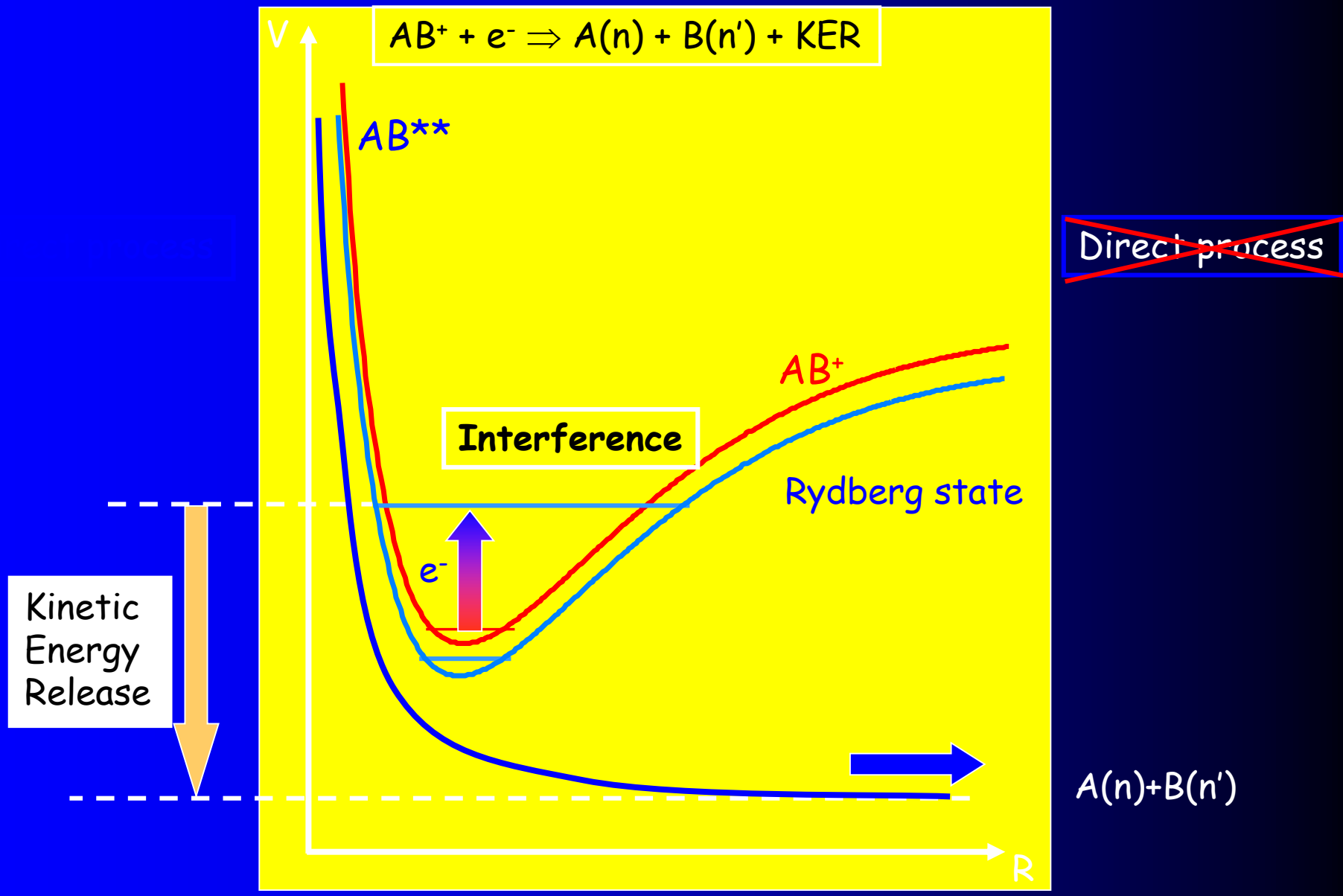

~~Direct process~~

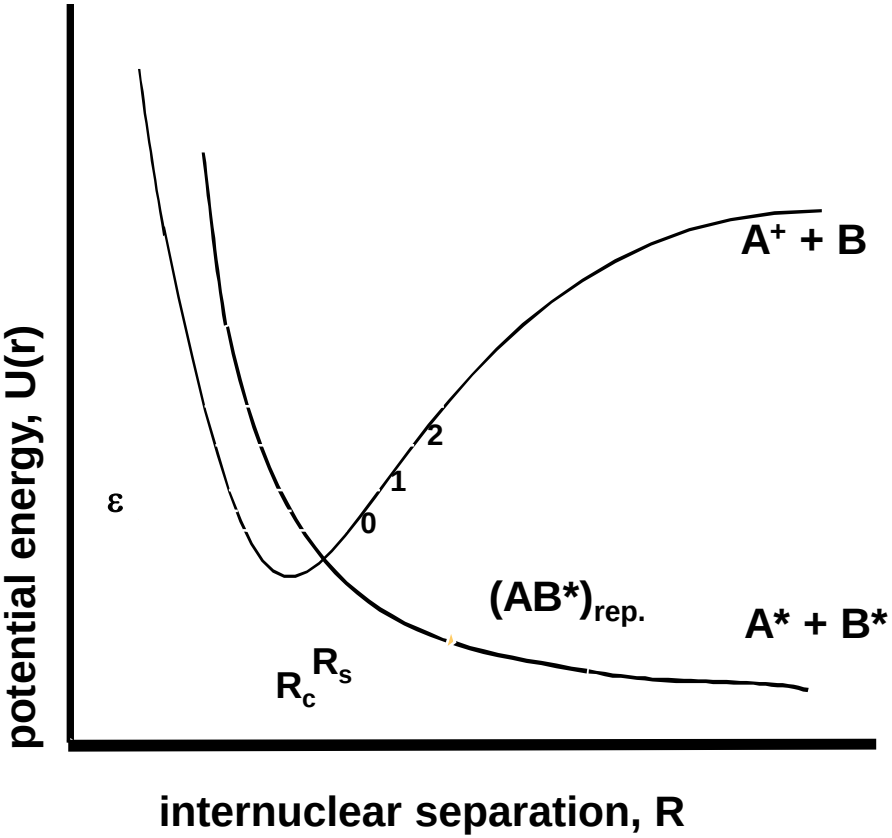

Direct mechanism

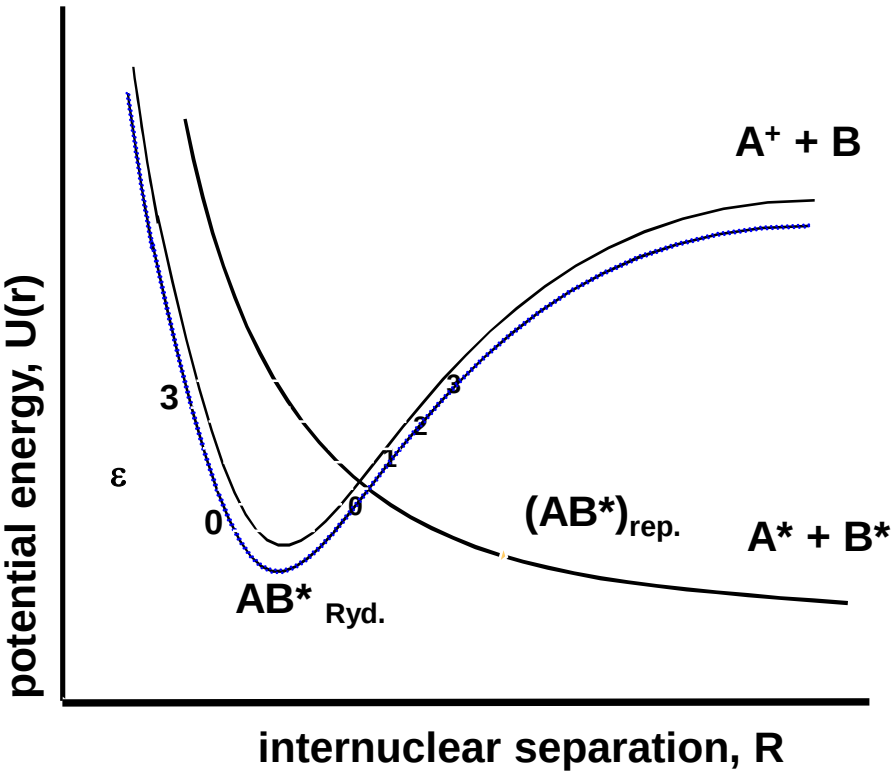

Indirect mechanism

Electron - Ion Collision- Recombination

Resonances

Autoionizing and pre-dissociating Rydberg states

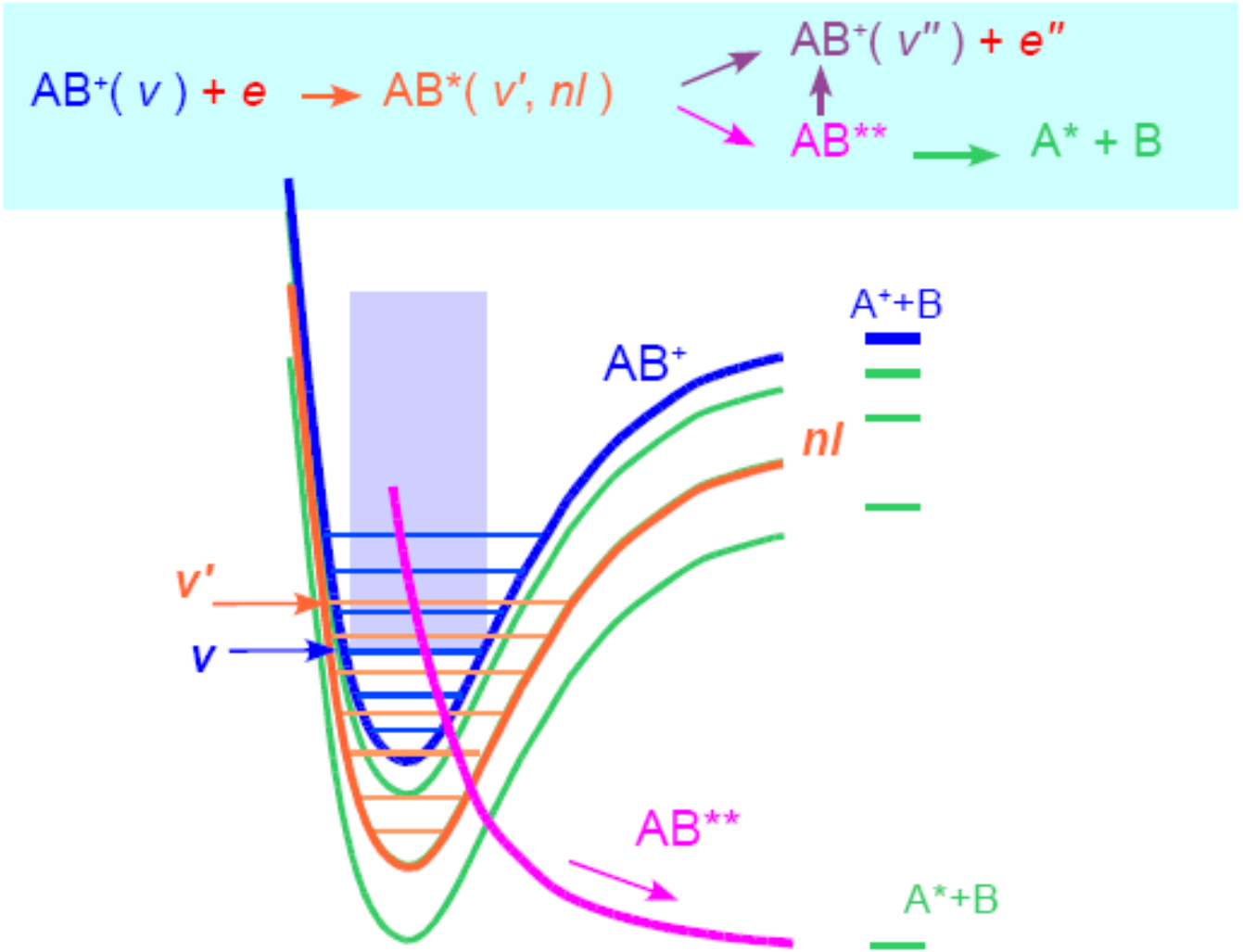

$H_2^+ + e^-$

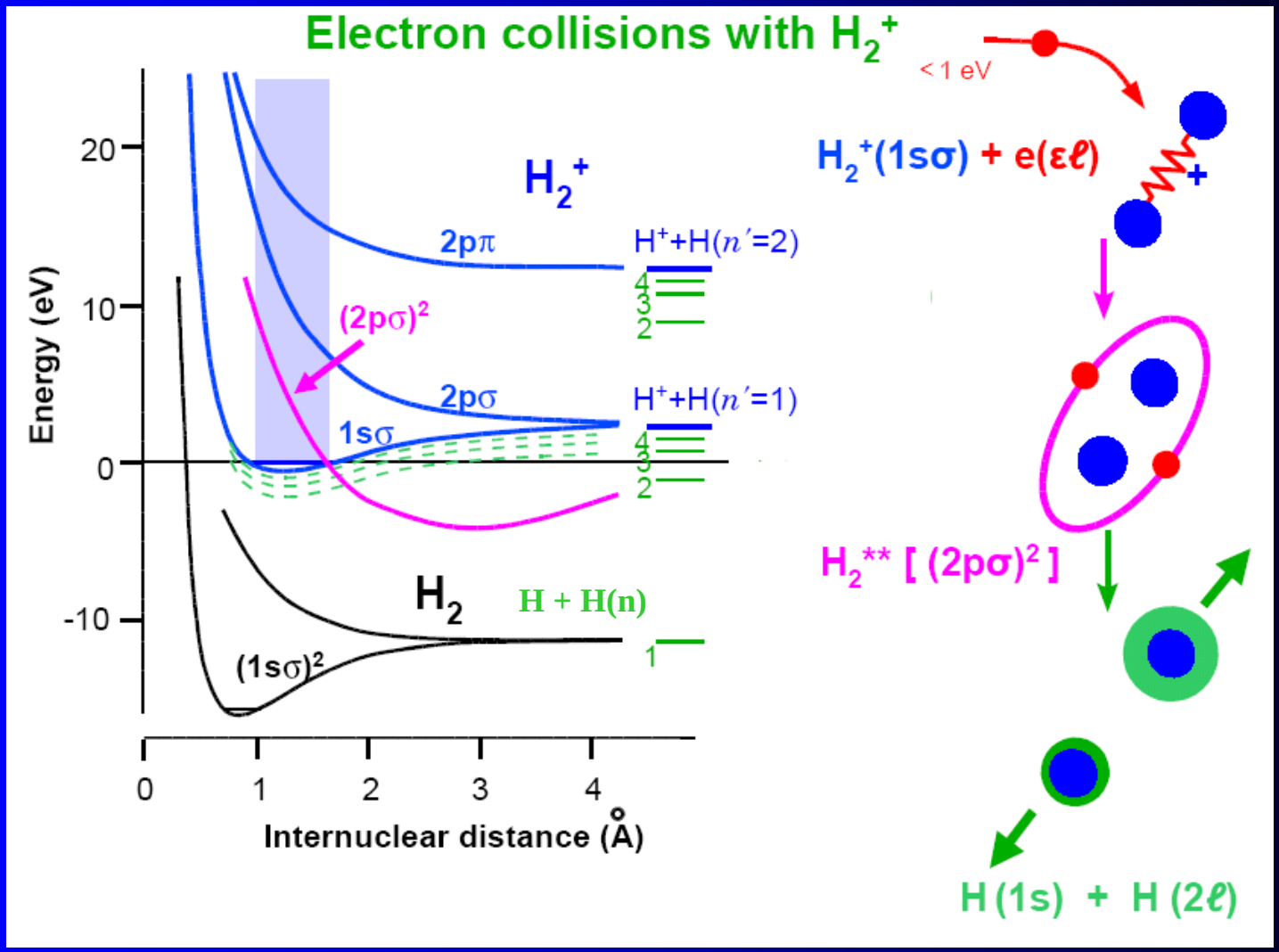
Electron collisions with H_2^+
< 1 eV
$H_2^+(1s\sigma) + e(\varepsilon\ell)$
H_2^+
$2p\pi$
$H^+ + H(n'=2)$
$(2p\sigma)^2$
$2p\sigma$
$H^+ + H(n'=1)$
$1s\sigma$
H_2
H + H(n)
$(1s\sigma)^2$
H_2^{**} [$(2p\sigma)^2$]
H (1s) + H (2ℓ)
Energy (eV)
20
10
0
-10
0
1
2
3
4
Internuclear distance (Å)

Next lecture: SA and absorption experiments (CRDS)

$O_2^+ + e^-$

2001

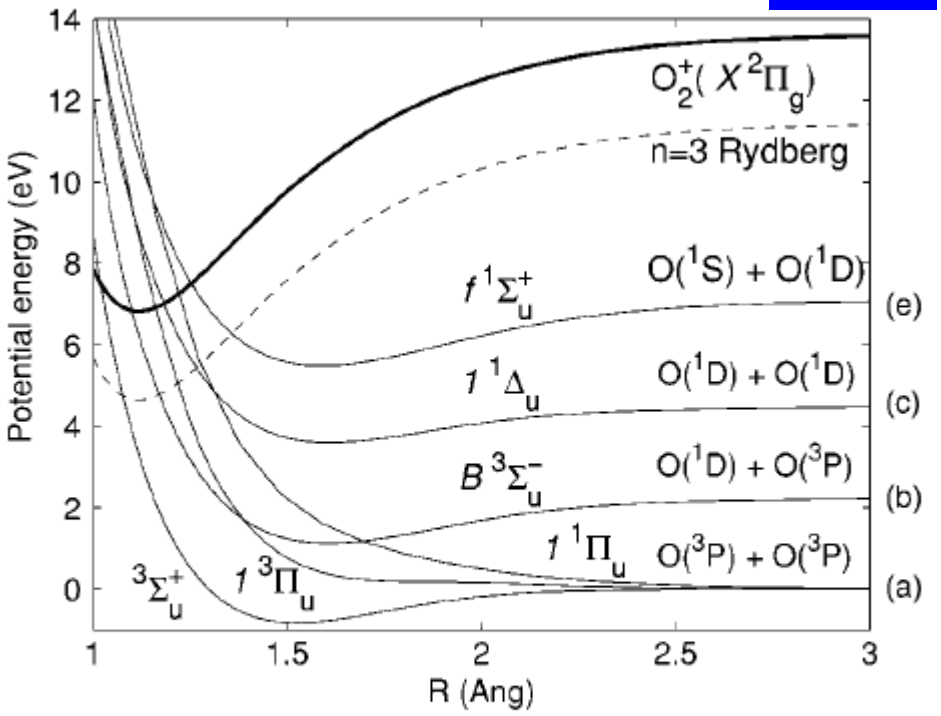

FIG. 1. Schematic of the diabatic potential curves relevant for the DR of O_2^+. The dissociation limits connected with each valence capture state are given on the right. The labels (a)–(c), and (e) refer to Eqs. (1a)–(1c) and (1e), respectively.

Five exothermic channels are available for vibrational ground state O_2^+ ions in zero relative energy collisions with electrons. They are summarized as follows with the associated kinetic energy releases:

$$O_2^+(X^2\Pi_g, v=0) + e^- \rightarrow O(^3P) + O(^3P) + 6.65 \text{ eV} \quad (1a)$$

$$\rightarrow O(^3P) + O(^1D) + 4.99 \text{ eV} \quad (1b)$$

$$\rightarrow O(^1D) + O(^1D) + 3.02 \text{ eV} \quad (1c)$$

$$\rightarrow O(^3P) + O(^1S) + 2.77 \text{ eV} \quad (1d)$$

$$\rightarrow O(^1D) + O(^1S) + 0.80 \text{ eV}. \quad (1e)$$

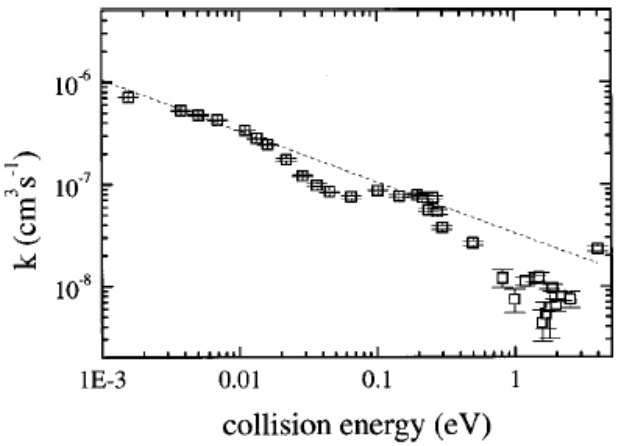

FIG. 2. DR rate coefficient k as a function of electron collision energy from 1 meV to 5 eV. Statistical errors are shown at the 1σ level. The dotted line shows the threshold $E^{-1/2}$ behavior. Both the rate coefficient and the energy are shown on a logarithmic scale.

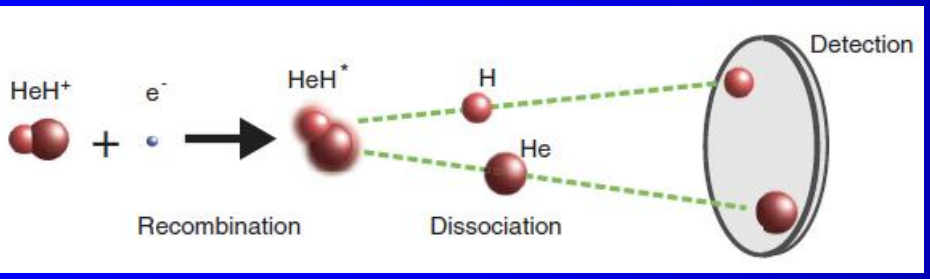

THEORETICAL FRAMEWORK

The states involved: exemple for He_2^+/He_2 system

He_2^+

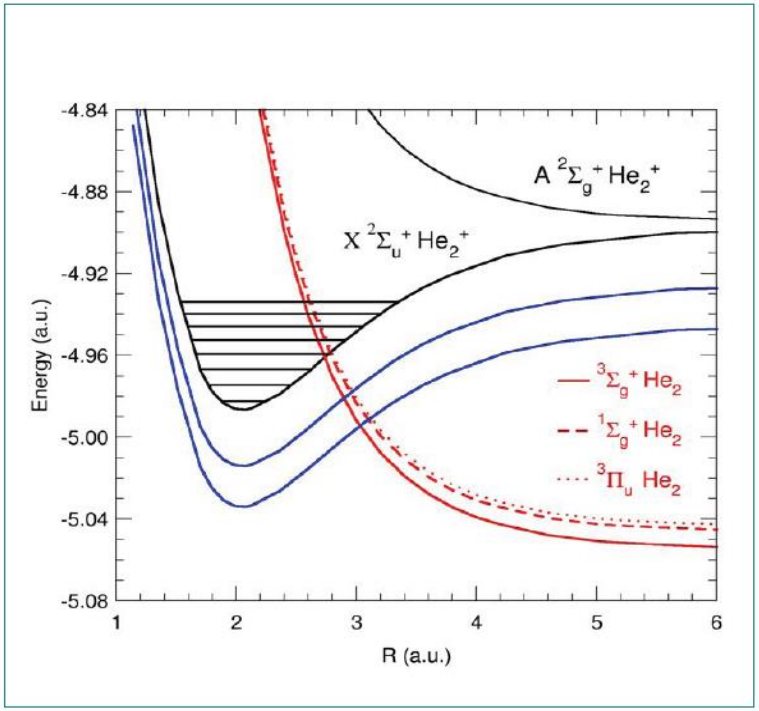

2004 DR6 Mosbach

I. Schneider, et al., DR2004 Mosbach

Theoretical background

Dissociative Recombination without a Curve Crossing

Theory predicted: DR rate coefficient is vary small ~ **10^{-11} cm^3s^{-1}**

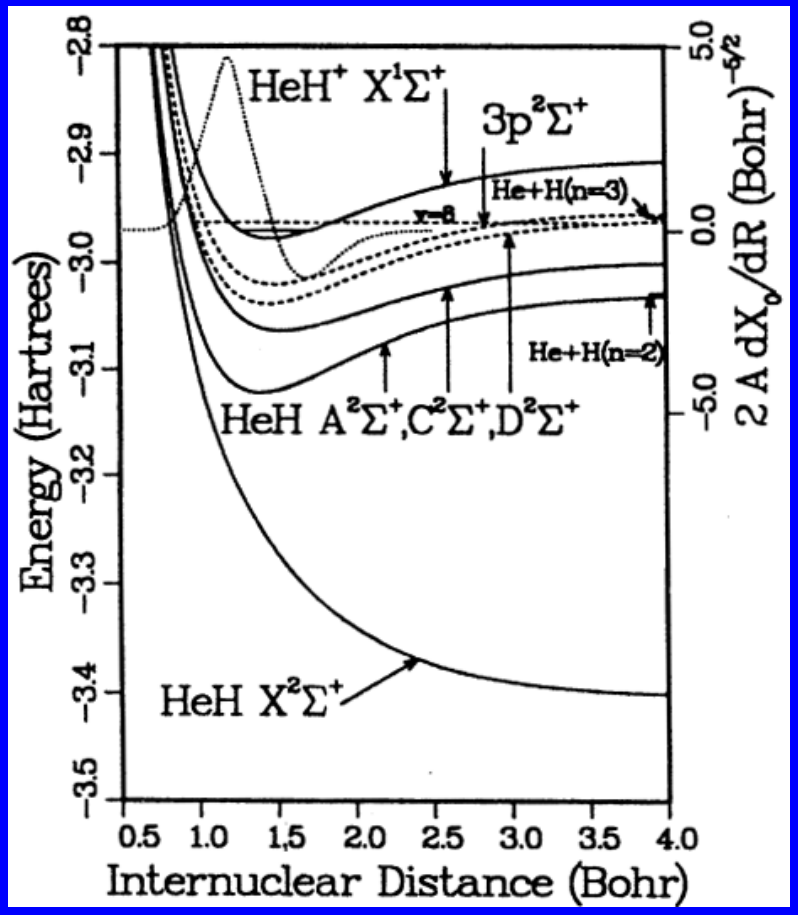

HeH^+ and HCO^+ ions- examples of a non-crossing case. However, experiments gave $\alpha \approx 2\times10^{-8}$ and $\alpha \approx 2\times10^{-7}$ cm^3s^{-1}

A new mechanism has been proposed!

Multi-step indirect dissociative recombination ("tunneling mode" recombination)

hartree (symbol: E_h or Ha), also known as the **Hartree energy**, 27.211386245988(53) eV

Recombination HeH^+

358 | NATURE | VOL 568 | 18 APRIL 2019

LETTER

https://doi.org/10.1038/s41586-019-1090-x

Astrophysical detection of the helium hydride ion HeH^+

Rolf Güsten[1]*, Helmut Wiesemeyer[1], David Neufeld[2], Karl M. Menten[1], Urs U. Graf[3], Karl Jacobs[3], Bernd Klein[1,4], Oliver Ricken[1], Christophe Risacher[1,5] & Jürgen Stutzki[3]

Extended Data Table 2 | Reaction rates used herein

Reaction	Rate coefficient [$cm^3\ s^{-1}$]	Notes
$He^+ + H \rightarrow HeH^+ + h\nu$	1.4×10^{-16}	1
$HeH^+ + e \rightarrow He + H$	$3.0 \times 10^{-10}\ (T/10^4\ K)^{-0.47}$	2
$HeH^+ + H \rightarrow He + H_2^+$	$1.2 \times 10^{-9}\ (T/10^4\ K)^{-0.11}$	3

(1) The rate coefficient (in $cm^3\ s^{-1}$) was obtained by averaging the published cross-sections[25] over a Maxwell–Boltzmann distribution, and applies to temperatures in the range 5,000 K to 20,000 K. The published cross-sections are for collisions in which He^+ (1*s*) and H (1*s*) are in the singlet state (total spin 0), but as only one-quarter of collisions will have spin 0, the rate has been reduced by a factor of four. Values in the literature[13,36,37] vary widely. (2) This value corrects an error in the computation[27] of the thermal rate coefficient from the cross-section measurements. Taking as valid the primary data of ref. [27], namely, the merged-beam cross-sections given in their figure 3, the thermal rate coefficients was recomputed by applying the methods developed;, for example, for the calculation of the dissociative recombination cross-section of HCl^+ (ref. [26]); we find the thermal rate coefficient to be an order of magnitude below that originally computed[27]. (3) Ref. [35] shows the rate coefficient obtained from quantum calculations.

Recombination HeH^+

Science **2019** REPORTS

Cite as: O. Novotný *et al.*, *Science* 10.1126/science.aax5921 (2019).

Quantum-state–selective electron recombination studies suggest enhanced abundance of primordial HeH^+

Oldřich Novotný[1]*, Patrick Wilhelm[1], Daniel Paul[1], Ábel Kálosi[1,2], Sunny Saurabh[1], Arno Becker[1], Klaus Blaum[1], Sebastian George[1,3], Jürgen Göck[1], Manfred Grieser[1], Florian Grussie[1], Robert von Hahn[1], Claude Krantz[1], Holger Kreckel[1], Christian Meyer[1], Preeti M. Mishra[1], Damian Muell[1], Felix Nuesslein[1], Dmitry A. Orlov[1], Marius Rimmler[1], Viviane C. Schmidt[1], Andrey Shornikov[1], Aleksandr S. Terekhov[4], Stephen Vogel[1], Daniel Zajfman[5], Andreas Wolf[1]

[1]Max-Planck-Institut für Kernphysik, Saupfercheckweg 1, 69117 Heidelberg, Germany. [2]Charles University, 18000 Praha, Czech Republic. [3]Universität Greifswald, Institut für Physik, 17487 Greifswald, Germany. [4]Rzhanov Institute of Semiconductor Physics, Novosibirsk 630090, Russia. [5]Weizmann Institute of Science, Rehovot 76100, Israel.
*Corresponding author. Email: oldrich.novotny@mpi-hd.mpg.de

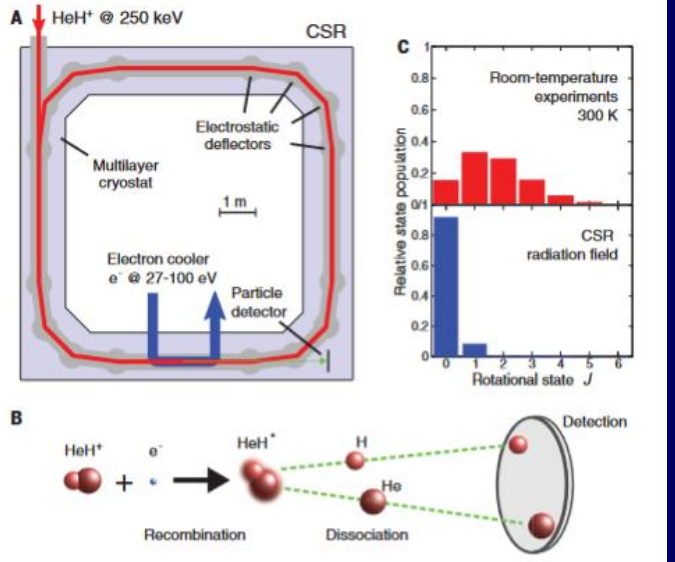

Fig. 1. Dissociative recombination in the cryogenic storage ring, CSR. (**A**) Scheme of the CSR ring structure with the injected and stored HeH^+ ion beam (red), merged electron beam (blue), reaction products (green), and particle detector. (**B**) Reaction scheme and position-sensitive detection of coincident fragments. (**C**) Equilibrium rotational state populations of HeH^+ for previous studies (300 K) and the estimated radiation field in the CSR.

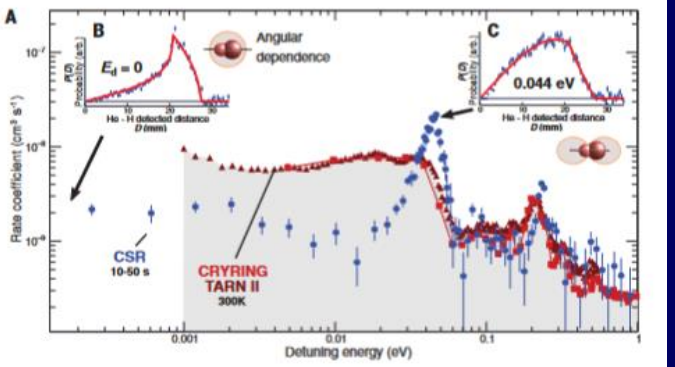

Fig. 2. DR for rotationally cold HeH^+. (**A**) Blue circles indicate the merged-beams rate coefficient α_{DR} as a function of the detuning energy E_d after relaxation to >50% $J = 0$ (this experiment, 10 s < t < 50 s, mean ± SD); absolute scaling uncertainty ±20% (SEM). Red symbols represent room temperature data from (*11*) (squares, absolute scaling uncertainty ±10% SEM) and from (*12*) [triangles, scaled to (*11*) at 0.03 eV]. (**B**) Fragment distance distribution projected into the detector plane for E_d = 0 (blue) with fit (*19*) for isotropic angular distribution (red). (**C**) Projected fragment distance distribution for E_d = 0.044 eV (blue) with fit (*19*) for a $|Y_{10}|^2$ angular distribution of the fragments (red). The angular dependences in (B) and (C) are indicated schematically. arb., arbitrary units.

Recombination HeH^+

PHYSICAL REVIEW LETTERS **124,** 043401 (2020)

2020

Dissociative Recombination of Cold HeH^+ Ions

Roman Čurík*
J. Heyrovský Institute of Physical Chemistry, ASCR, Dolejškova 3, 18223 Prague, Czech Republic

Dávid Hvizdoš
J. Heyrovský Institute of Physical Chemistry, ASCR, Dolejškova 3, 18223 Prague, Czech Republic and Institute of Theoretical Physics, Faculty of Mathematics and Physics, Charles University in Prague, V Holešovičkách 2, 180 00 Prague, Czech Republic

Chris H. Greene
Department of Physics and Astronomy, Purdue University, West Lafayette, Indiana 47907, USA and Purdue Quantum Science and Engineering Institute, Purdue University, West Lafayette, Indiana 47907, USA

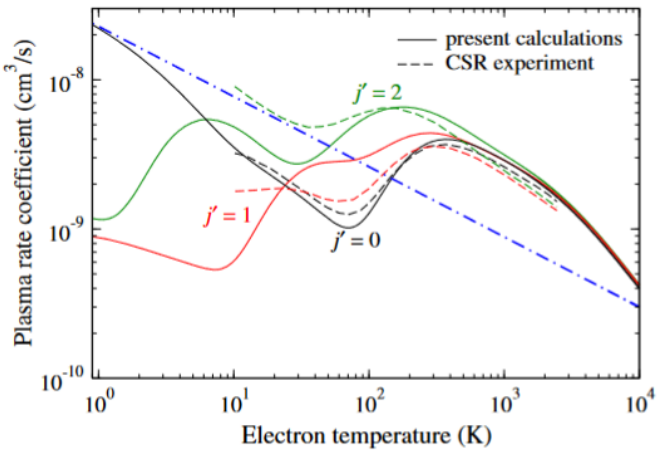

FIG. 5. Plasma rate coefficients are shown for different initial rotational states $j' = 0, 1, 2$. The solid curves result from the present theory, while the dashed curves are taken from the experiment at the CSR [4]. The dot-dashed line represents data employed by Guesten *et al.* [1] in their chemistry kinetics simulations of NGC 7027.

Quantum-state-selective electron recombination studies suggest enhanced abundance of primordial HeH^+

Oldřich Novotný[1*], Patrick Wilhelm[1], Daniel Paul[1], Ábel Kálosi[1,2], Sunny Saurabh[1], Arno Becker[1], Klaus Blaum[1], Sebastian George[1,3], Jürgen Göck[1], Manfred Grieser[1], Florian Grussie[1], Robert von Hahn[1], Claude Krantz[1], Holger Kreckel[1], Christian Meyer[1], Preeti M. Mishra[1], Damian Muell[1], Felix Nuesslein[1], Dmitry A. Orlov[1], Marius Rimmler[1], Viviane C. Schmidt[1], Andrey Shornikov[1], Aleksandr S. Terekhov[4], Stephen Vogel[1], Daniel Zajfman[5], Andreas Wolf[1]

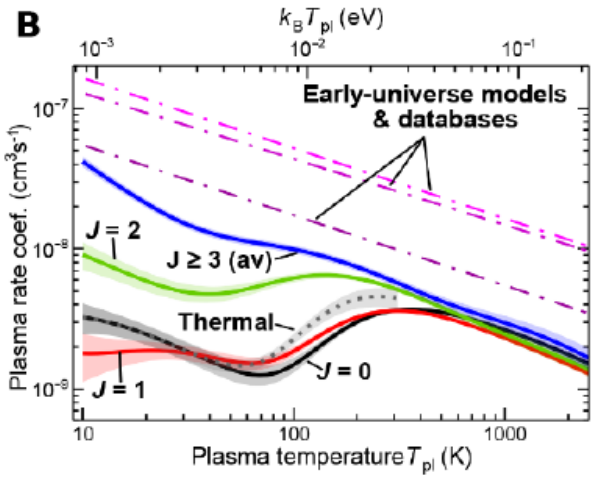

Fig. 4. Rotational-state selective DR rates for HeH^+. (A) Merged-beams rate coefficients $\alpha^J_{DR}(E_d)$ for $J \leq 2$ and average for $J \geq 3$ (mainly 3 and 4; mean ± SD). The dashed lines mark the shift of the maximum as J increases. (B) Full lines: single-J plasma rate coefficients $\alpha^J_{DR,pl}(T_{pl})$ for $J \leq 2$ and average for $J \geq 3$ (mainly 3 and 4; mean with shaded areas as ± SD). Dotted: fully thermal rate coefficient $\alpha_{DR,therm}(T_{rot} = T_{pl})$. Dashed-dotted: values applied in early-universe models (*21*, *22*) and astrochemistry databases (*23*–*25*). See (*19*) for further discussion, numerical fitting functions and parameters.

Concept of recombination rate coefficient (plasma binary reactions)

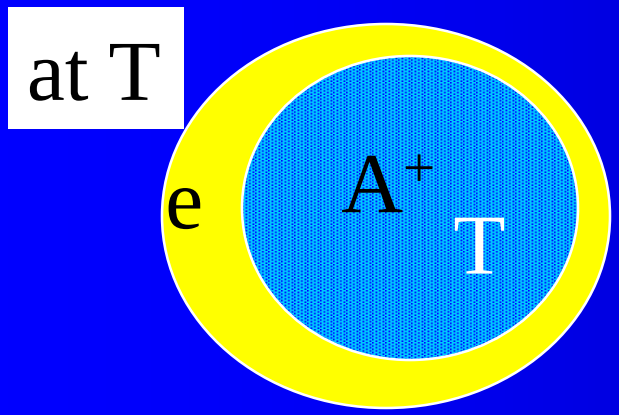

$e^- + A^+ \rightarrow$ products

$dN_A/dt = -\alpha n_e N_A$

RECOMBINATION RATE COEFFICIENT

$\alpha = \alpha(T)$

$\sigma = \sigma(v) = \sigma(\varepsilon)$

Collision rate coefficient, Recombination rate coefficient

$\alpha = \langle \sigma u_r \rangle$

$H_3^+ + e^- \rightarrow H + H_2; 3H$

Single collision

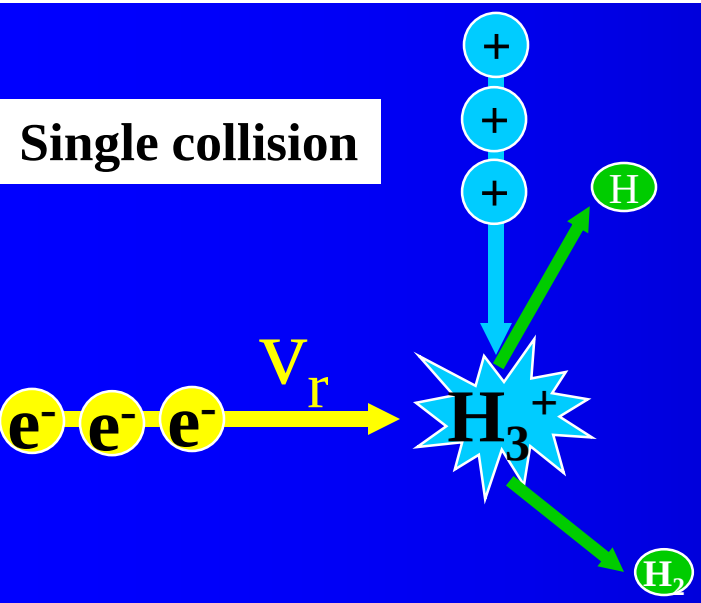

$\sigma(v_r)$ **recombination cross section**

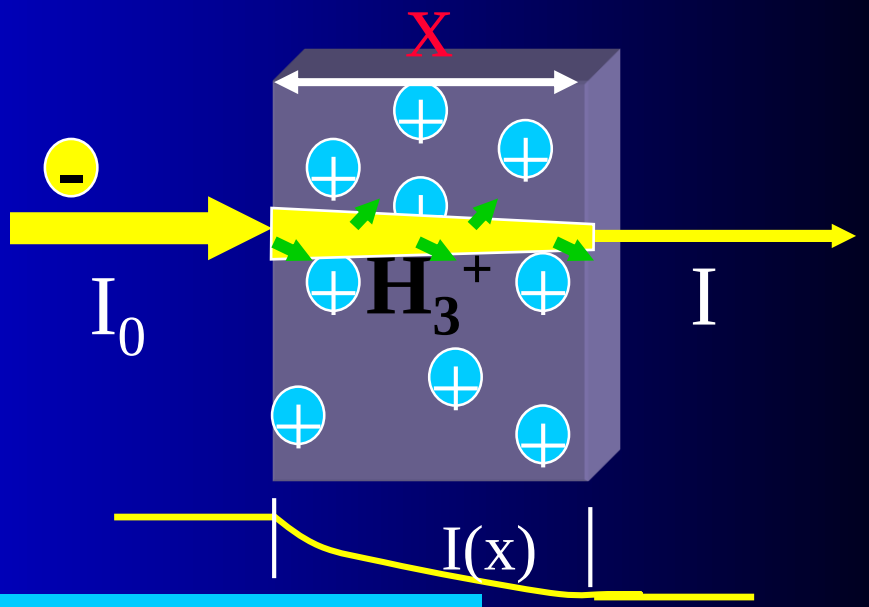

$I=I_0\exp(-\sigma n_i x)$

$k(T)=<v\sigma>$

Multiple collision

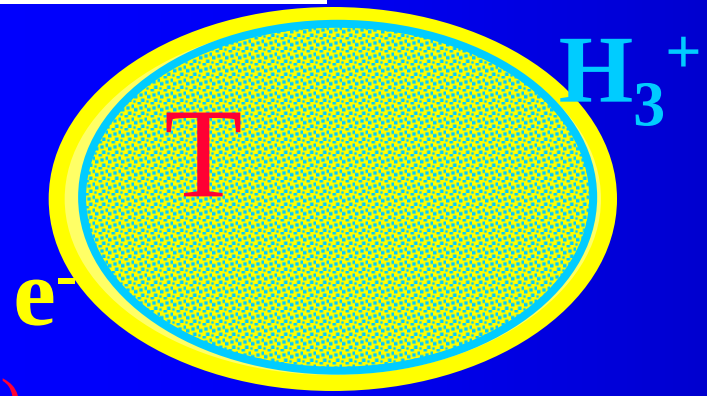

k(T)

recombination rate coefficient

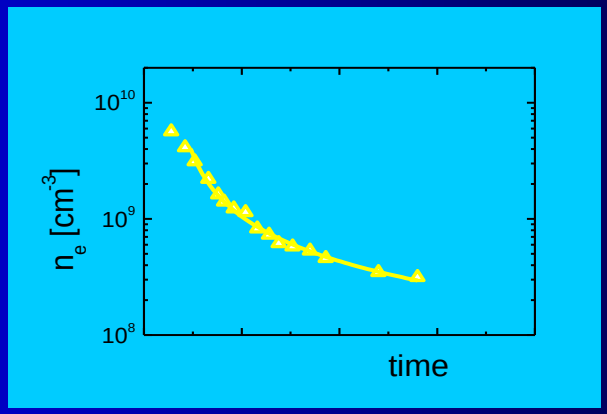

$dn_i/dt=-kn_in_e$

Cross sections measured obtained in Ion Storage Ring experiments

Quo vadis??

$HD^+ + e^-$

Dissociative recombination

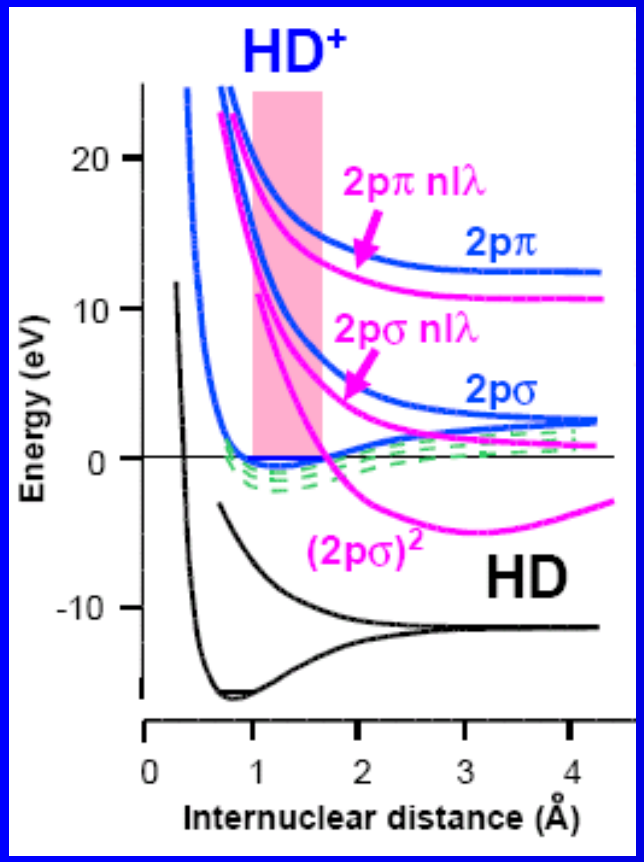

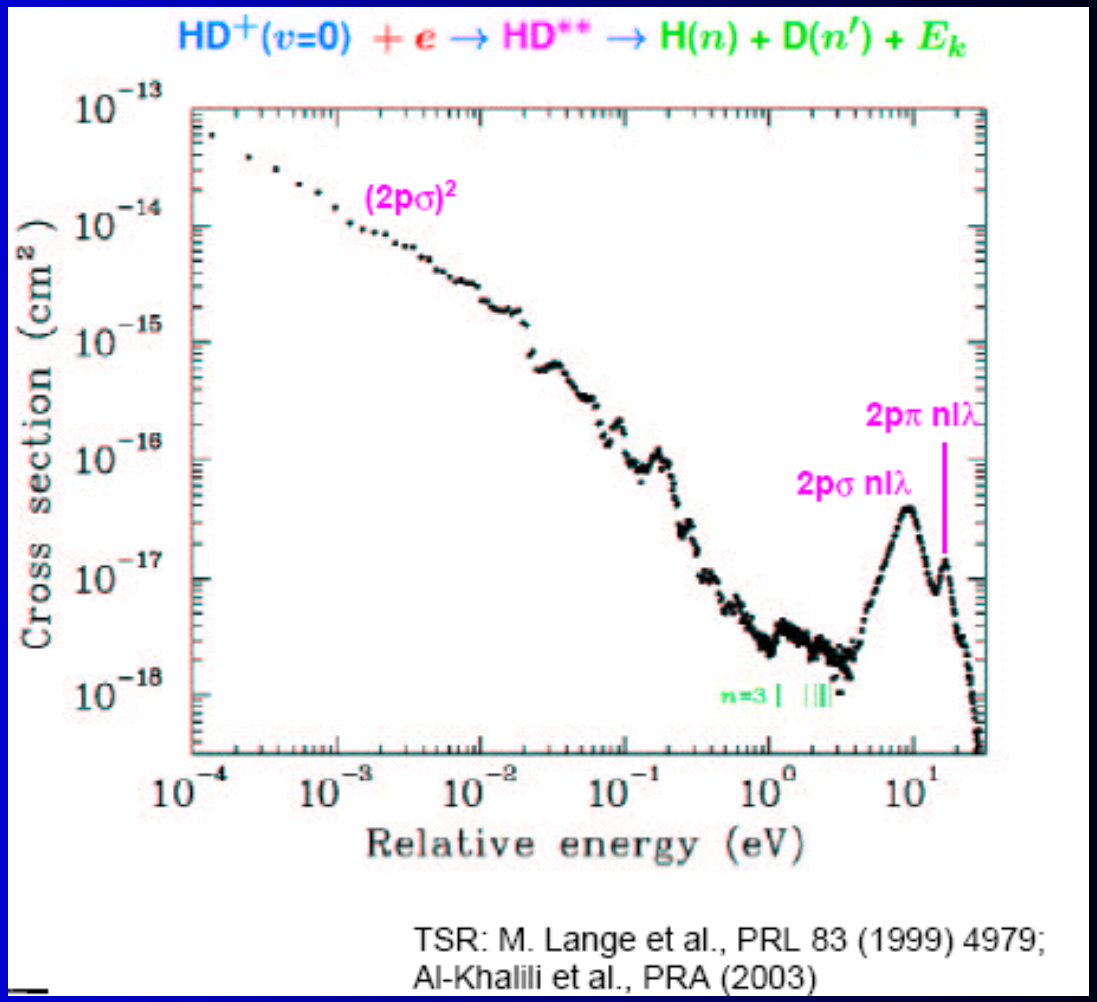

TSR: M. Lange et al., PRL 83 (1999) 4979;
Al-Khalili et al., PRA (2003)

Dissociative recombination HD+

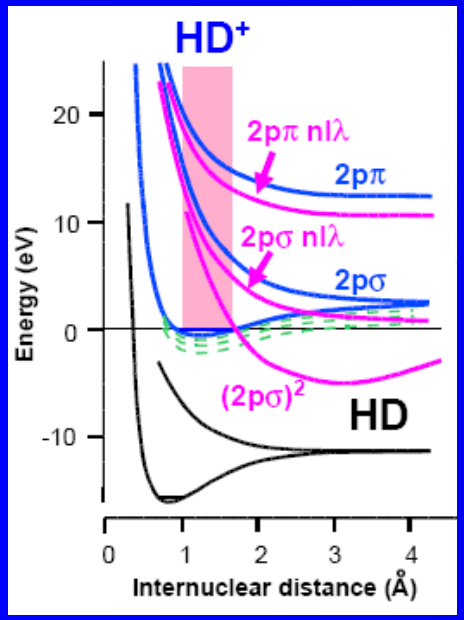

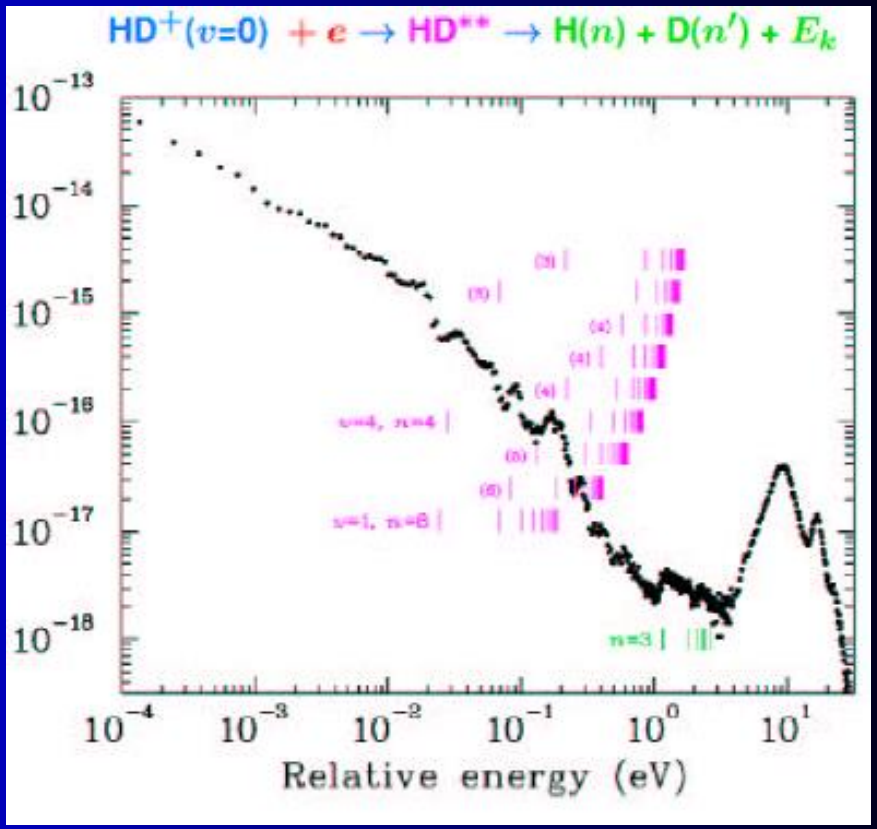

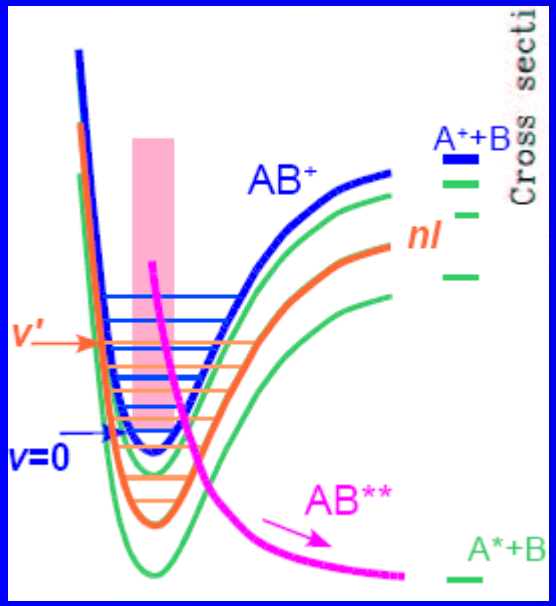

Scan of electron ion relative energy E

Electron temperature kT_{Per}=4meV (30meV for E>0.3eV)

kT_{Par}=0.1meV

Energy resolution ~4….8 meV (E< 0.08eV)

Absolute accuracy of cross section ca. +- 30%

Recombination H_2^+

Electron collisions with H_2^+

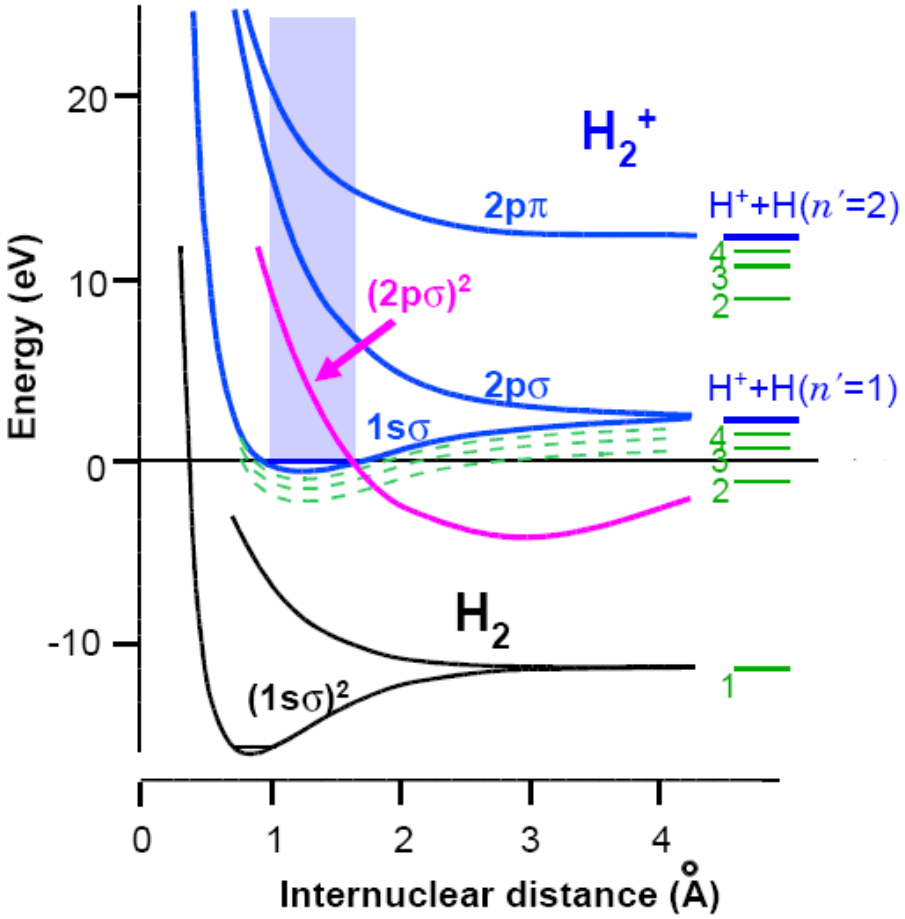

H. Takagi, J. Phys. B, 26, 4815 (1993)

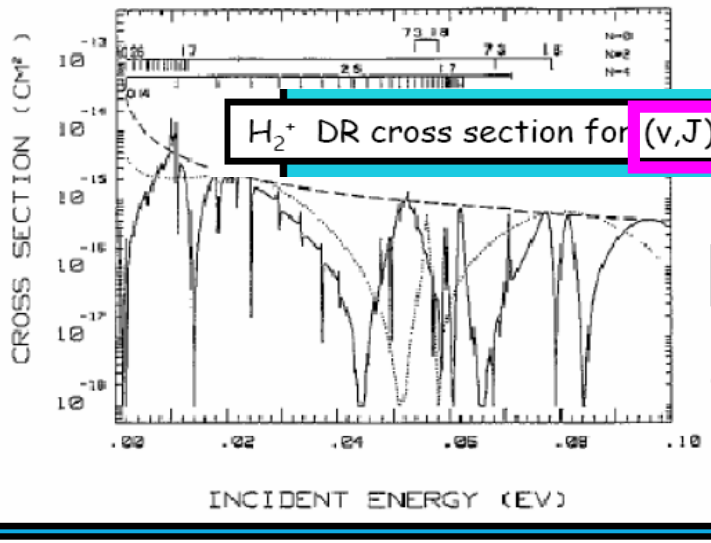

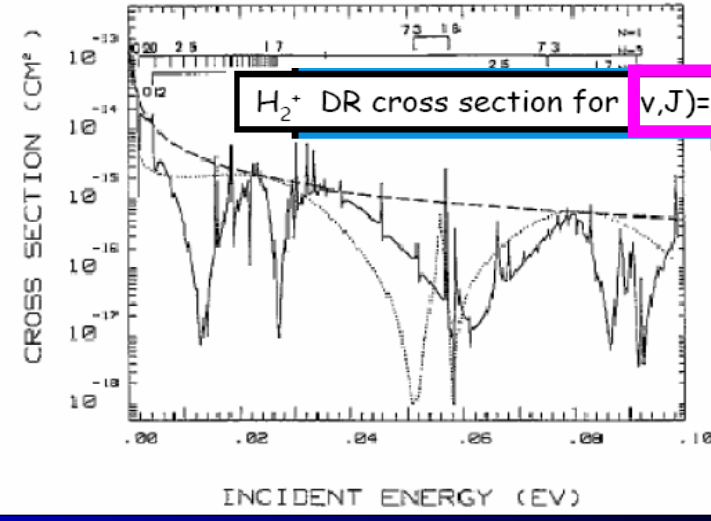

Recombination NO^+

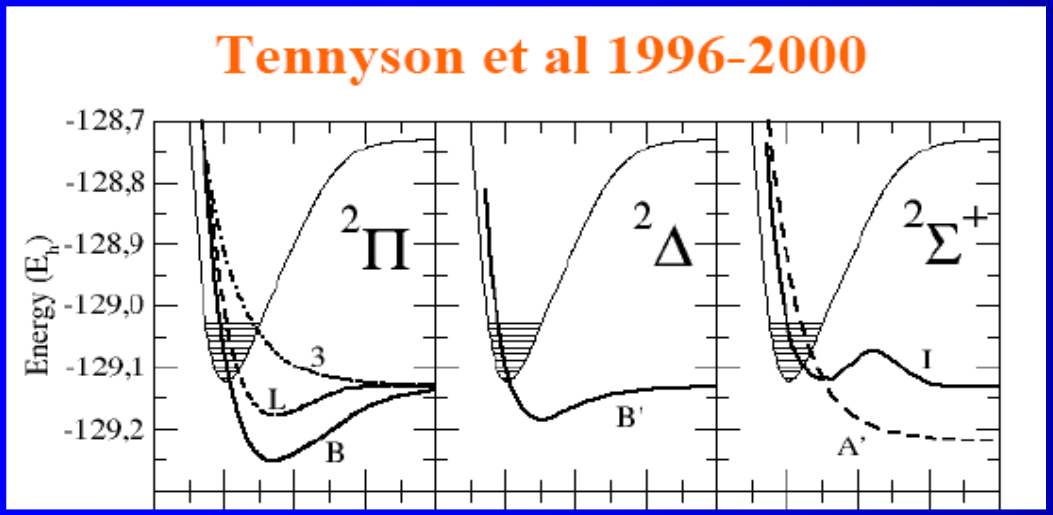

Recombination of H_3^+

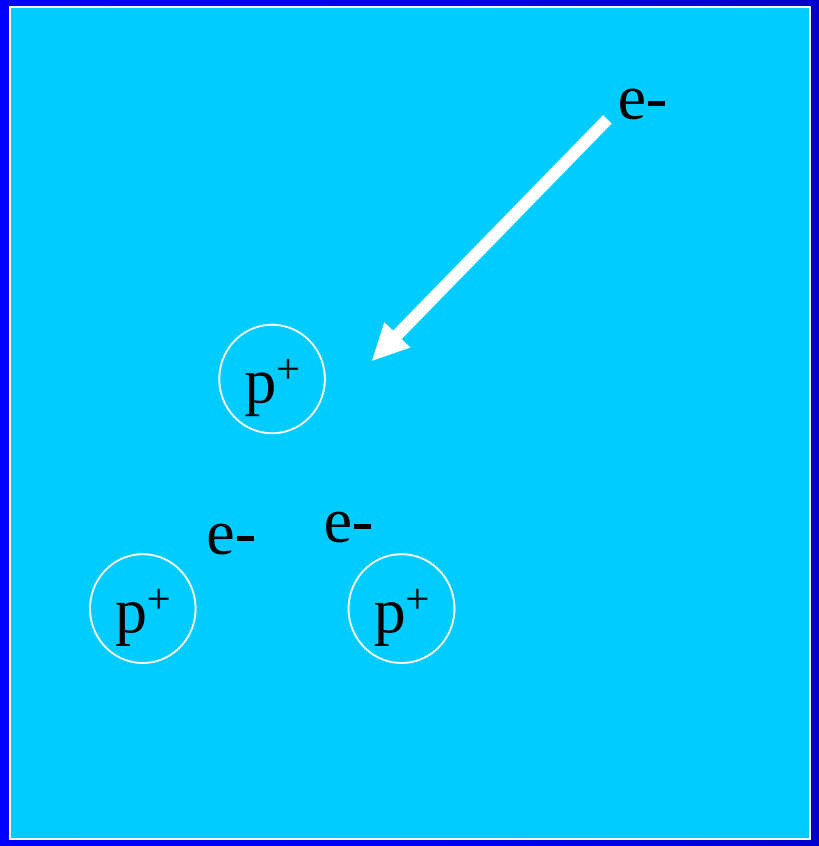

$$H_3^+ + e^- \rightarrow H+H+H$$

$$\rightarrow H_2+H$$

$$\rightarrow H_3^* \quad (?)$$

Tunneling dissociative recombination

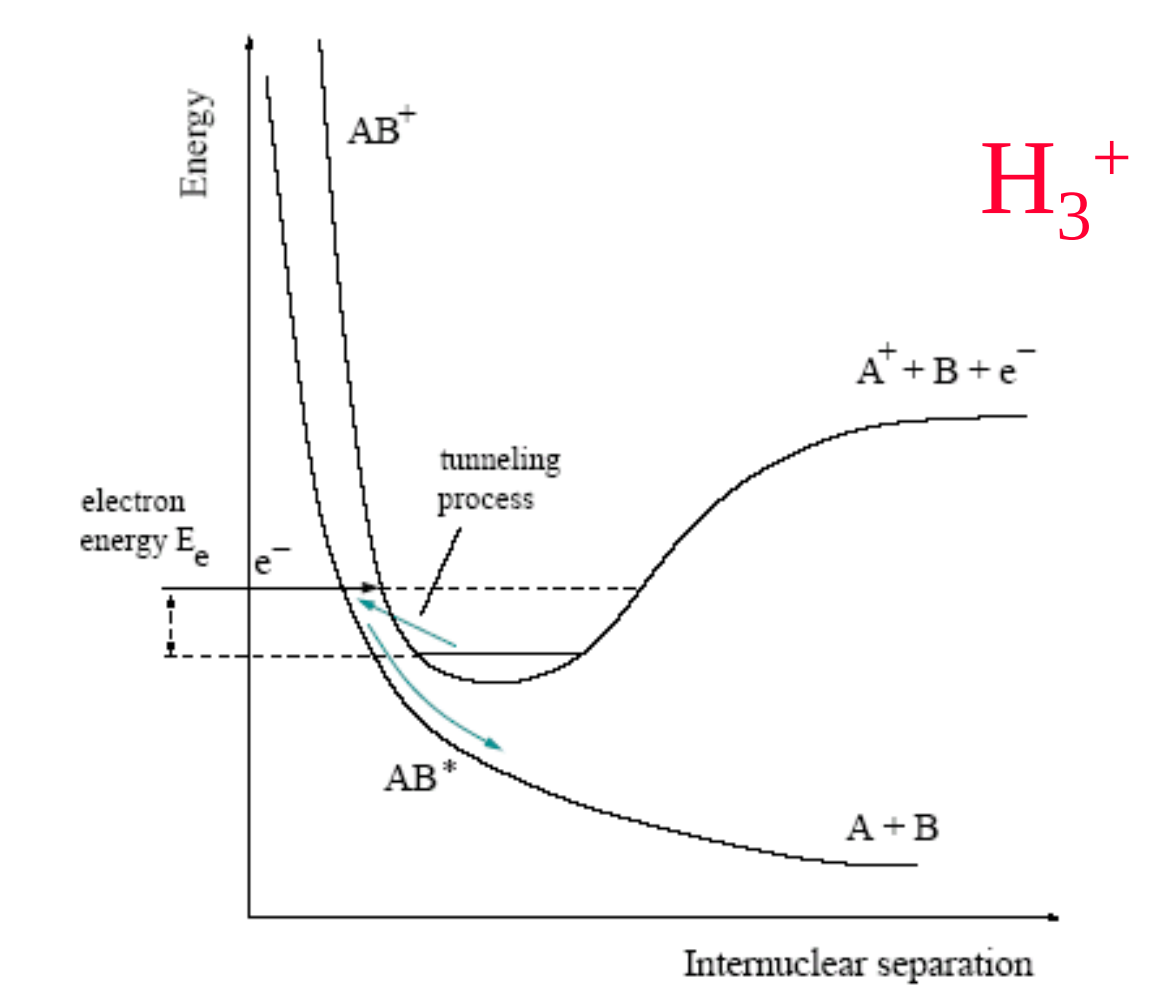

Figure 4.3: *Sketch of tunneling mode dissociative recombination.*

Tunneling dissociative recombination

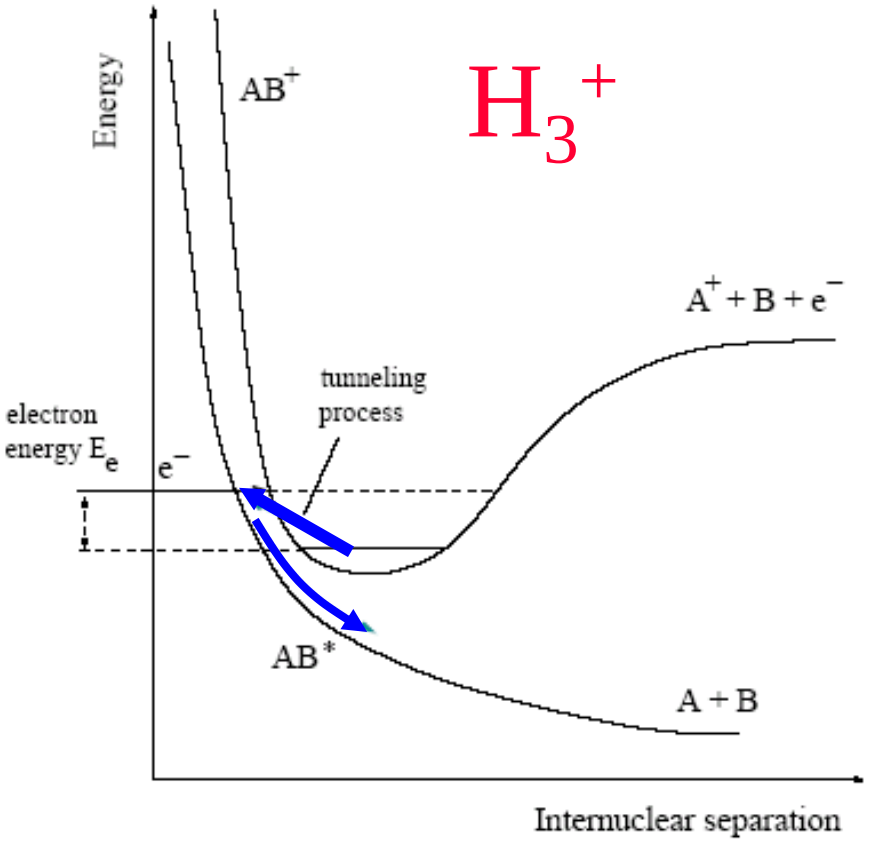

Figure 4.3: *Sketch of tunneling mode dissociative recombination.*

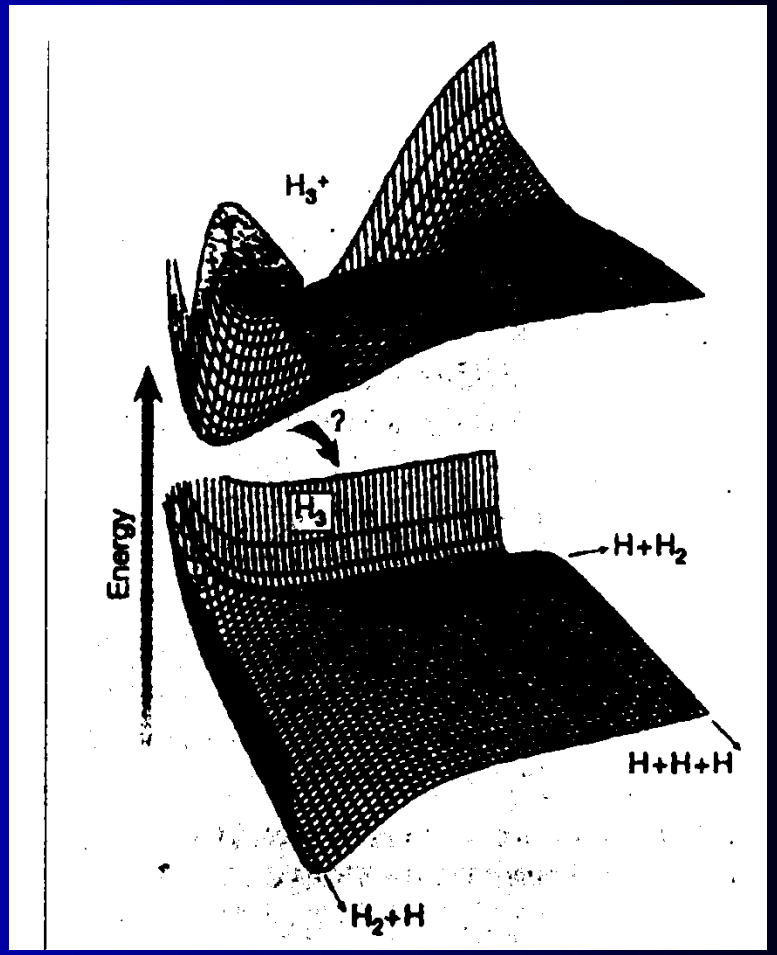

Dissociative recombination of H_3^+ . Relevant potential curves

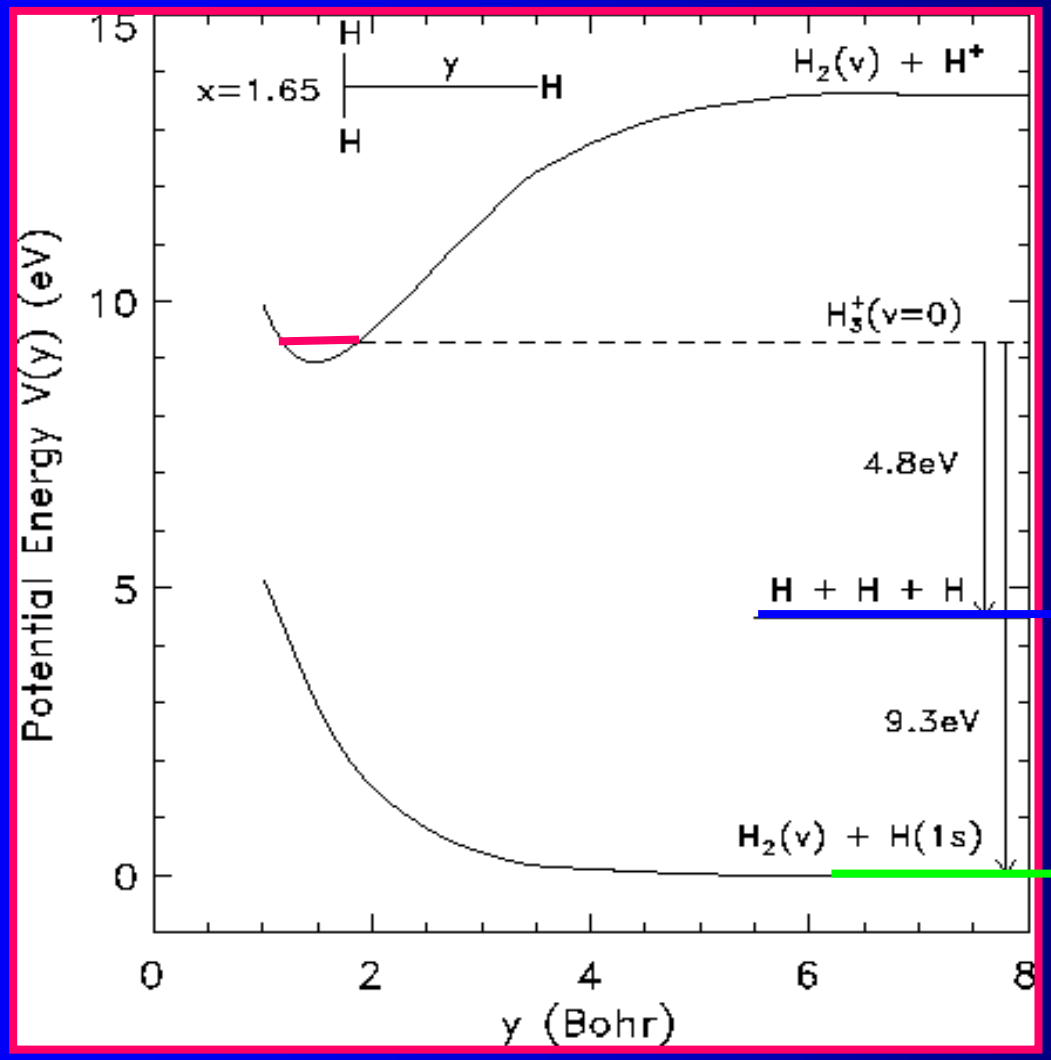

3-body decay

2-body decay

Dissociative recombination of H_3^+

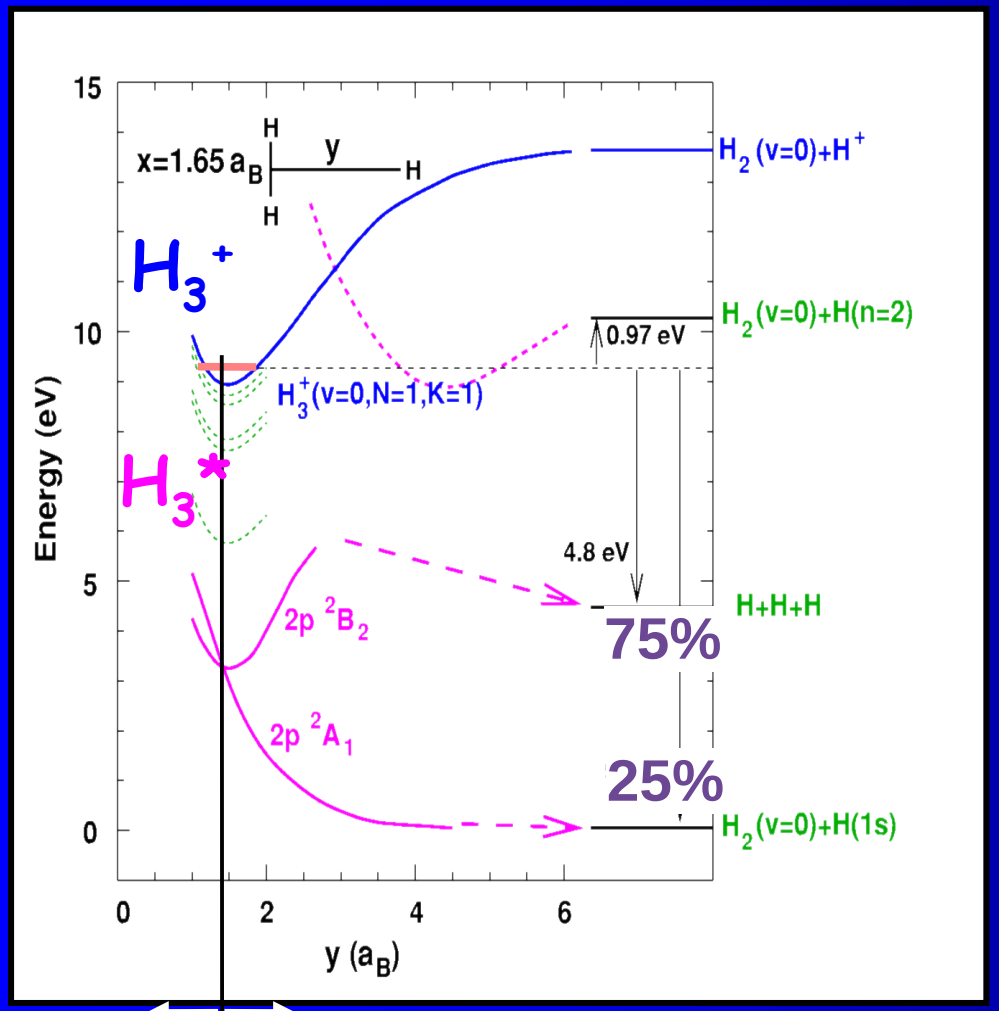

Symmetric deformation

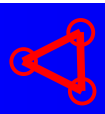

Remote curve crossing

Electron capture via Jahn-Teller coupling of electronic and ro-vibrational motion

Prototype system for electron capture and dissociation mechanisms in polyatomic species

Three atomic ions

Dissociative recombination of H_3^+

Prototype system for electron capture and dissociation mechanisms in polyatomic species

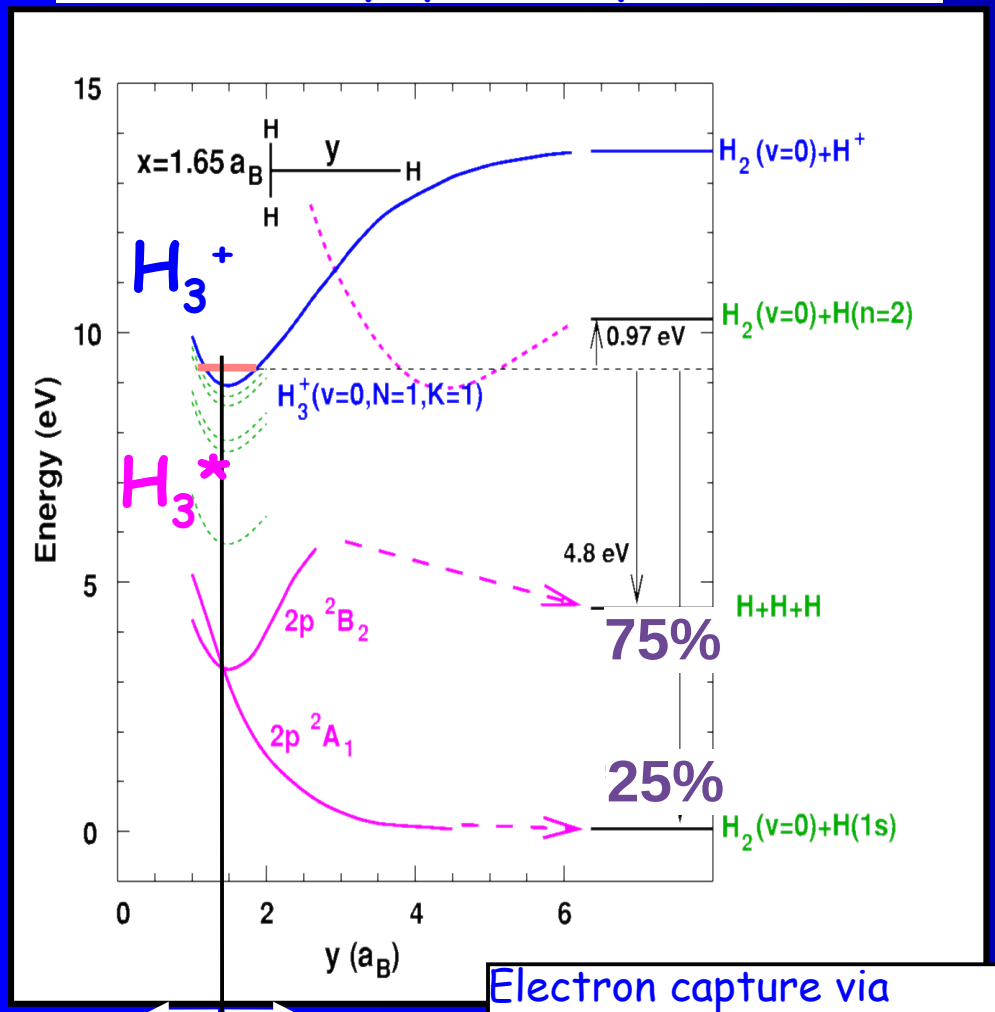

Symmetric deformation

Electron capture via Jahn-Teller coupling of electronic and ro-vibrational motion

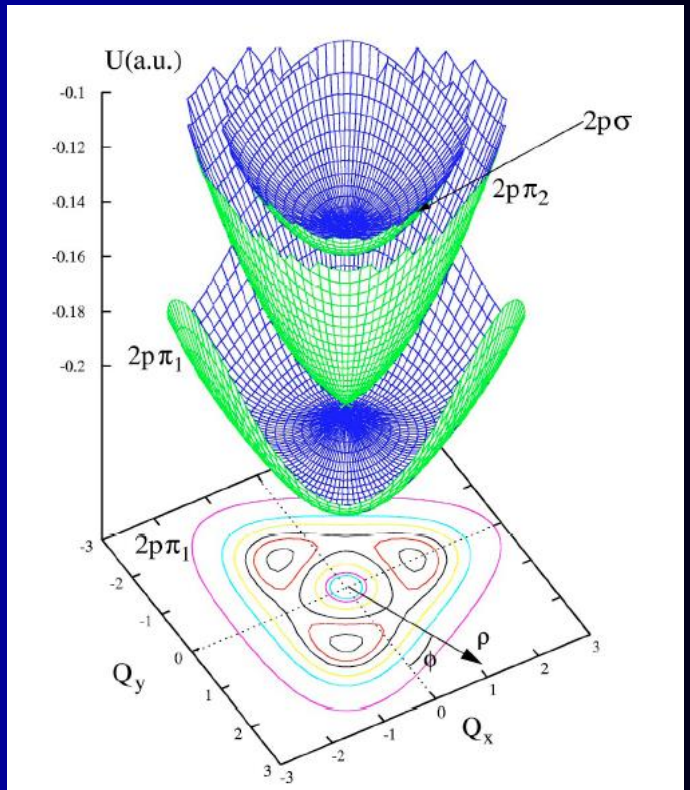

FIG. 4. The figure demonstrates how the Jahn-Teller effect produces a high rate of dissociative recombination. One $2p\sigma$ potential surface and two $2p\pi$ potential surfaces [47] of the neutral molecule are shown. The conical intersection is produced by Jahn-Teller coupling. When an electron arrives, it scatters first into a low-lying vibrationally excited Rydberg state $\{01^1\}$. Then, after the nuclei vibrate, the system finds its way with high probability into a $2p\pi$ state having high vibrational excitation, near the point of conical intersection. The contour plot at the bottom of the figure represents the lowest $2p\pi_1$ surface. All three potential surfaces are shown in the reduced 2D space of dimensionless normal coordinates. The coordinates used here are the normal asymmetric Q_x, Q_y coordinate, with ρ and ϕ their polar components [17,18]. The third vibrational coordinate—the symmetric stretch coordinate Q_1—is kept constant for this graph.

2004 - 2007

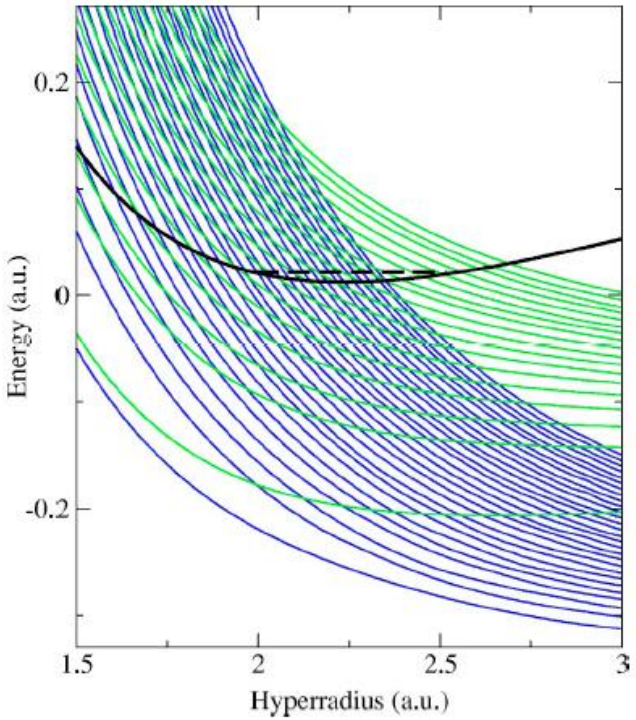

FIG. 1. The problem of DR of H_3^+ in the hyperspherical adiabatic approximation. The lowest hyperspherical adiabatic potential (thick full line) of the H_3^+ and number of hyperspherical adiabatic potentials of the neutral molecule (thin lines). Lower family of lines (darker lines) dissociate to the H_2+H channel; the upper family (lighter lines) dissociate to the H+H+H channel. To calculate hyperspherical adiabatic curves we used the three-dimensional H_3^+ potential from Ref. [48] and the H_3 potential from Refs. [35–37]. Since the density of hyperspherical states is high, only every tenth H_3 potential curve is shown in the figure. The dashed line shows the position of the ground vibrational level of the ion, which is the only one populated in the relevant experiments.

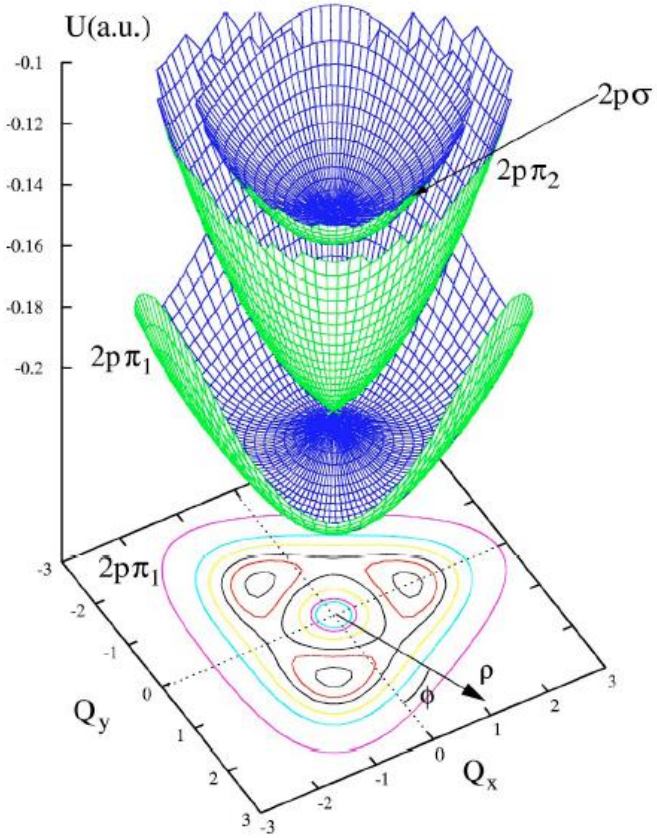

FIG. 4. The figure demonstrates how the Jahn-Teller effect produces a high rate of dissociative recombination. One $2p\sigma$ potential surface and two $2p\pi$ potential surfaces [47] of the neutral molecule are shown. The conical intersection is produced by Jahn-Teller coupling. When an electron arrives, it scatters first into a low-lying vibrationally excited Rydberg state $\{01^1\}$. Then, after the nuclei vibrate, the system finds its way with high probability into a $2p\pi$ state having high vibrational excitation, near the point of conical intersection. The contour plot at the bottom of the figure represents the lowest $2p\pi_1$ surface. All three potential surfaces are shown in the reduced 2D space of dimensionless normal coordinates. The coordinates used here are the normal asymmetric Q_x, Q_y coordinate, with ρ and ϕ their polar components [17,18]. The third vibrational coordinate—the symmetric stretch coordinate Q_1—is kept constant for this graph.

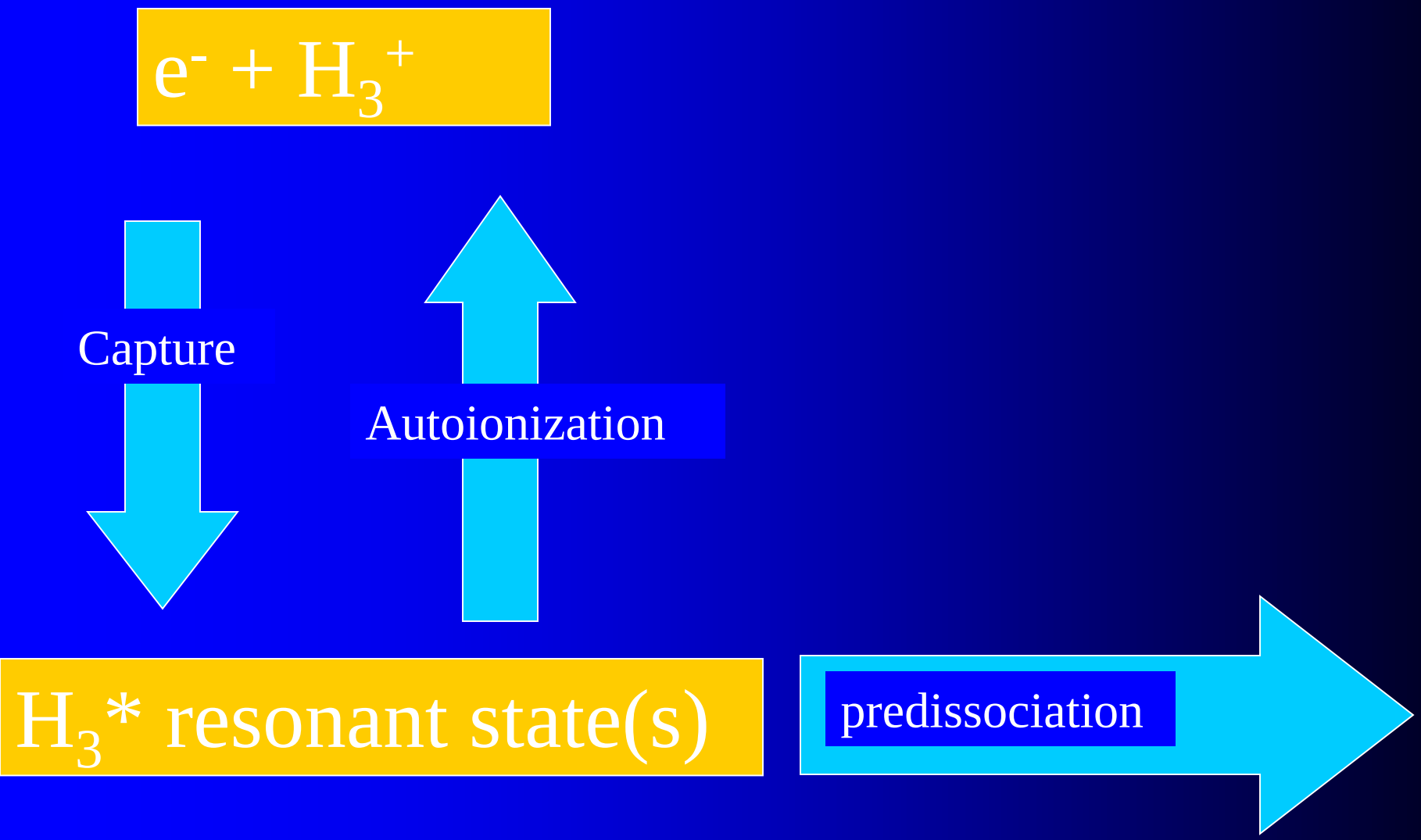

To get high recombination rate, we need

(a) efficient capture

(b) predissociation faster than auto-ionization

Cosmic-ray ionisation rate $\gamma \sim 3 \times 10^{-17} s^{-1}$

Dense Clouds

Barnard 68 (João Alves)

Formation

$$H_2 \xrightarrow{h\nu} H_2^+ \xrightarrow{H_2} H_3^+$$

$$d[H_3^+]/dt \sim \gamma . [H_2]$$

a) DENSE CLOUDS:

$H_3^+ + CO$ $\quad d[H_3^+]/dt \sim -k_{CO} x [H_3^+] x [CO]$

$(k_{CO} = 2 \times 10^{-9} cm^3 s^{-1})$

$[H_3^+] = \gamma / k_{CO} \cdot [H_2]/[CO] =$ **$\sim 1 \times 10^{-4} cm^{-3}$**

~OK with observation

Cosmic-ray ionisation rate $\gamma \sim 3 \times 10^{-17} s^{-1}$

Formation

$$H_2 \xrightarrow{h\nu} H_2^+ \xrightarrow{H_2} H_3^+$$

$$d[H_3^+]/dt \sim \gamma . [H_2]$$

b) DIFFUSE CLOUDS:

$H_3^+ + e^-$ $\quad d[H_3^+]/dt \sim - \alpha_{DR} [H_3^+][e^-]$

$\alpha_{DR} = 2 \times 10^{--7} cm^3 s^{-1} \times (T/300)^{-0.65}$ (the value from 2005)

$[H_3^+] = \gamma/\alpha_{DR} . [H_2]/[C] = \sim 1 \times 10^{-7} cm^{-3}$

~ NO with observation

… history is repeating itself ….

$$H_3^+ + e^- \Rightarrow H + H_2, 3H$$

RSDM 2012

DR 2013

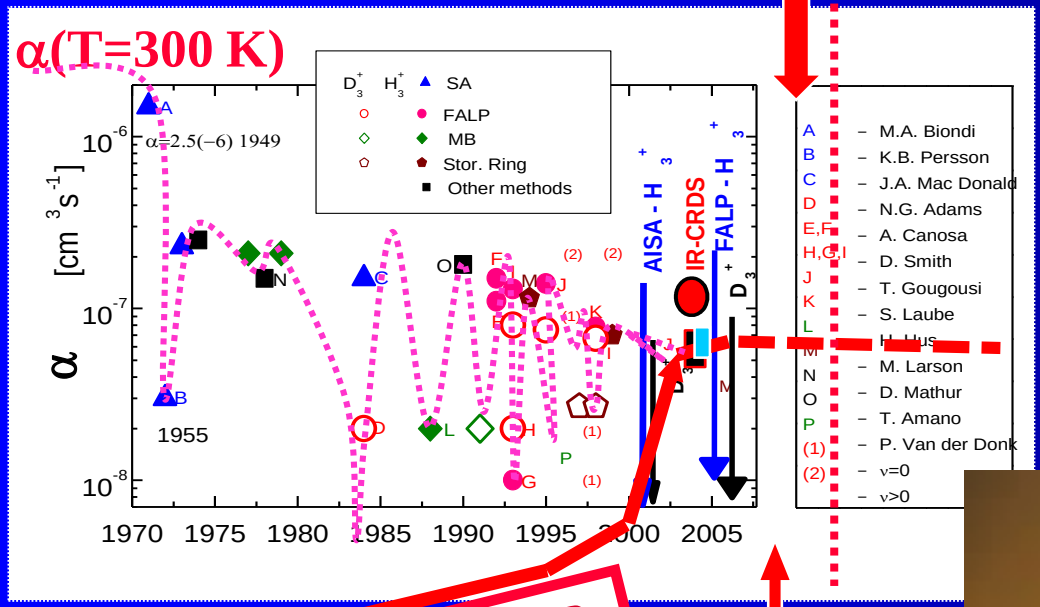

THEORY OF DR

Doubts 2011

"Presently no rate coefficient measurement with a confirmed temperature below 300 K exists".

Petrignani *et al.* Phys. Rev. A (2011)

and … history repeated itself .

M. Larsson et al, CP Letters (2008)

… One remaining problem is to understand the plasma afterglow experiments.

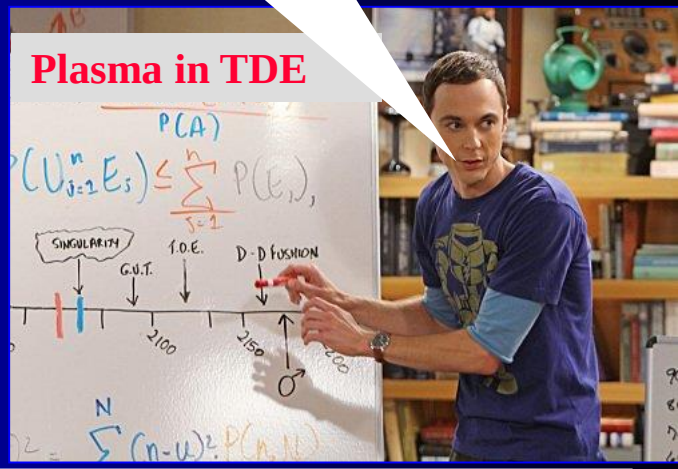

…. many times it was concluded, that the task was finished….

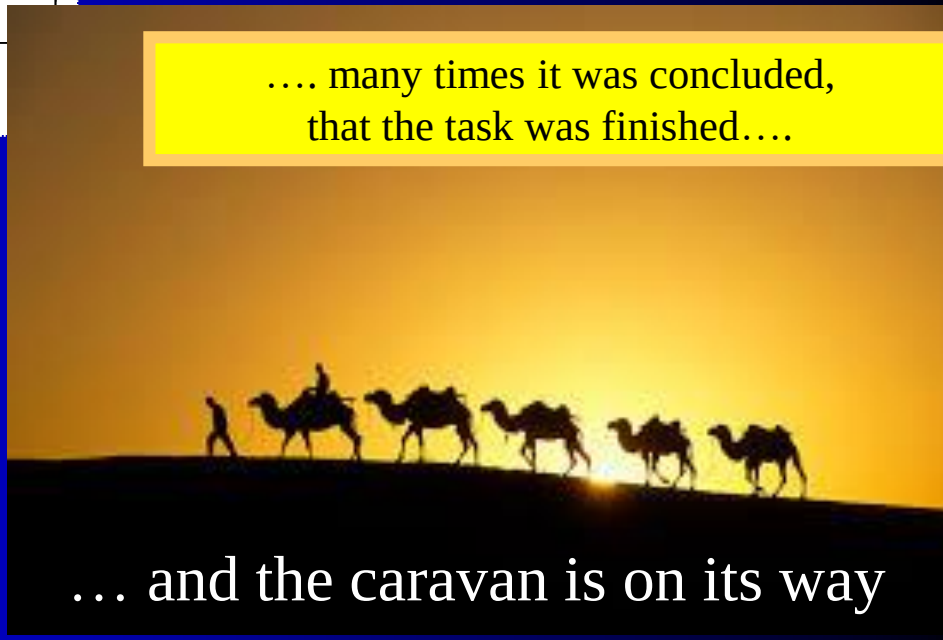

… and the caravan is on its way

Calculated life time from Slava

Slava 30 08 07

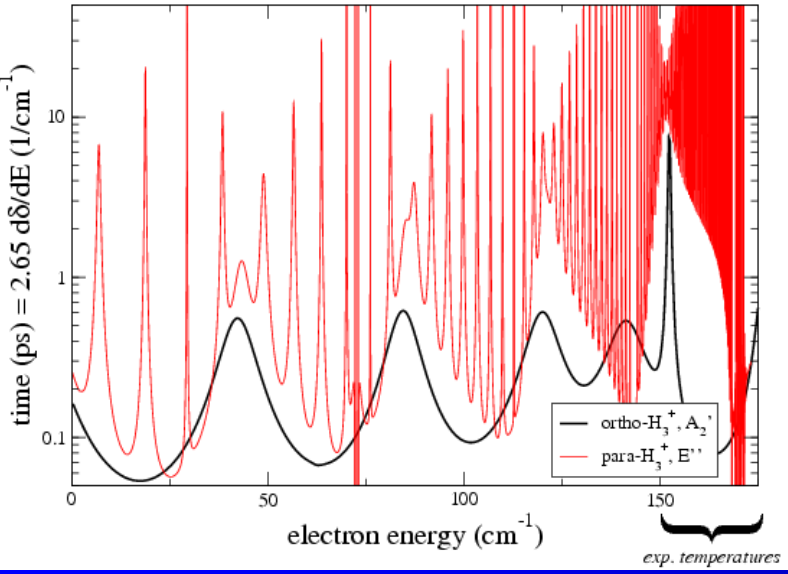

$$H_3^+ + e \Leftrightarrow H_3^* \rightarrow$$

$$H_3^+ + e \rightarrow H_3^*$$

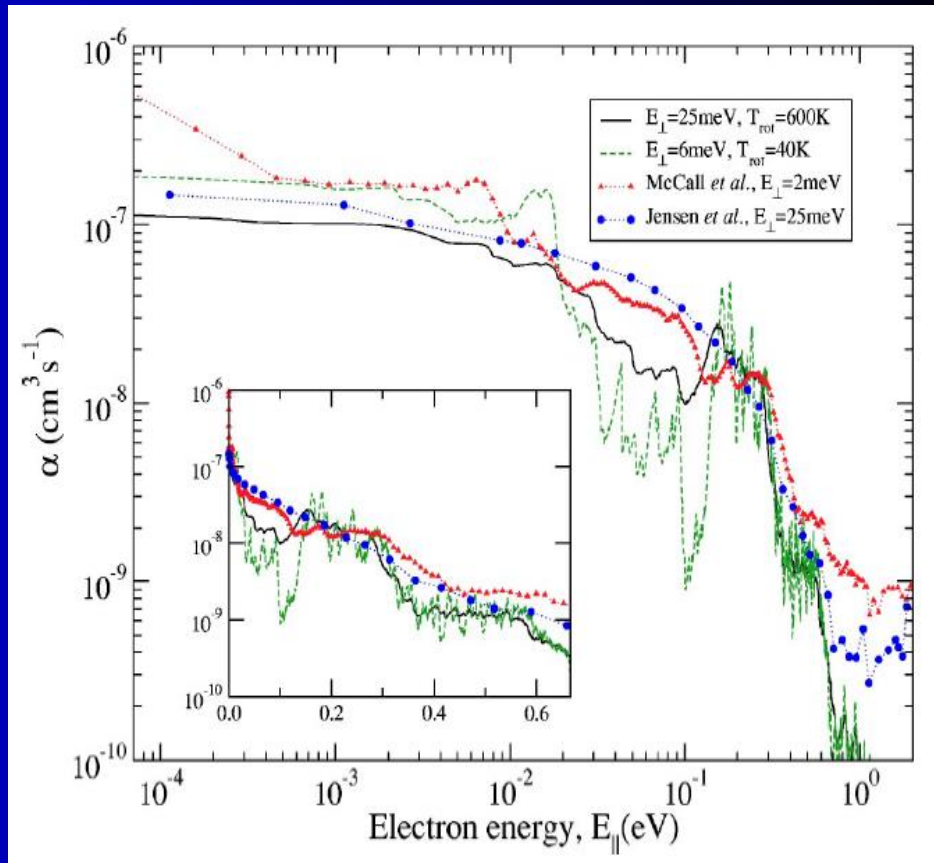

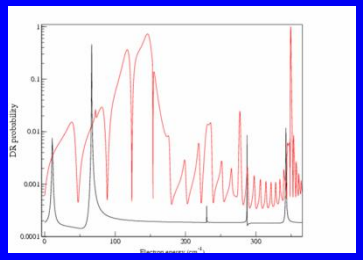

Dear Juraj and Chris, I'm sending you the figure with the DR probabilities for two different symmetries (red and black curves). The red curve corresponds to the rotational autoionization region. Fro this figure you can have an idea about the widths of the resonances. With best wishes, Slava

Recombination rate coefficients

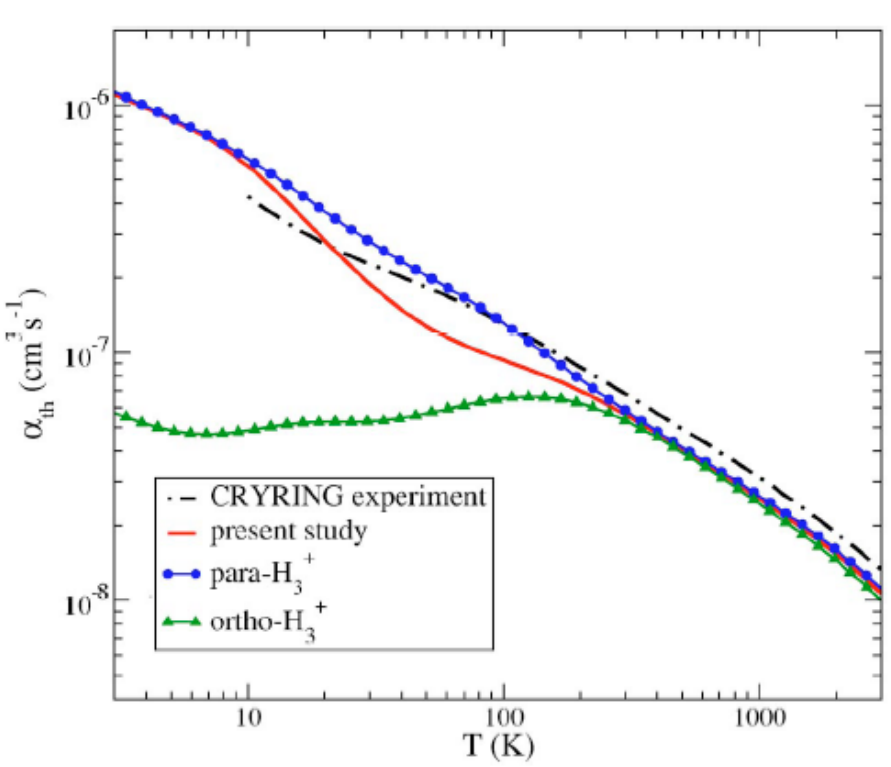

FIG. 5. (Color online) The present theoretical thermal rate coefficient for dissociative recombination of H_3^+ is compared with the experimental rate coefficient deduced from the storage ring experiment of McCall and coworkers (Refs. 9 and 10).

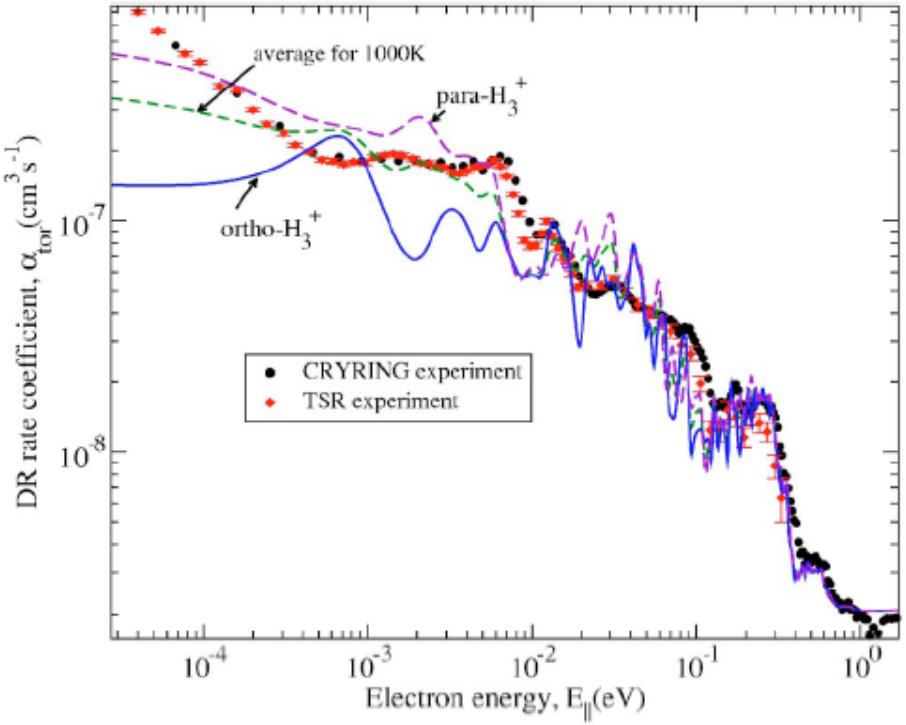

FIG. 3. (Color online) This figure compares the theoretical DR rate coefficient to the high-resolution storage ring experiment of Kreckel *et al.*[12] carried out at TSR. The experimental resolution parameters are $\Delta E_{\|}$ and $\Delta E_{\perp}$ are 25 μeV and 0.5 meV, respectively. The theoretical curve shown has been calculated with these parameters and rotational temperature T_{rv} =1000 K. The figure also shows the theoretical DR rate coefficients calculated separately for ortho- and paraconfigurations of H_3^+ with the same parameters $\Delta E_{\|}$, $\Delta E_{\perp}$, and T_{rv}.

The battle ship enters the stage

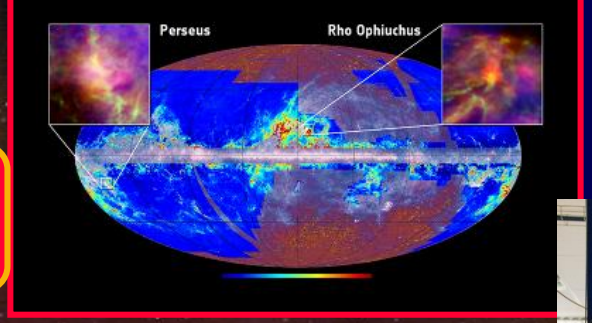

H_3^+ is fundamental

FALP

10-8

Πλασμα

Cryo-SA-CRDS

Cryo-NIR-CRDS

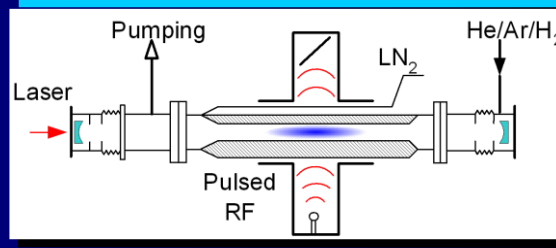

AISA

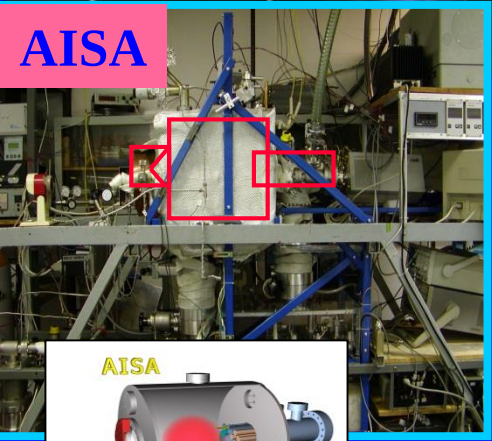

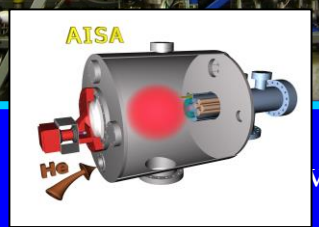

Cryo-FALP

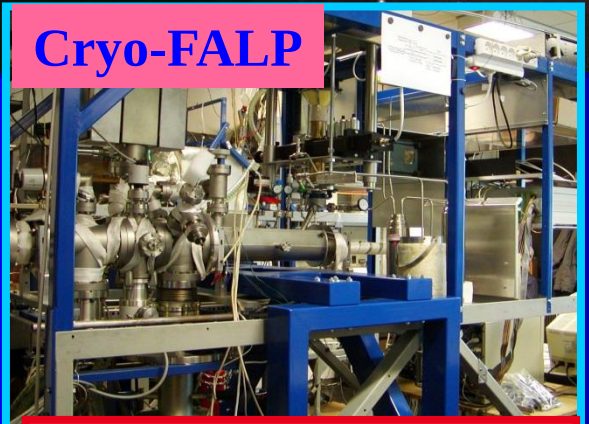

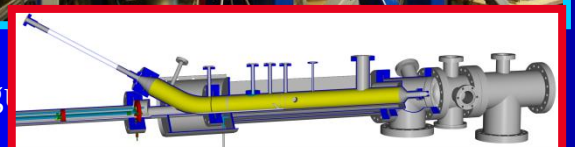

versity Prag

Pulsed (stationary) afterglow

Discharge pulse

microwave, UV, x-ray, e-beam

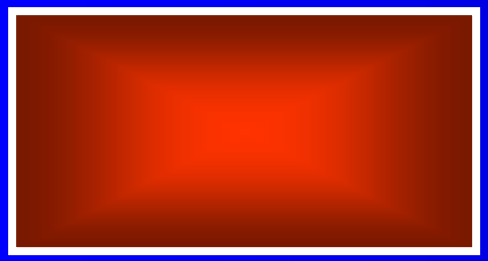

Plasma chamber
He: ~ 1 –20 Torr
Ar: 10 to 30 %
+ molecules

Measure $n_e(t)$

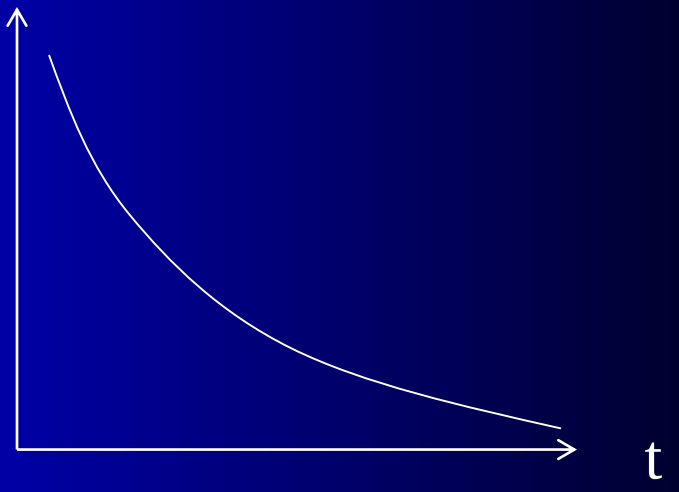

Get:

$$\frac{dn_e}{dt} = -\alpha n_e^{\,2} + (diffusion)$$

$$n_e(t) = \frac{n_{e0}}{1+\alpha n_{e0} t}$$

We measure effective – apparent binary recombination rate coefficient

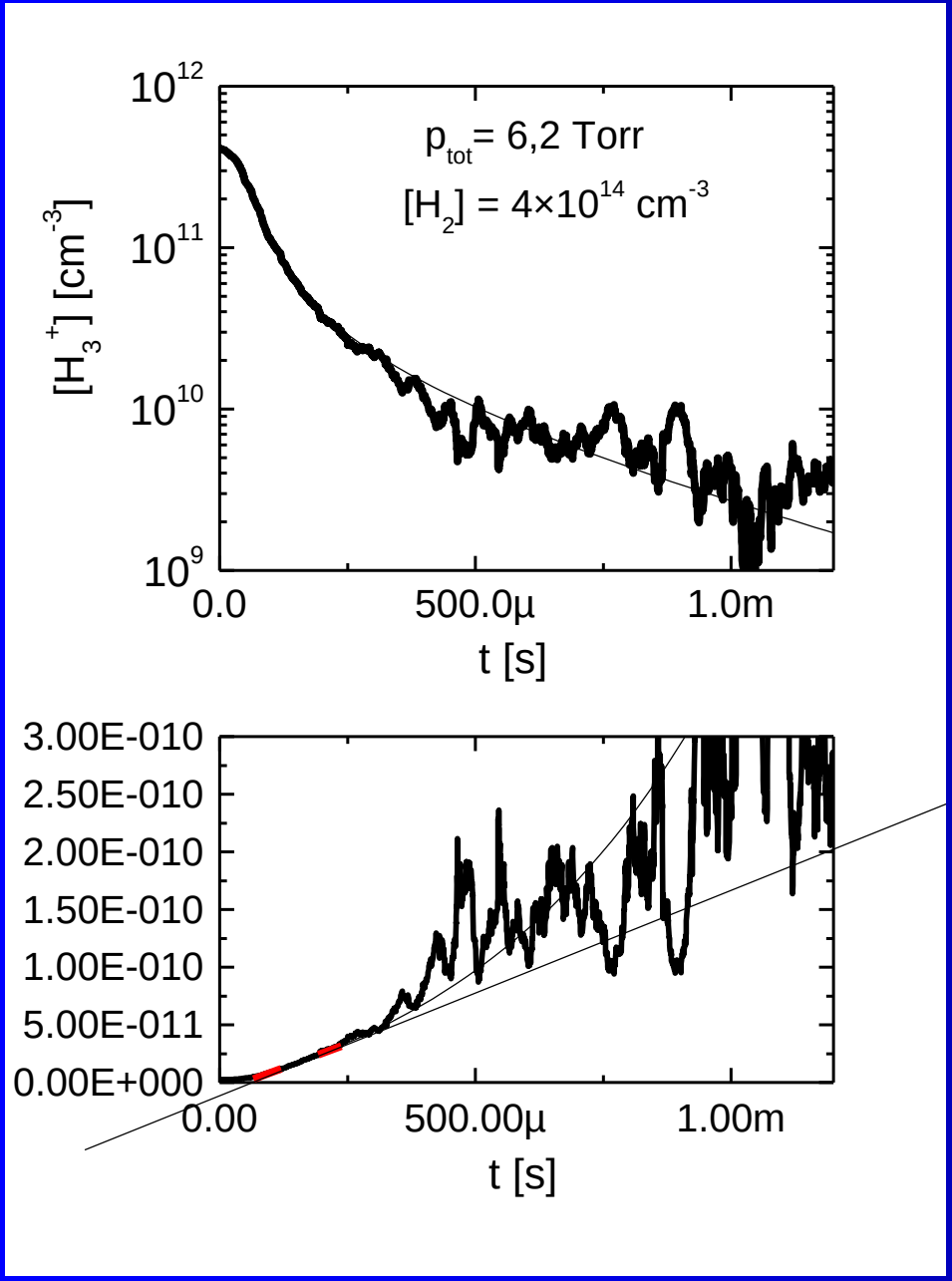

Quasineutral H_3^+ dominated plasma

$$\frac{\mathrm{d}n_\mathrm{e}}{\mathrm{d}t} = -\alpha_\mathrm{eff} n_\mathrm{e}^2 - \frac{n_\mathrm{e}}{\tau_\mathrm{L}}$$

$$\frac{1}{[H_3^+]} = \frac{1}{[H_3^+]_0} + \alpha t$$

We measure effective – apparent binary recombination rate coefficient

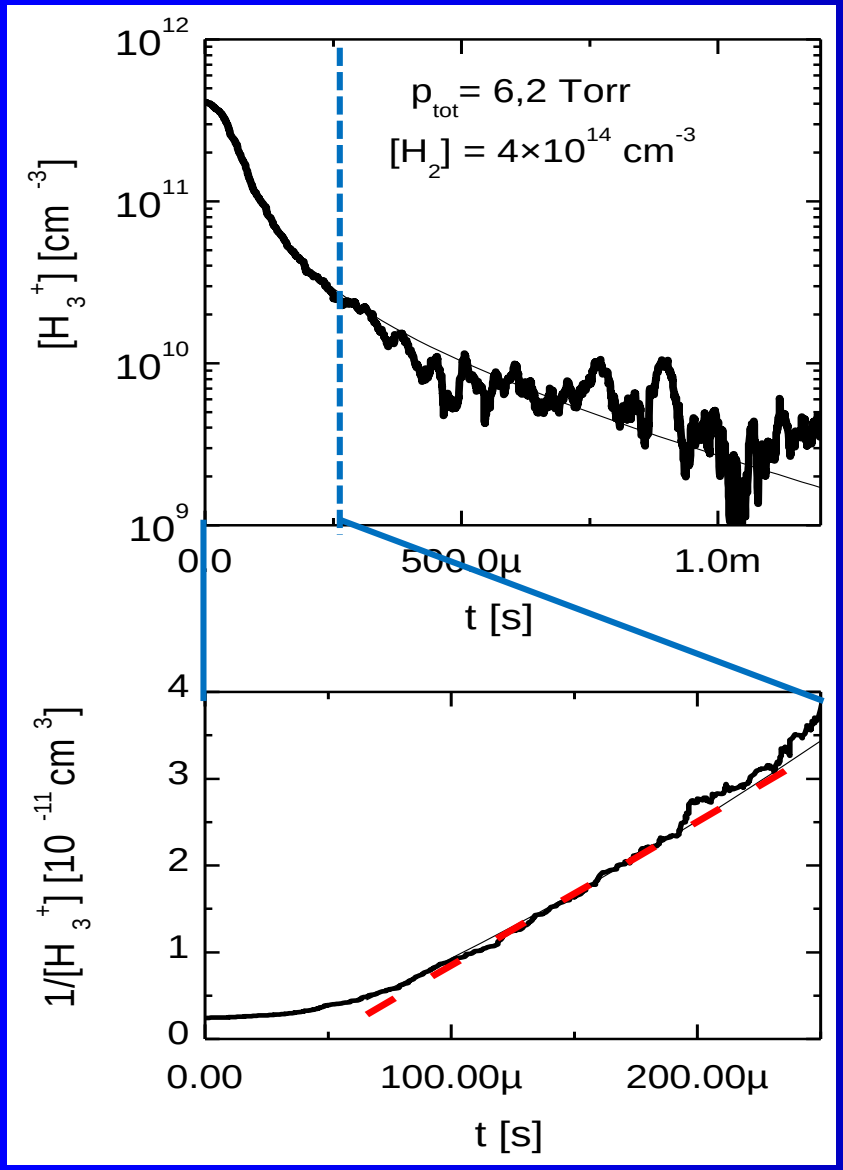

Quasineutral H_3^+ dominated plasma

$$\frac{\mathrm{d}n_\mathrm{e}}{\mathrm{d}t} = -\alpha_\mathrm{eff} n_\mathrm{e}^2 - \frac{n_\mathrm{e}}{\tau_\mathrm{L}}$$

$$\frac{1}{[H_3^+]} = \frac{1}{[H_3^+]_0} + \alpha t$$

Decay in diffusion and recombination governed plasma

$$\frac{dn_e}{dt} = -\alpha\, n_e^2 - \frac{D_a}{\Lambda^2} n_e$$

$$\frac{1}{n_e} = \alpha\, \frac{\exp(\nu t) - 1}{\nu_D} + \frac{1}{n_0} \exp(\nu_D t)$$

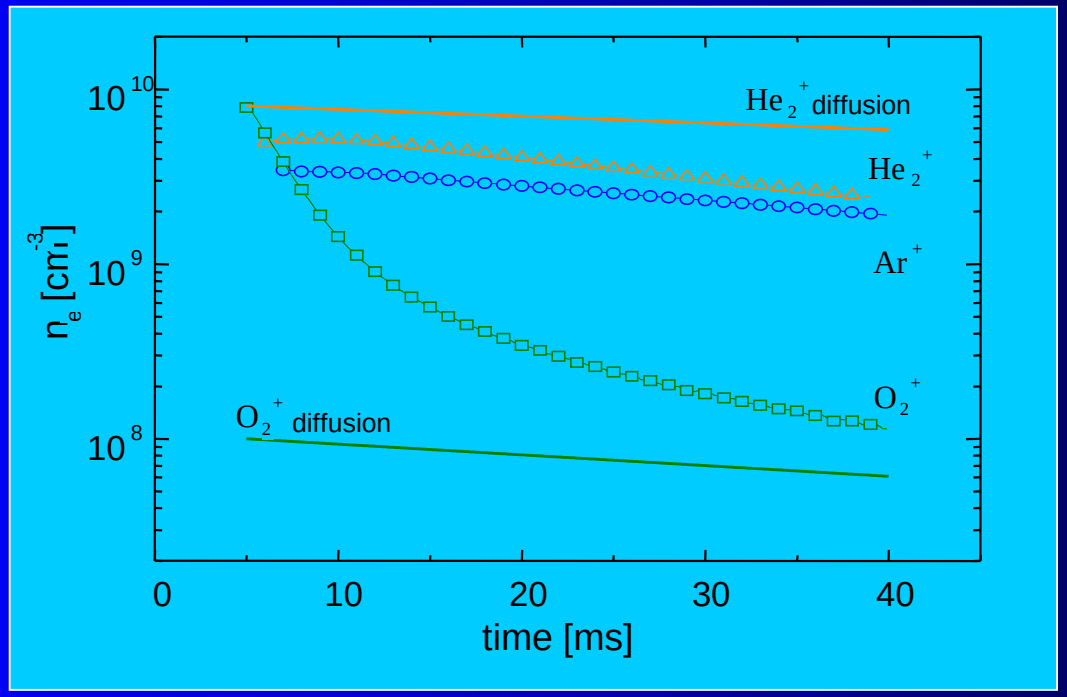

Decay in diffusion and recombination governed plasma

$$\frac{dn_e}{dt} = -\alpha\, n_e^2 - \frac{D_a}{\Lambda^2} n_e$$

$$\frac{1}{n_e} = \alpha\, \frac{\exp(\nu t) - 1}{\nu_D} + \frac{1}{n_0}\exp(\nu_D t)$$

Limit for t -->0

$$\frac{1}{n_e} = \alpha\, \frac{(1+\nu_D t) - 1}{\nu_D} + \frac{1}{n_0}(1+\nu_D t)$$

$$\frac{1}{n_e} = \alpha t + \frac{1}{n_0}(1)$$

Limit for large t

$$\frac{1}{n_e} = \left(\frac{\alpha}{\nu_D} + \frac{1}{n_0}\right)\exp(\nu_D t)$$

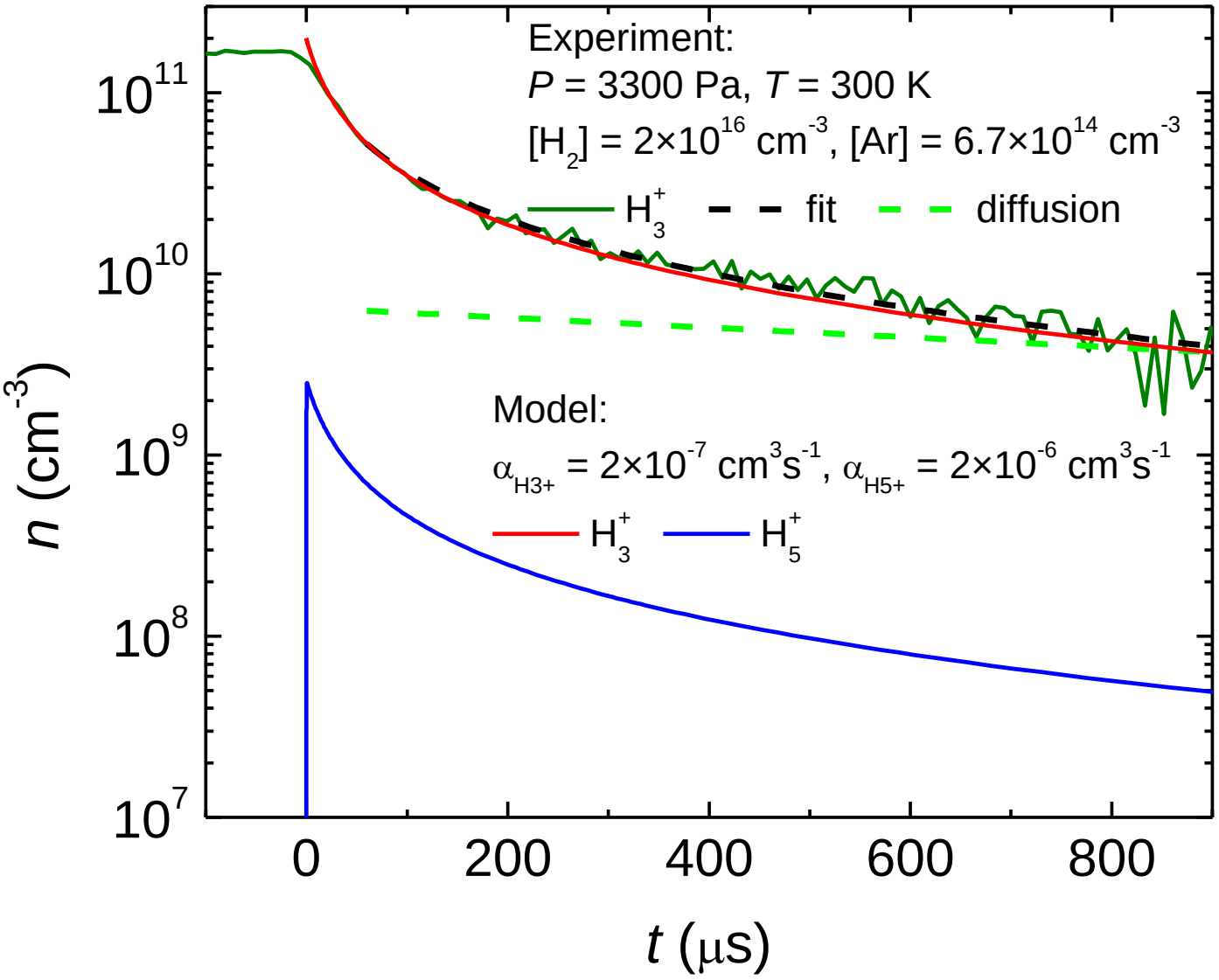

Srovnani modelu a experimentu. Pocatecni podminka: $[H_3^+] = n_e = 2\times10^{11}$ cm^{-3}.

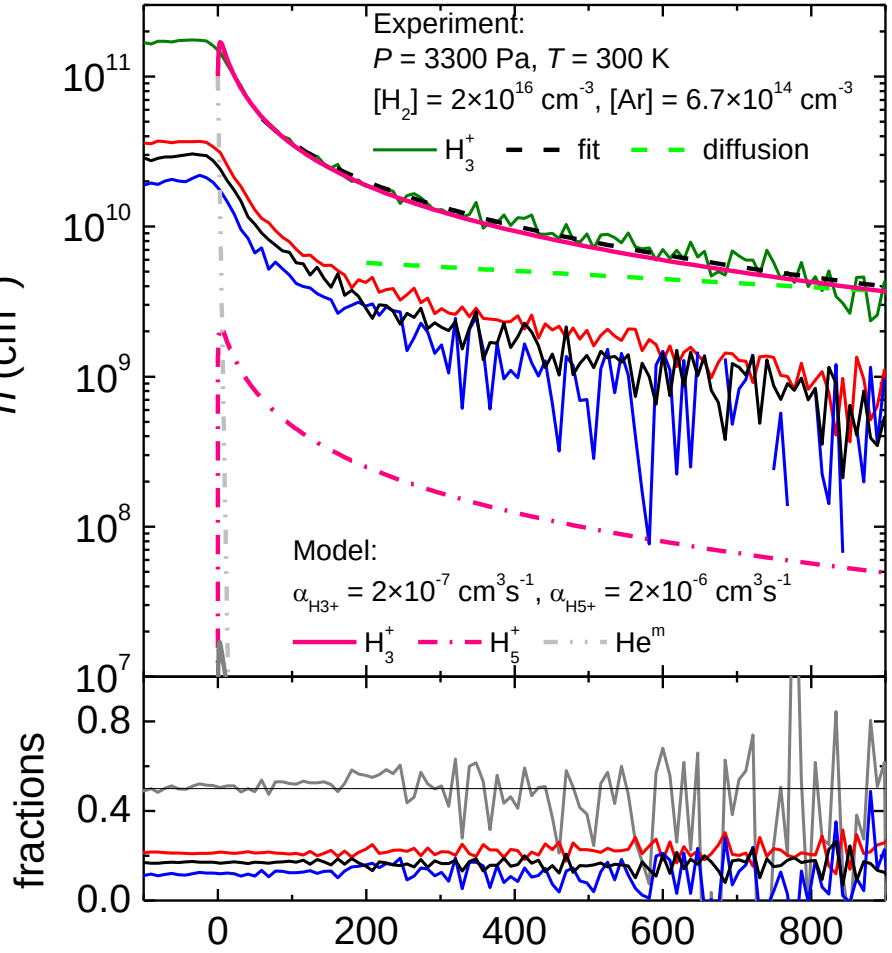

$$\frac{dn_e}{dt} = -[\alpha_1 n_1(t) + \alpha_2 n_2(t)] n_e$$

$$\Rightarrow \alpha_{eff}(t) = [\alpha_1 f_1(t) + \alpha_2 f_2(t)]$$

$$f_1 + f_2 = 1$$

Model + data. Pocatecni podminka: $n_e = He^m = [H_3^+]$.

Poznamka. Namerene τ difuznich ztrat 1.6 ms. Teoreticke τ pri danem tlaku je 1.8 ms (odpovida cca 4×10^{10} cm^{-3} koncentraci necistot (pri 2×10^{-9} cm^3s^{-1} rychlosti reakce H_3^+ s necistotami). Namerena koncentrace vody $[H_2O] = 5\times10^{10}$ cm^{-3} ($[He] = 8\times10^{17}$ cm^{-3}).

If there are 2 or more ion species, the fast recombining species disappears first

$$\frac{dn_e}{dt} = -[\alpha_1 n_1(t) + \alpha_2 n_2(t)] n_e$$

$$\Rightarrow \alpha_{eff}(t) = [\alpha_1 f_1(t) + \alpha_2 f_2(t)]$$

$$f_1 + f_2 = 1$$

Diffusion and recombination

$$\frac{dn_e}{dt} = -\alpha\, n_e^2 - \frac{D_a}{\Lambda^2} n_e$$

$$\frac{1}{n_e} = \alpha\, \frac{\exp(\nu t) - 1}{\nu} + \frac{1}{n_0} \exp(\nu t)$$

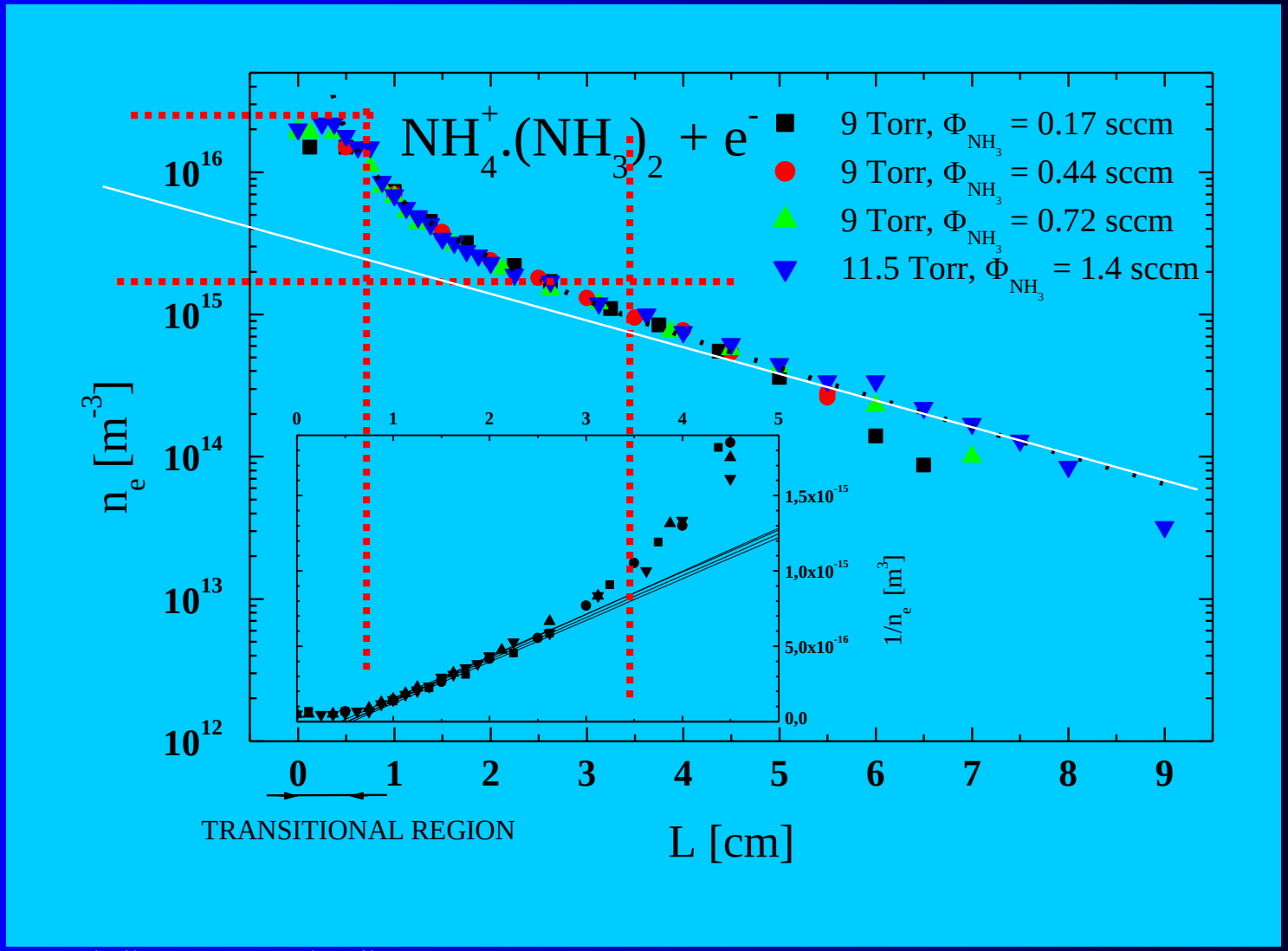

J. Glosík, G. Bánó, R. Plašil, A. Luca, P. Zakouril,
Study of the electron ion recombination in high pressure flowing afterglow. Recombination of $NH_4^+.(NH_3)_2$,
International J. Mass Spectrom., **189**, 103-113 (1999)

Advanced analyze O_2^+

$$dn_e / dt = -\alpha[O_2^+]n_e - \nu_D n_e - \nu_R n_e = -\alpha n_e^2 - \nu_D n_e - \nu_R n_e$$

$$\frac{1}{n_e} - \frac{1}{n_0} = \alpha(t_e - t_0)$$

$$-n_e'/n_e^2 = \alpha + (\nu_D + \nu_R)/n_e$$

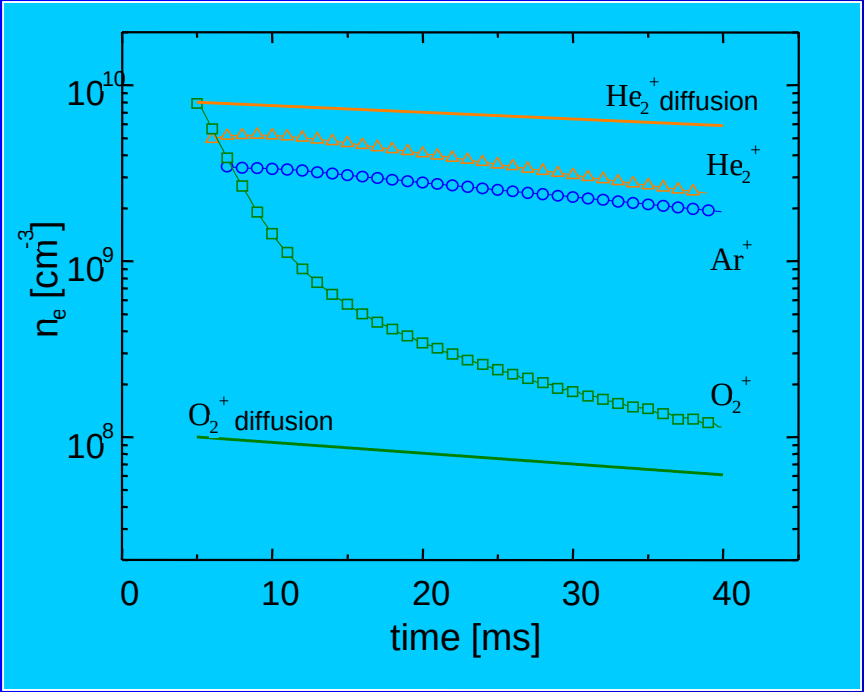

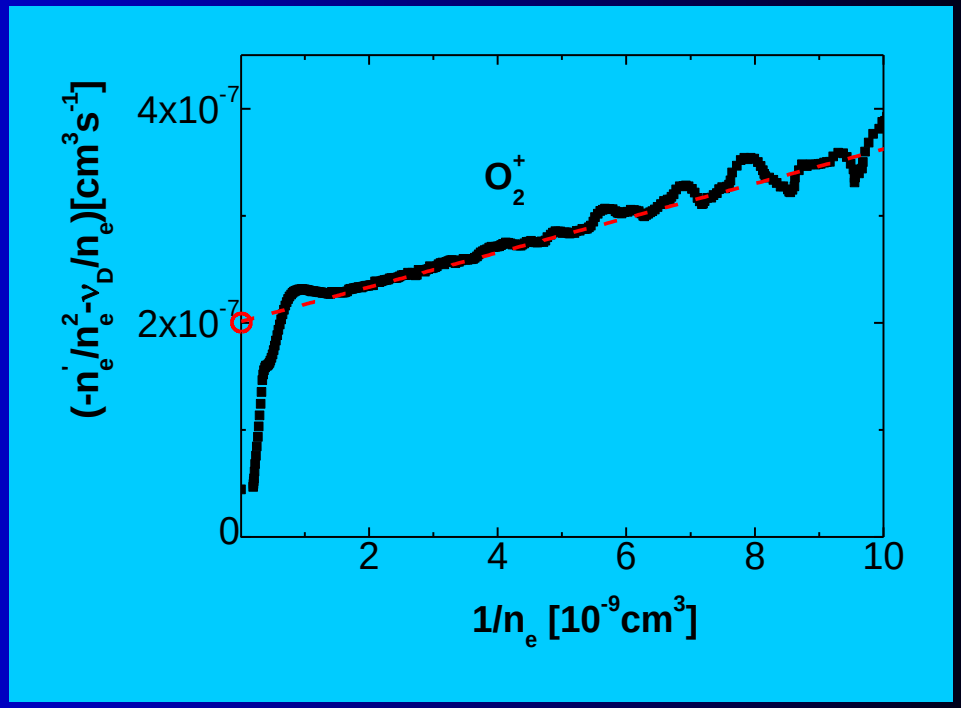

Stationary afterglow (M. Biondy, R. Johnsen)

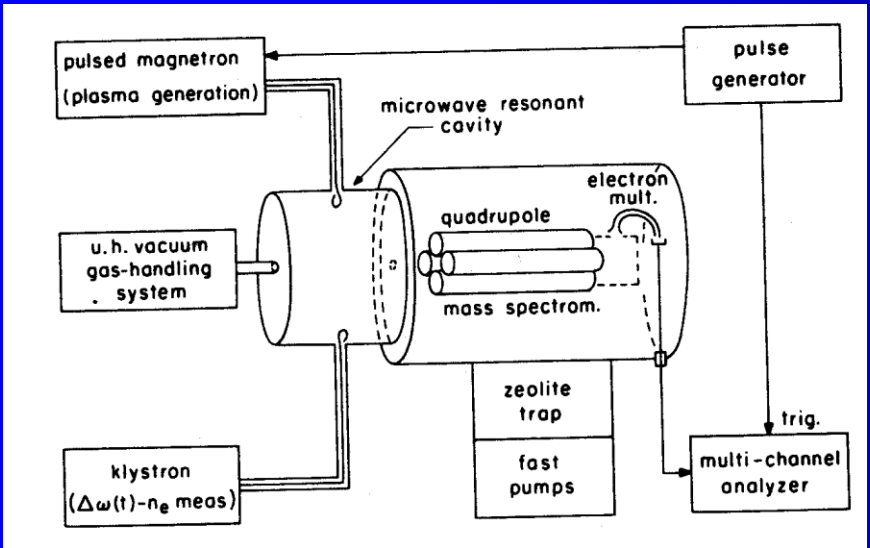

M.T.Leu, M.A. Biondy, R. Johnsen
recombination of H_3^+ and H_5^+

μw SA

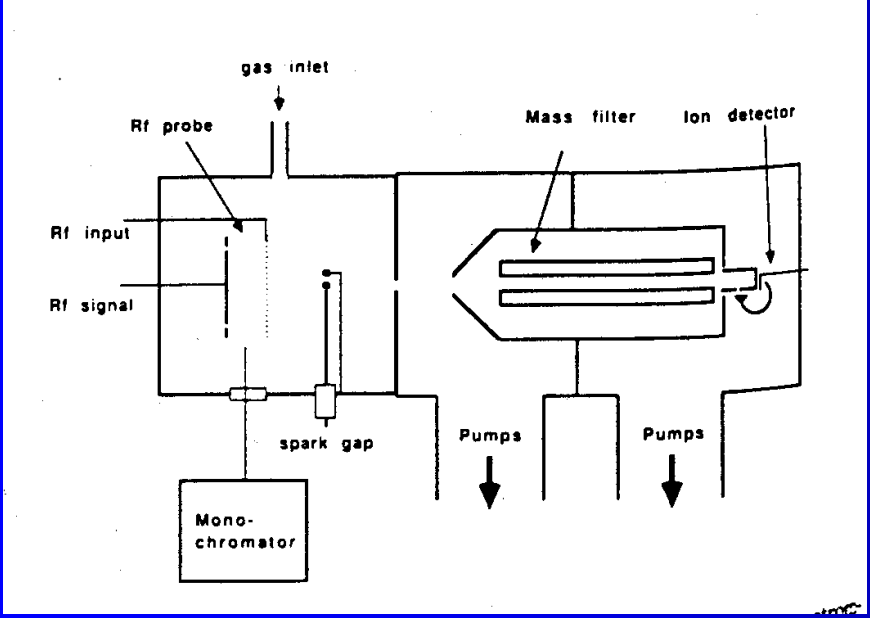

R. Johnsen N4+ recombination
at 300-800 Torr a= $2.6 \times 10^{-6} cm^3 s^{-1}$

High pressure SA

RF probe, spark discharge

Exp. No.1

ADVANCED INTEGRATED STATIONARY AFTERGLOW

AISA

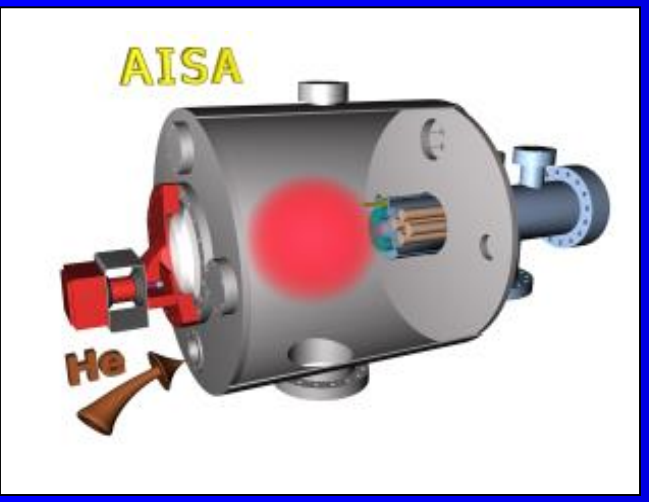

PULSED STATIONARY AFTERGLOW

20-100ms decay

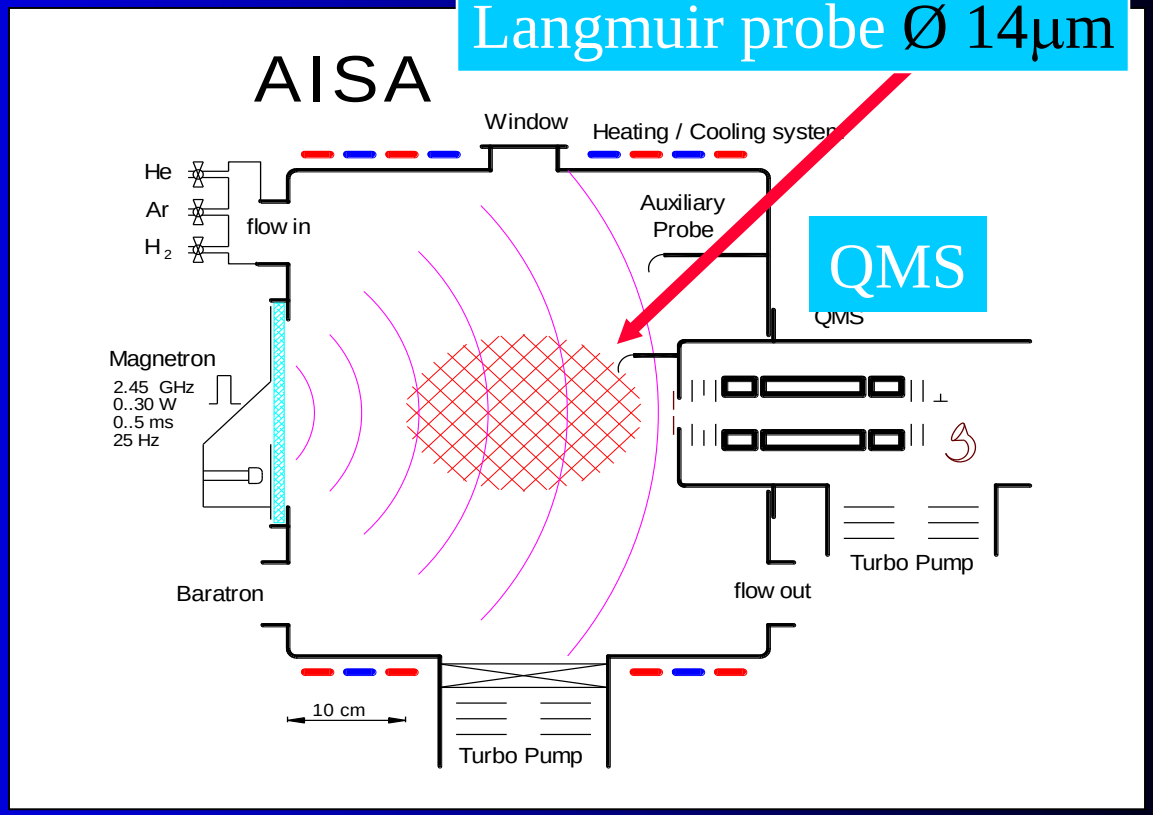

40 cm diameter

UHV - 10^{-9} Torr

External magnetron

2 Torr of He/Ar/H_2

CALCULATION OF PLASMA DECAY IN CYLINDER

DIFFUSION AND RECOMBINATION

τ_D=60 ms, α=1x10^{-7}cm^{3}s^{-1} and α=5x10^{-9}cm^{3}s^{-1}

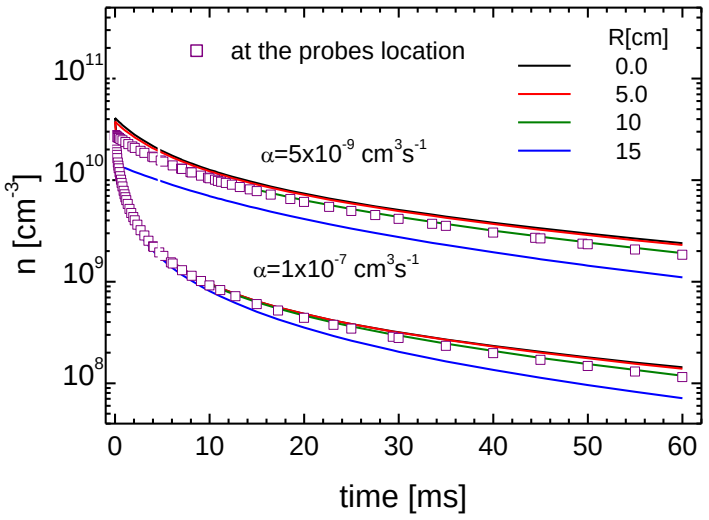

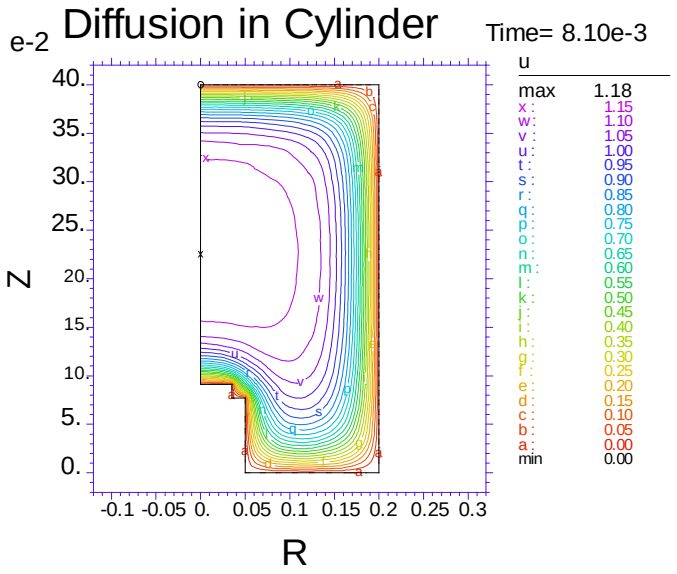

RECOMBINATION AND DIFFUSION

in $He/O_2^+/e^-$ plasma (2 Torr, τ_D~60ms)

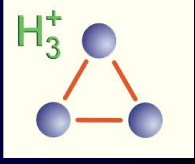

$\alpha(O_2^+, 300K) = 2x10^{-7} cm^3 s^{-1}$

O_2^+

$$O_2^+ + e^- \Rightarrow neutral \quad products$$

$$\frac{d[O_2^+]}{dt} = -\alpha[O_2^+]n_e - \frac{n_e}{\tau_D}$$

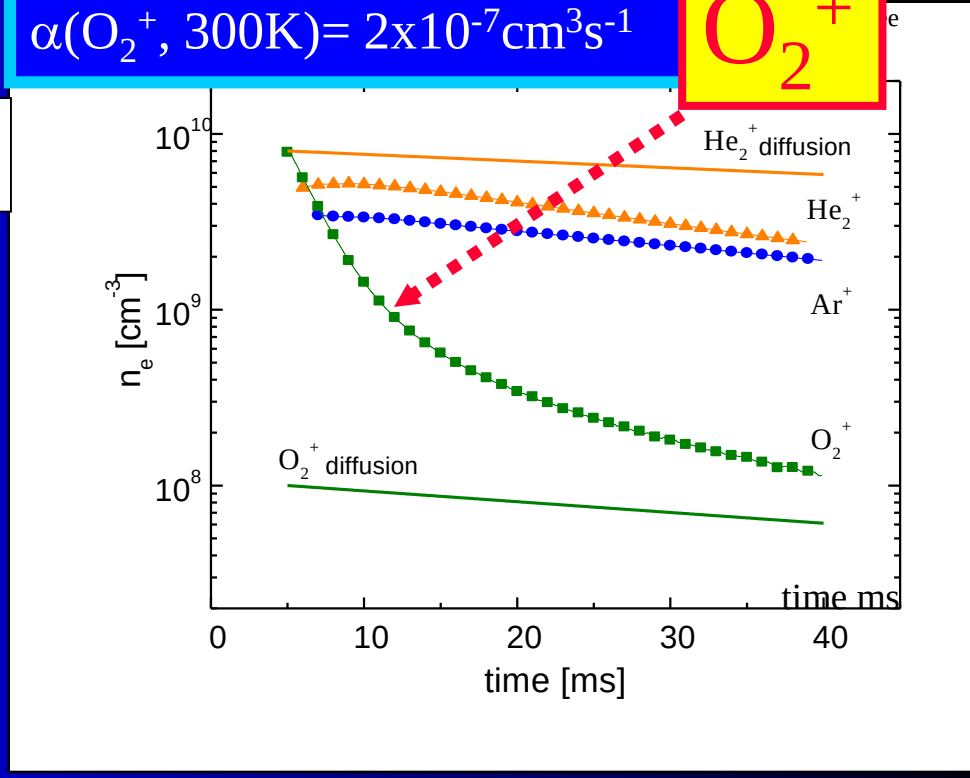

Only recombination:

$$1/n_e = 1/n_{e0} + \alpha t$$

Only diffusion

$$n_e = n_{e0} \exp(-t/\tau_D)$$

With recombination and diffusion

$$n_e = \frac{1}{\alpha\tau_D \exp(t/\tau_D) + \frac{1}{n_0}\exp(t/\tau_D)}$$

Formation of H_3^+ in He/Ar/H_2 mixture

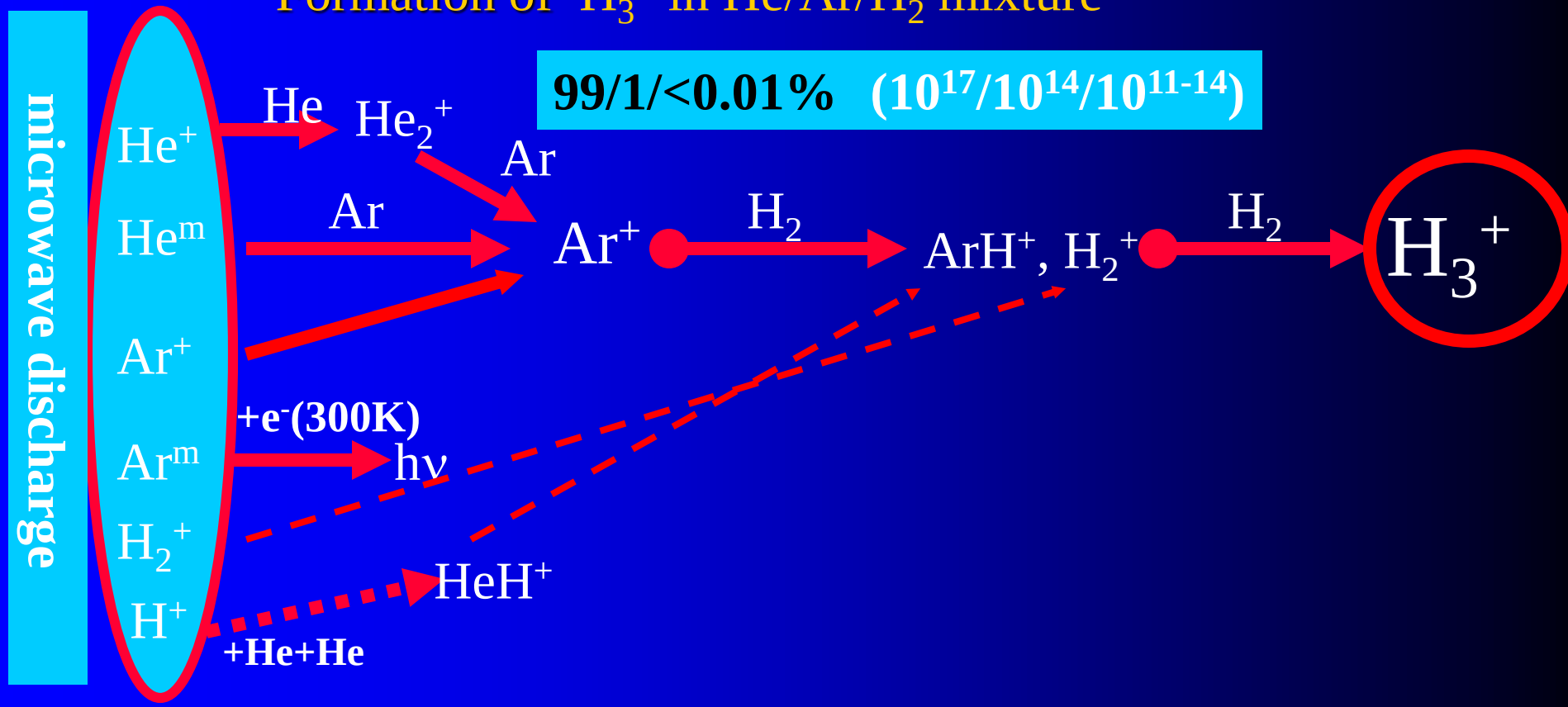

FORMATION:

Ion molecule reactions during the early afterglow

Formation of H_3^+ in He/Ar/H_2 mixture

microwave discharge

He^+ He^m Ar^+ Ar^m H_2^+

$10^{17}/10^{14}/10^{11}$

Ar → Ar^+ —H_2→ ArH^+, H_2^+ —H_2→ H_3^+

Changes due to the ion molecule reactions during the early afterglow

He/Ar

He/Ar/H_2

He/Ar/D_2

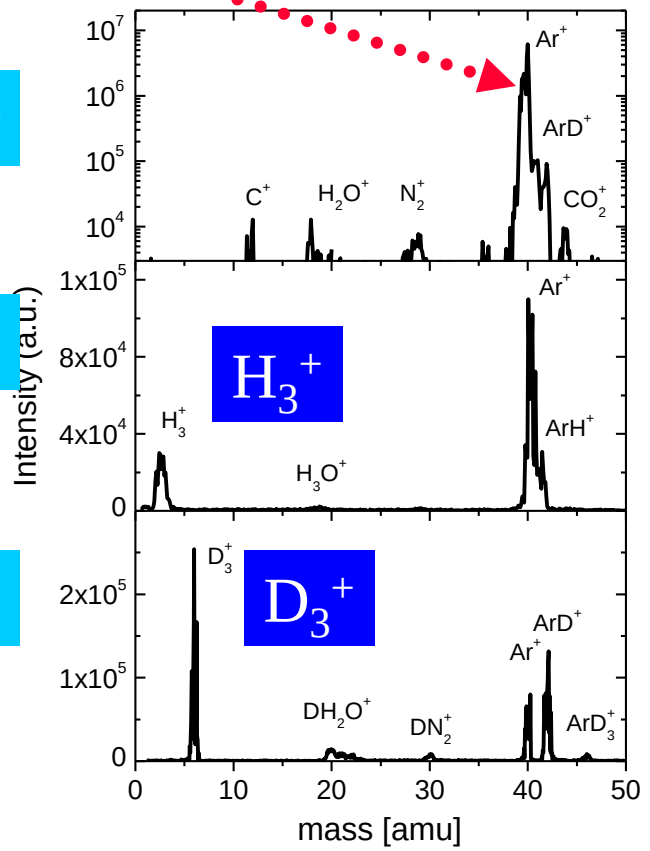

VT - AISA

2 Torr of He/Ar/H_2

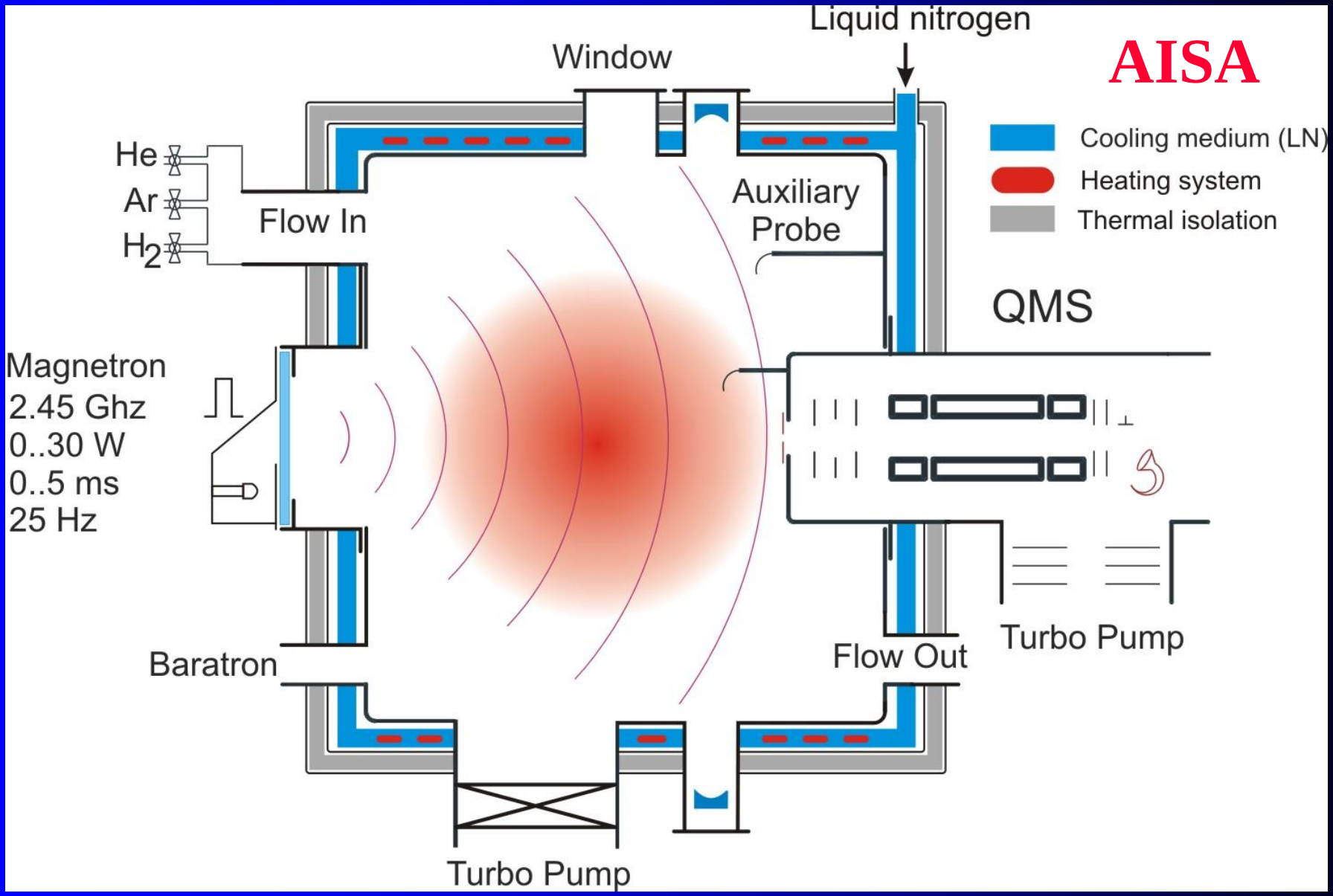

Formation of H_3^+ in He/Ar/H_2 mixture

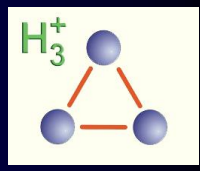

Calculated from kinetic model

He^+
He^m, Ar^m
Ar^+

Ar, H_2 → Ar^+ → (H_2) ArH^+, H_2^+ → (H_2) H_3^+

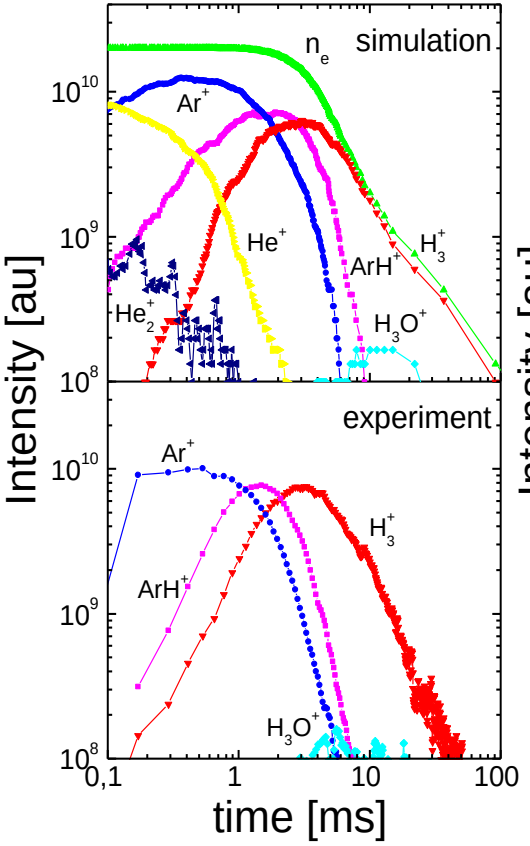

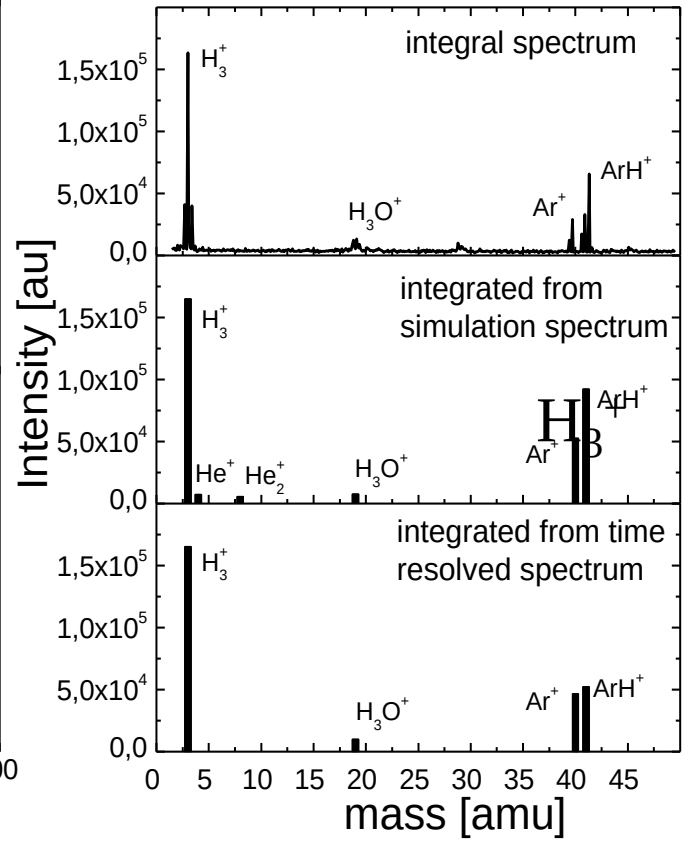

Formation of H_3^+ in He/Ar/H_2 mixture

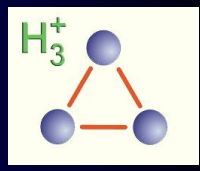

He^+
He^m, Ar^m
Ar^+

Ar, H_2 → Ar^+ → H_2 → ArH^+, H_2^+ → H_2 → H_3^+

Calculated from kinetic model

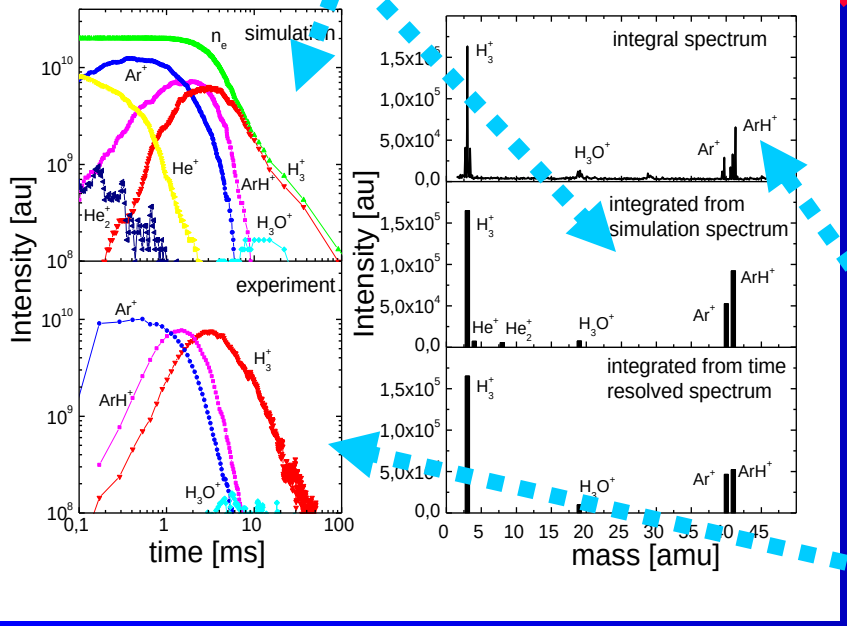

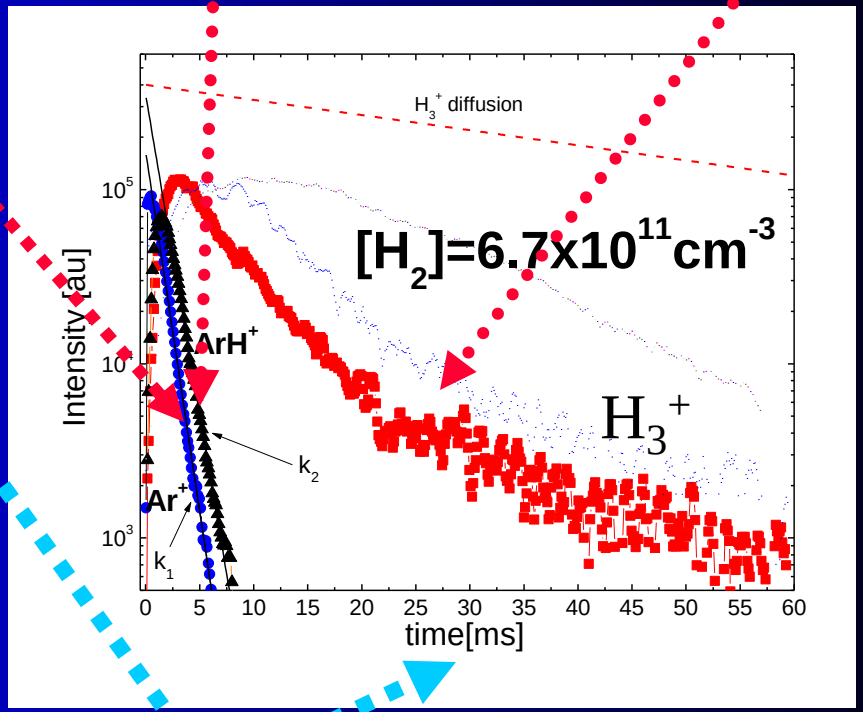

Measured time evolution

Time resolved mass spectra

Rates of the decays are dependent on $[H_2]$

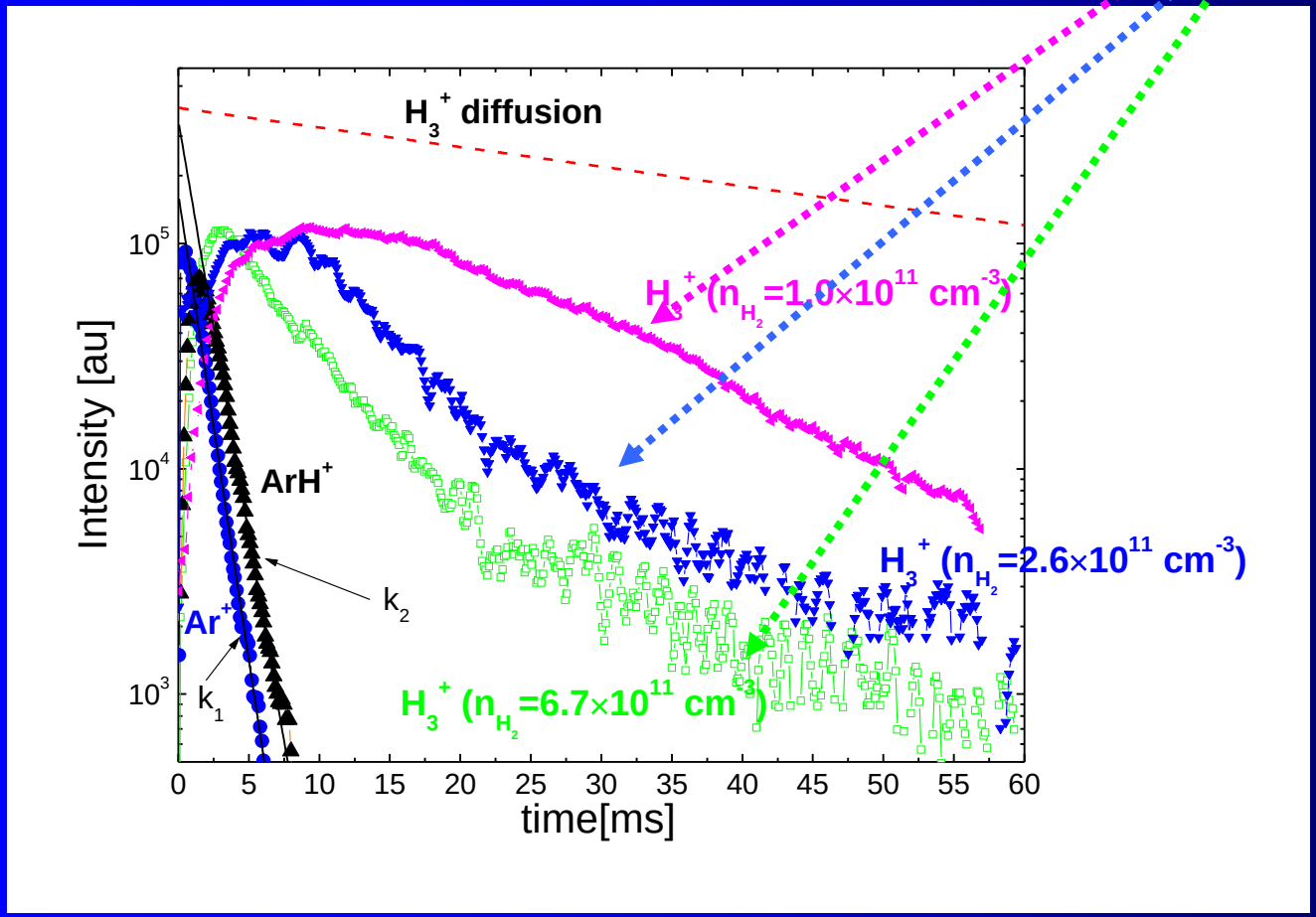

Time resolved mass spectra

$$\frac{dn_e}{dt} = -[\alpha_1 n_1(t) + \alpha_2 n_2(t)]n_e$$

$$\Rightarrow \alpha_{eff}(t) = [\alpha_1 f_1(t) + \alpha_2 f_2(t)]$$

$$f_1 + f_2 = 1$$

OBSERVED DEPENDENCE ON $[H_2]$!!

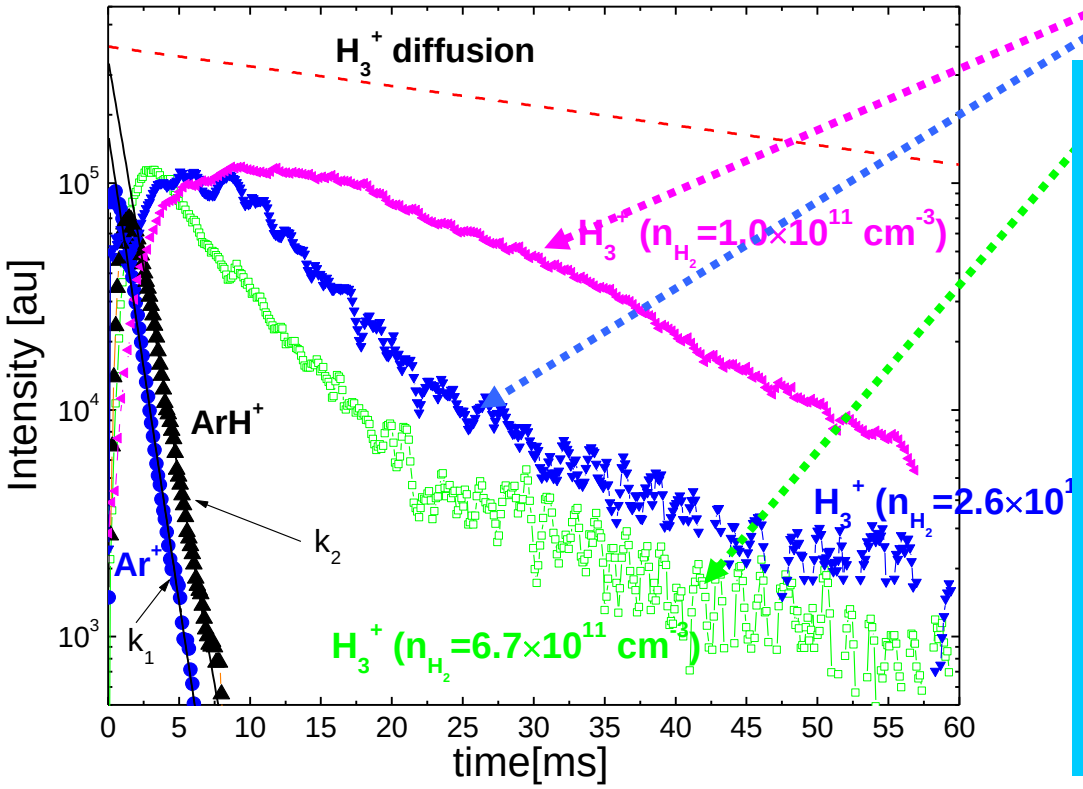

H_3^+ *fraction*

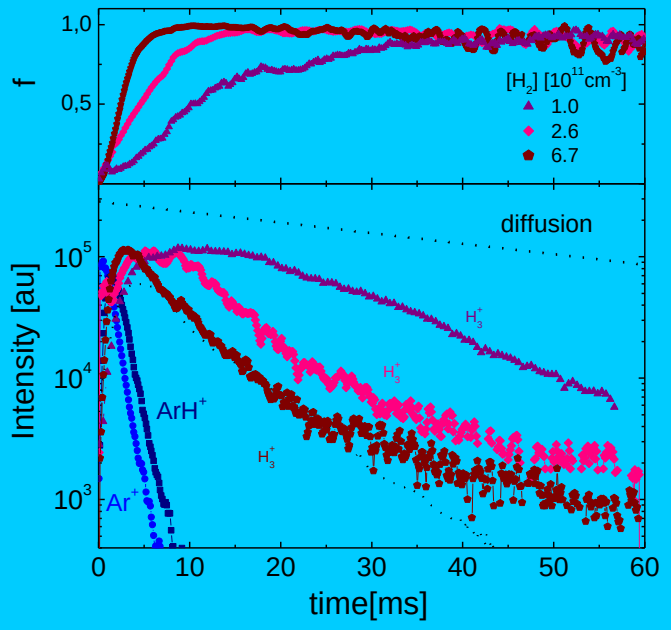

It is only qualitative information, not sufficient to obtain α

Correction to ion composition 1

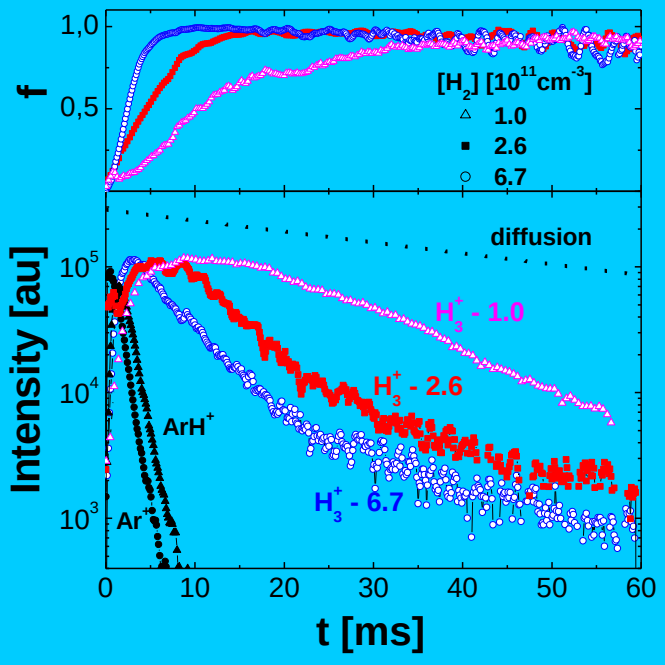

$$f = H_3^+ / \Sigma_{ions}$$

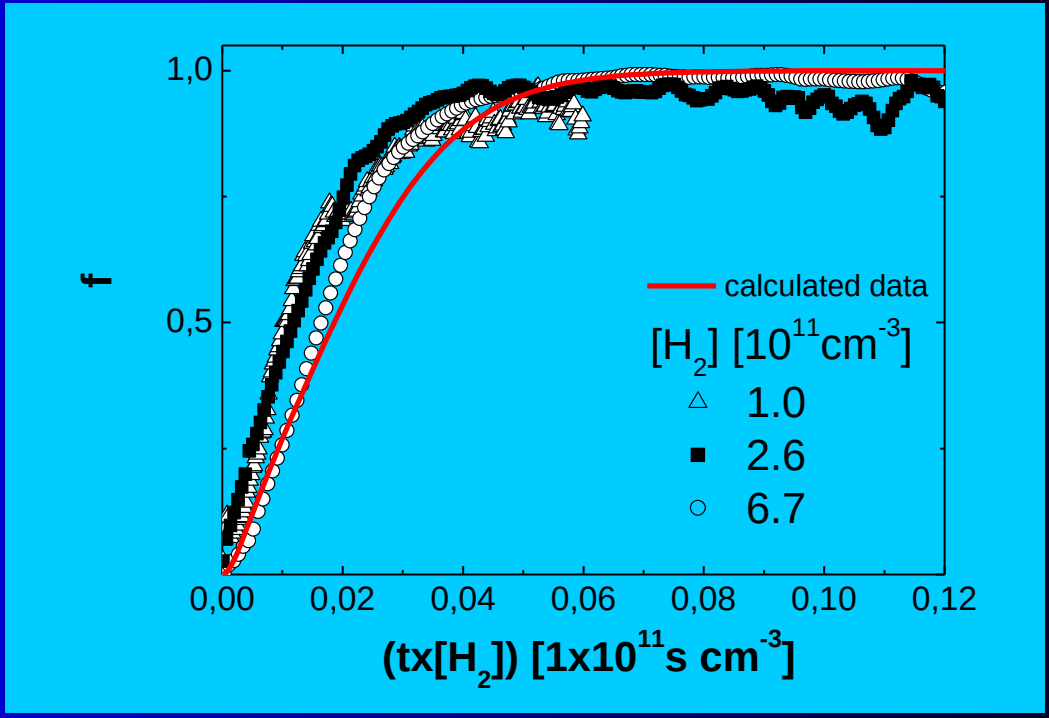

Plasma Sources Sci. Technol. **18** (2009) 025031 (7pp) doi:10.1088/0963-0252/18/2/02503

Electron and gas temperature dependences of the dissociative recombination coefficient of molecular ions Ne_2^+ with electrons

O Mikuš[1], P Lukáč[1], I Morva[2], Z Zábudlá[1], J Trnovec[1] and M Morvová[2]

$$\alpha(T_e, T_g) \sim \alpha_0 T_e^{-\xi} T_g^{-\gamma},$$

$$Ne_2^+ + e \Leftrightarrow (Ne_2)^* \rightarrow Ne^* + Ne + \text{kin. energy}$$

$$\alpha_{Ne_2^+}(T_e, T_g) = (1.8 \pm 0.2) \times 10^{-7} (T_e/300\,\text{K})^{-0.42} (T_g/300\,\text{K})^{-0.7}\ \text{cm}^3\ \text{s}^{-1}$$

$$300\ \text{K} \leqslant T_e \leqslant 6300\ \text{K and } 300\ \text{K} \leqslant T_g \leqslant 500\ \text{K}.$$

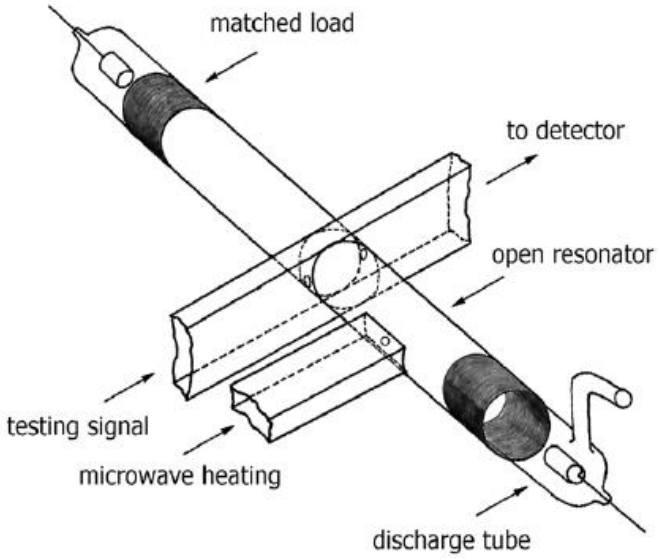

Figure 1. Cutaway view schematic of the open cylindrical TM_{011} cavity—wave guide section.

Plasma Sources Sci. Technol. **18** (2009) 025031

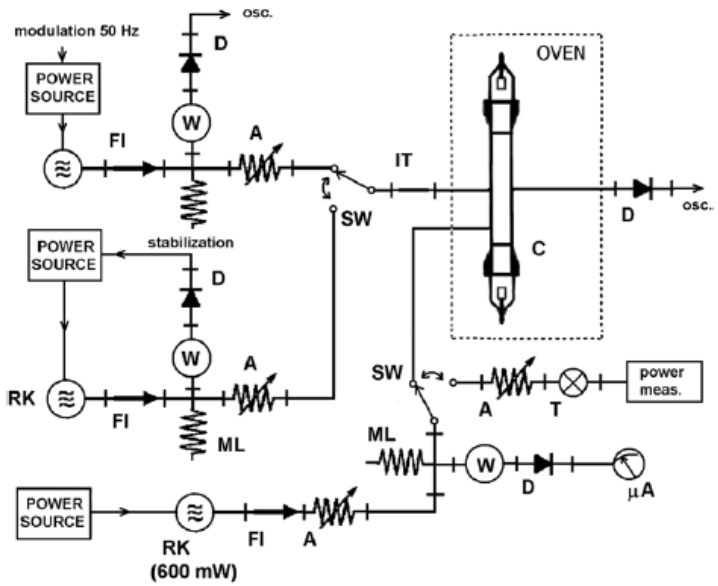

Figure 2. Diagram of the dual mode X-band microwave afterglow apparatus, FI—ferrite isolator, D—diode, A—attenuator, RK—reflex klystron, ML—matched load, W—wavemeter, T—thermistor, C—cavity, IT—impedance transformer, SW—microwave switch.

Next lecture: SA and absorption experiments

Table 1. Data of the dissociative recombination of Ne_2^+ ions.

α	T_g	T_e	ξ_g	ξ_e	Method of measurements	Method of heating	References
1.7×10^{-7}	300	300–11 000		0.43	Microwave cavity	Travelling microwave	Frommhold *et al* [5]
1.4×10^{-7}	450–900	$= T_g$		0.5	Double probe	Shock wave	Cunningham and Hobson [6]
1.4×10^{-7}	900–3500	$= T_g$		1.5	Double probe	Shock wave	
1.4×10^{-7}	300	1500–3000	—	1.5	Shock tube	Microwave	Chang *et al* [18]
?	300	?	—	0.9	Light quenching	Microwave cavity	Farhat [29]
?	300	?	—	0.5–0.66	Light quenching	Microwave cavity	Taylor and Herskovitz [30]
2×10^{-7}	300	300–600	—	0.25	Microwave cavity	Microwave cavity	Hess [31]
2×10^{-7}	300	900–2400	—	0.4	Microwave cavity	Microwave cavity	
?	300	?	—	1.4	Light intensity	Microwave	Nygaard [32]
1.8×10^{-7}	300–500	$= T_g$		0.42	Microwave cavity	Oven heating	Kasner [33]
1.8×10^{-7}	300	300–4600	—	0.49	Microwave cavity	Travelling microwave	Philbrick *et al* [34]
?	300	10 000–25 000	—	0.36	Relaxation disch. current	Glow discharge	Vinogradov *et al* [35]
1.8×10^{-7}	300	300–1500	—	0.36	Microwave cavity	Microwave cavity	Lukáč *et al* [36]
?	300	?	—	0.4; 1.4	Light intensity	Microwave	Tálsky [37]
1.8×10^{-7}	300	300–6000	—	0.42	Microwave cavity	Travelling microwave	Our results [19]
1.5×10^{-7}	300–10 000	300–10 000	?	0.5–1.5	Theoretical	Theoretical	Ngassam *et al* [10]
1.8×10^{-7}	300–550	300–6000	0.7	0.42	Micowave cavity	Electrical oven and Travelling microwave	Present results

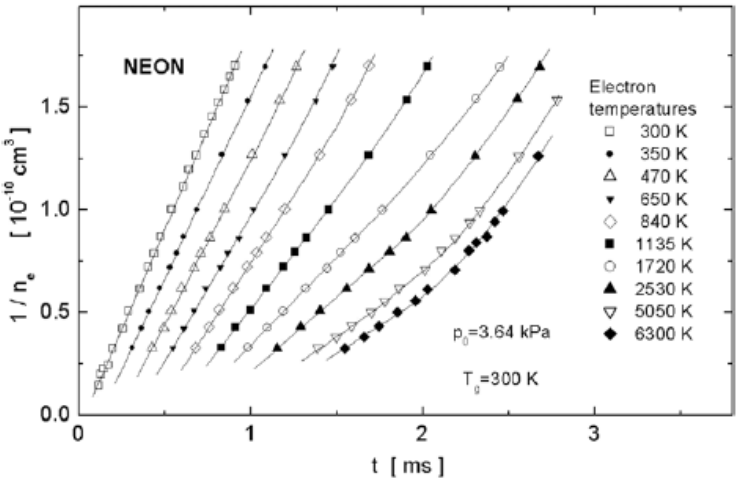

Figure 3. The reciprocal of the 'average microwave electron density' $\langle 1/n_e \rangle$ as a function of the afterglow time (t) for different electron temperatures when $T_{gas} = 300$ K. The time zero point has been displaced 0.1 ms for various curves for clarity.

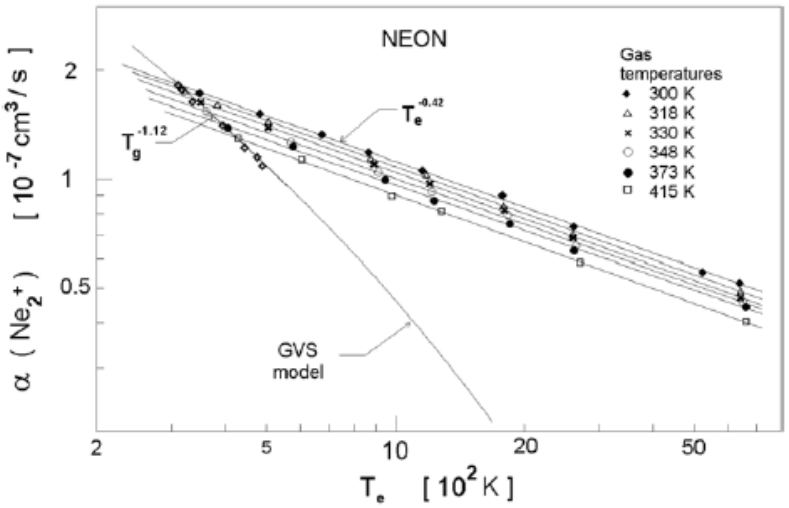

Figure 5. Dissociative recombination coefficient α (Ne_2^+) as a function of the electron temperature (T_e) at various gas temperatures. The GVS model assumes that $T_g = T_e = T$. (The figure is plotted in a log–log scale.)

Eliminating the electron temperature dependence of the recombination coefficients, we can describe the gas and electron temperature dependence in the form

$$\alpha(T_e, T_g) = \alpha(T_g)(T_e/300K)^{-0.42}\,\mathrm{cm^3\,s^{-1}}$$

or

$$\alpha(T_e, T_g) = (1.8 \pm 0.2) \times 10^{-7} \times (T_e/300\,\mathrm{K})^{-0.42} \times (T_g/300\,\mathrm{K})^{-0.7}\,\mathrm{cm^3\,s^{-1}}$$

for the ranges of $300\,\mathrm{K} \leqslant T_e \leqslant 6500\,\mathrm{K}$ and $300\,\mathrm{K} \leqslant T_g \leqslant 550\,\mathrm{K}$.

Temperature dependence

Abstract. A cylindrical TM_{010} microwave cavity has been used not only to determine the average electron density decay rates in a plasma afterglow, but also to heat the electrons. In this way it was possible to measure the electron temperature dependence of the recombination coefficient of Ne_2^+ ions with electrons. At $T_e = 300$ K, a value of $\alpha(Ne_2^+) = (1{\cdot}8 \pm 0{\cdot}1) \times 10^{-7}$ cm^3 s^{-1} was obtained. Over the range $300 \leqslant T_e \leqslant 1500$ K, $\alpha(Ne_2^+)$ decreased as $T_e^{-0{\cdot}36}$.

$$\alpha = \alpha_0 T_e^{-\xi}$$

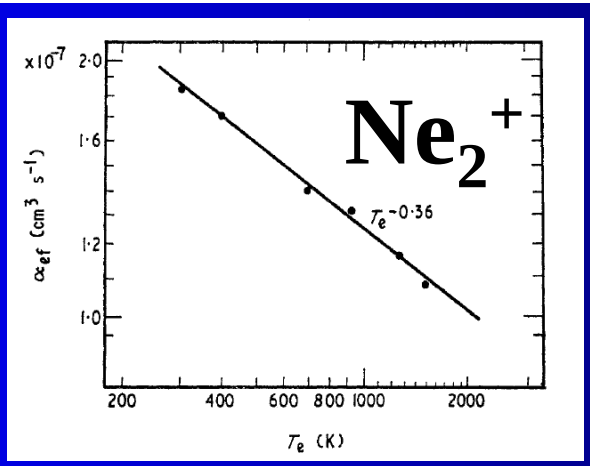

$$\alpha_{ef}(T_e) = \alpha_0(300\ \mathrm{K})\, T_e^{-0{\cdot}36}.$$

Multiple collision

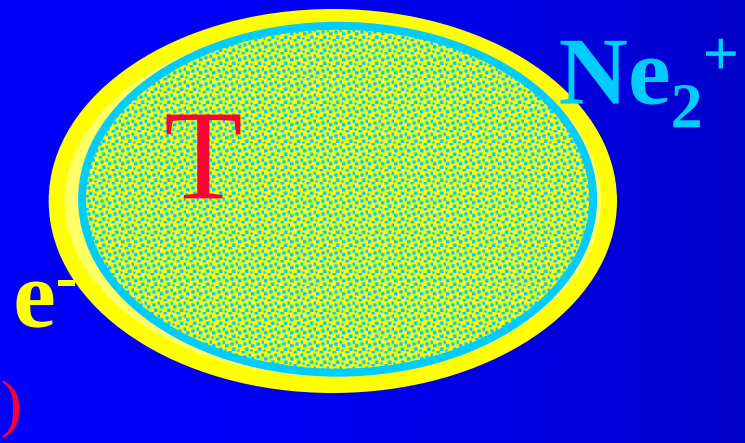

recombination rate coefficient

$$\alpha(Ne_3^+) = (1.1 \pm 0.1) \times 10^{-6} (T_e(\mathrm{K})/300)^{-0.36 \pm 0.04}\ \mathrm{cm}^3\ \mathrm{s}^{-1}$$

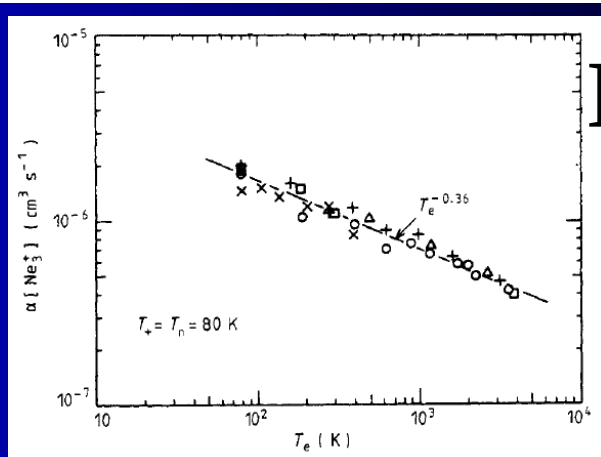

Figure 5. Measured values of the recombination coefficients $\alpha(Ne_3^+)$ plotted against electron temperature. The different symbols refer to runs taken on different days. The full curve is a least-squares fit of the form $\alpha \sim T_e^{-x}$ to the data.

In-situ satellite data

The points indicated by blue triangles are the $\alpha(NO^+)$ deduced from in-situ satellite data by

M. R. Torr, J. P. St-Maurice and D. G. Torr, J. Geophys. Res., **82** (1977) 3287.

The agreement between these data and the laboratory data is remarkable.

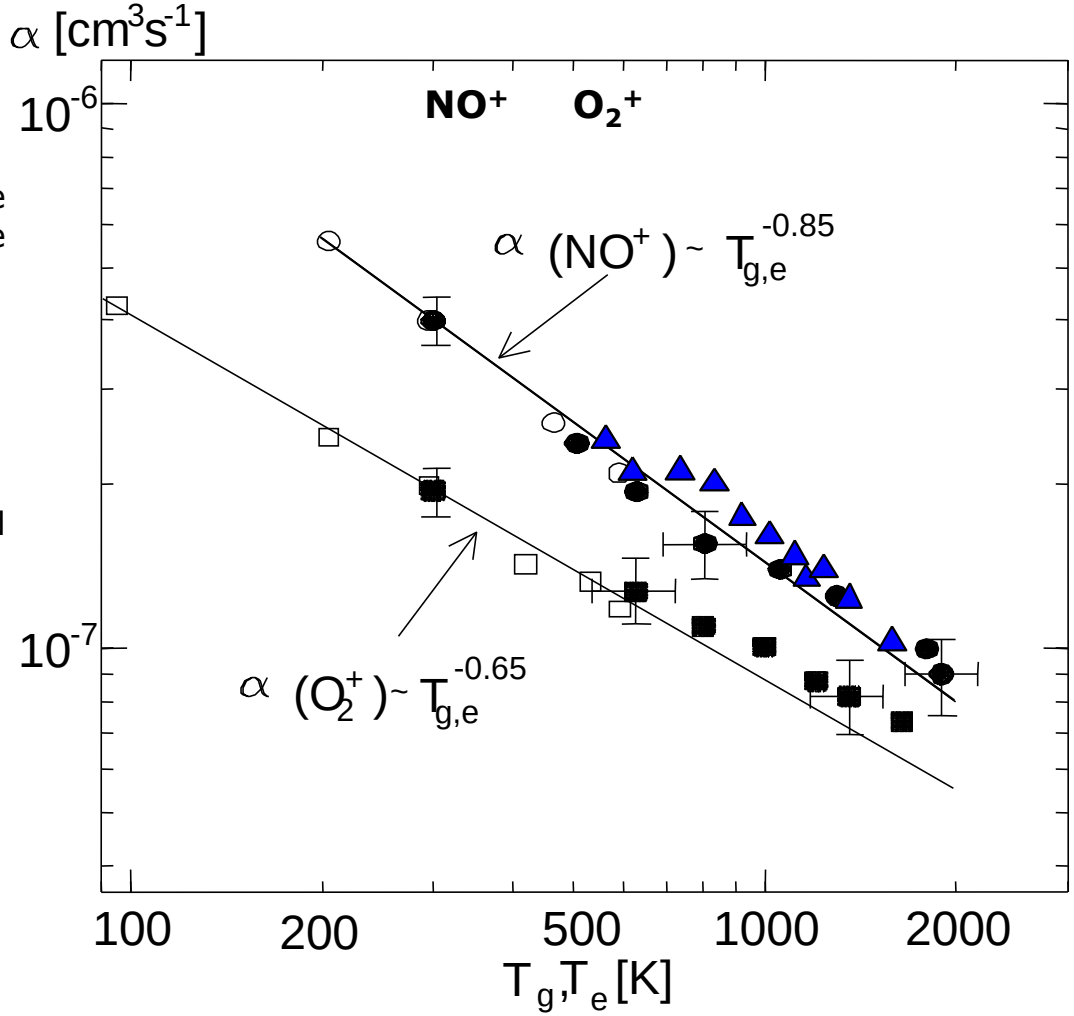

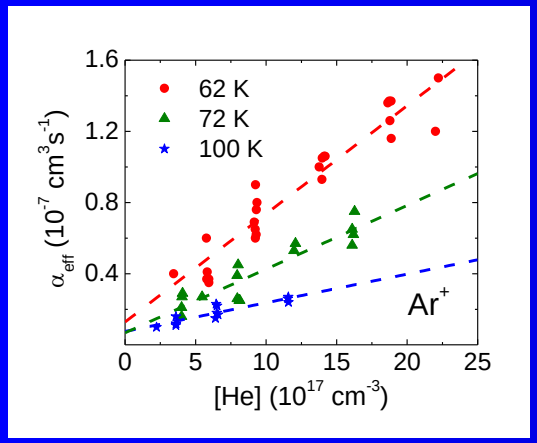
62 K
72 K
100 K
Ar+
αeff (10-7 cm3s-1)
[He] (1017 cm-3)

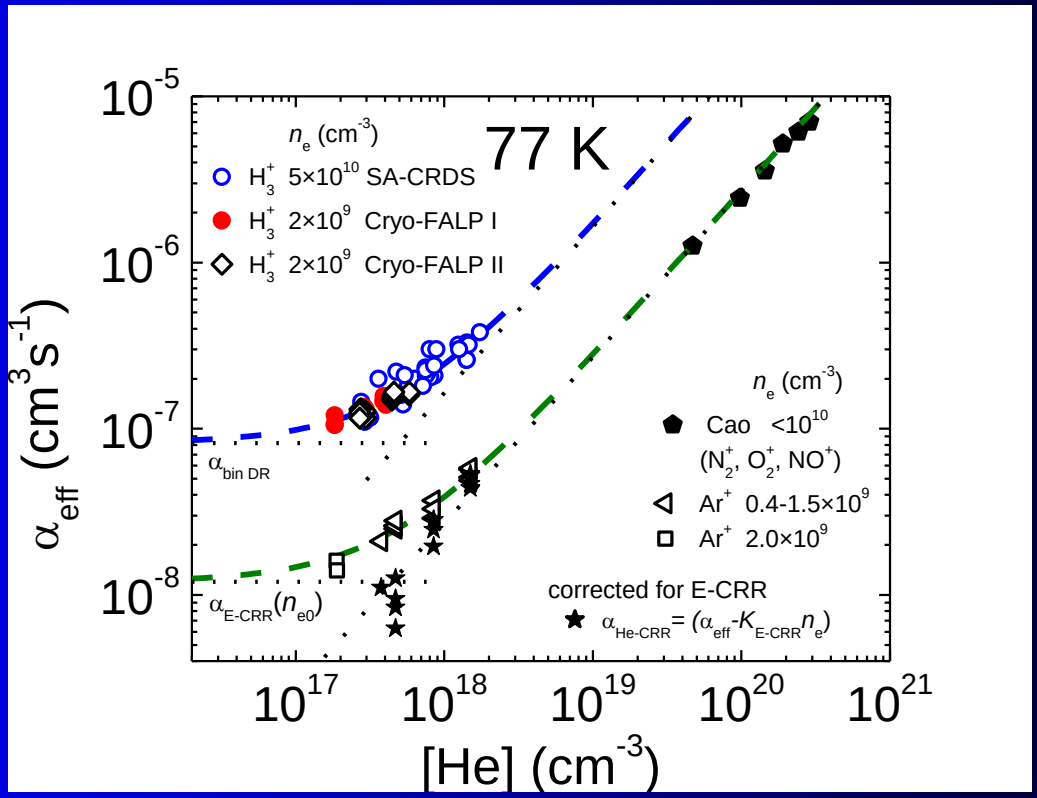
77 K
ne (cm-3)
H3+ 5×1010 SA-CRDS
H3+ 2×109 Cryo-FALP I
H3+ 2×109 Cryo-FALP II
αbin DR
αE-CRR(ne0)
ne (cm-3)
Cao <1010
(N2+, O2+, NO+)
Ar+ 0.4-1.5×109
Ar+ 2.0×109
corrected for E-CRR
αHe-CRR= (αeff-KE-CRRne)
αeff (cm3s-1)
[He] (cm-3)

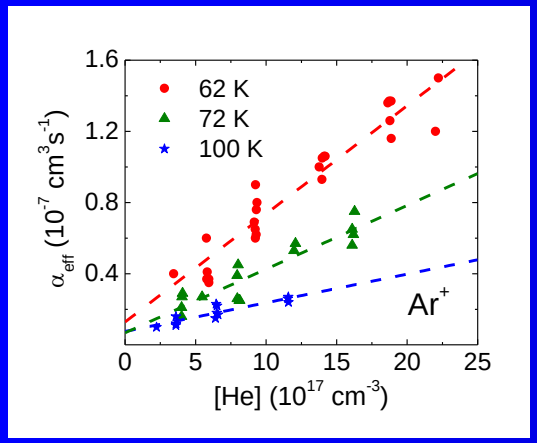
62 K
72 K
100 K
Ar+
αeff (10-7 cm3s-1)
[He] (1017 cm-3)

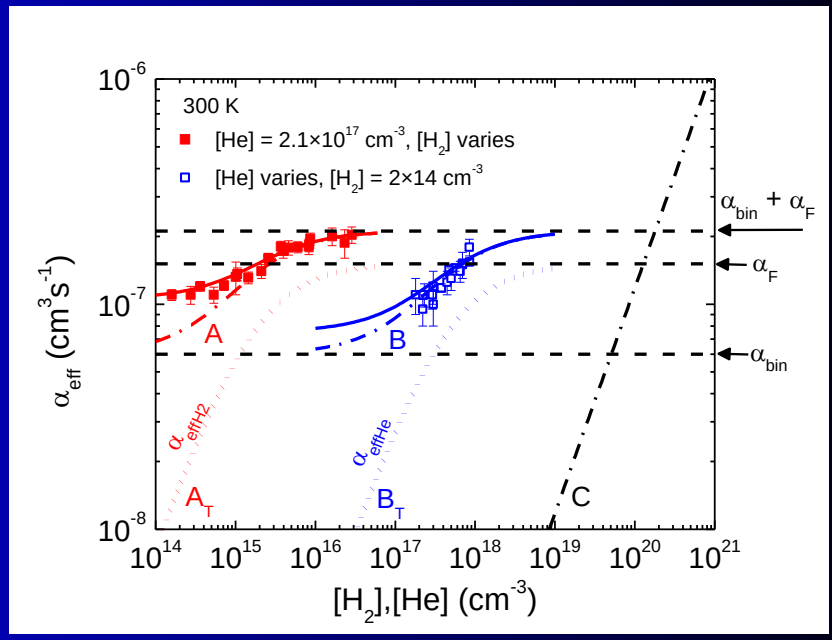
300 K
[He] = 2.1×10^17 cm^-3, [H2] varies
[He] varies, [H2] = 2×14 cm^-3
αbin + αF
αF
αbin
A
B
C
αeffH2
αeffHe
AT
BT
αeff (cm3s-1)
[H2],[He] (cm-3)

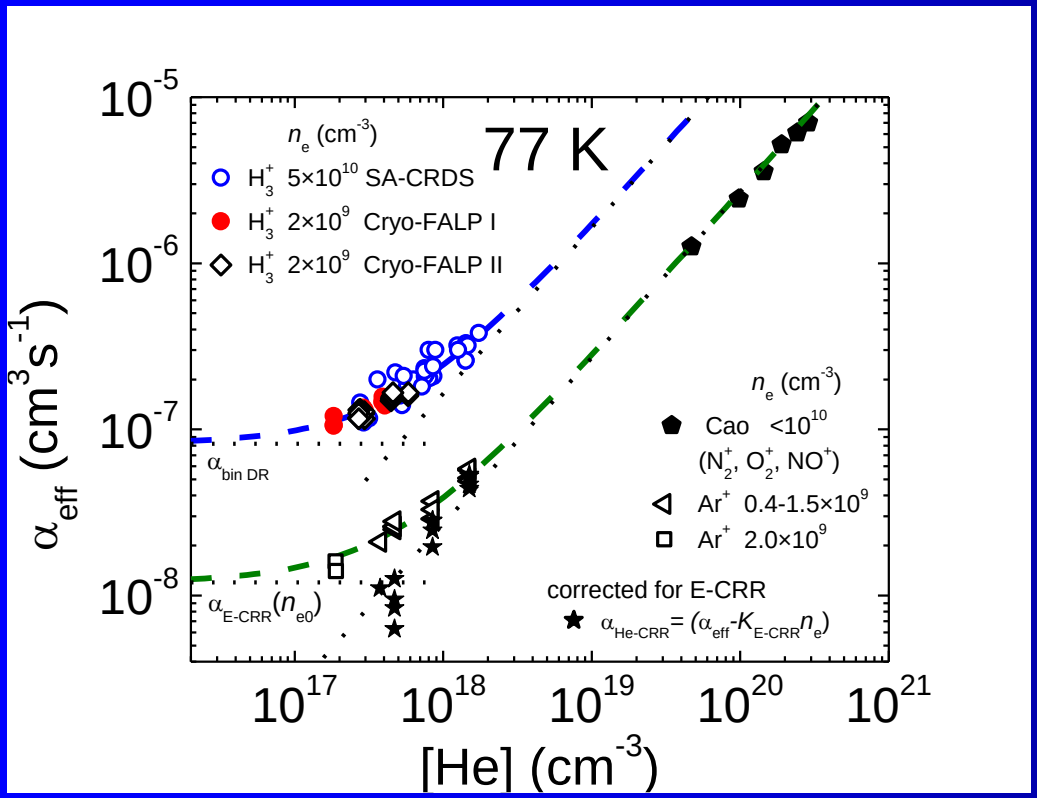
77 K
ne (cm-3)
H3+ 5×10^10 SA-CRDS
H3+ 2×10^9 Cryo-FALP I
H3+ 2×10^9 Cryo-FALP II
αbin DR
αE-CRR(ne0)
ne (cm-3)
Cao <10^10
(N2+, O2+, NO+)
Ar+ 0.4-1.5×10^9
Ar+ 2.0×10^9
corrected for E-CRR
αHe-CRR = (αeff - KE-CRR ne)
αeff (cm3s-1)
[He] (cm-3)

If there are 2 or more ion species, the fast recombining species disappears first

$$\frac{dn_e}{dt} = -[\alpha_1 n_1(t) + \alpha_2 n_2(t)] n_e$$

$$\Rightarrow \alpha_{eff}(t) = [\alpha_1 f_1(t) + \alpha_2 f_2(t)]$$

$$f_1 + f_2 = 1$$

Line intensity H_3^+

High sensitivity required

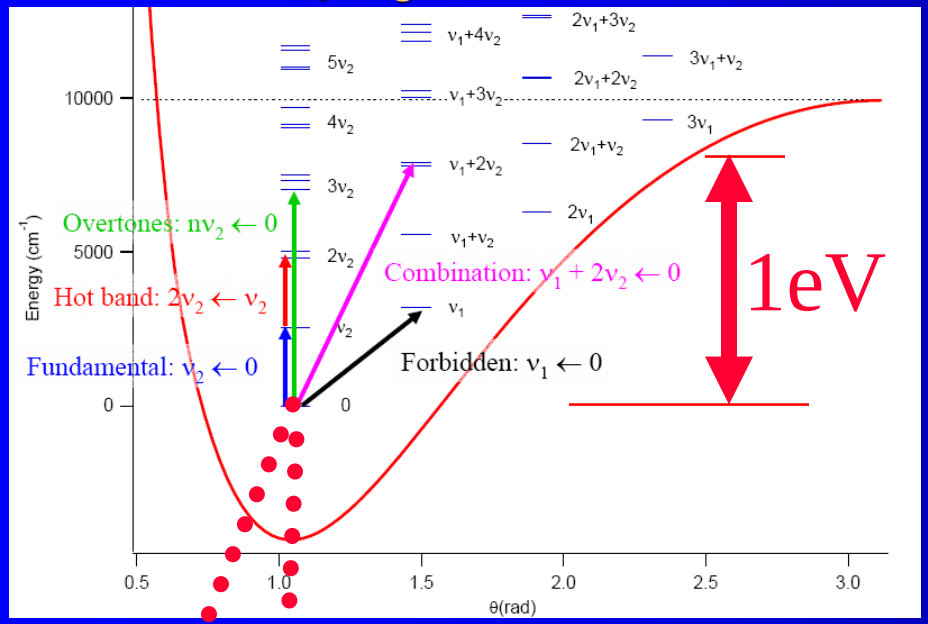

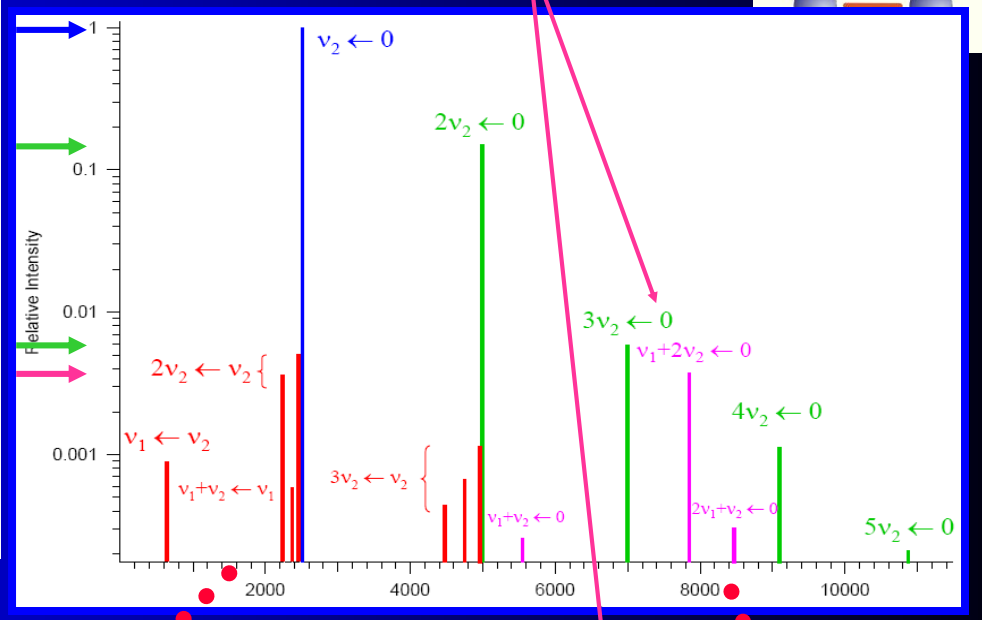

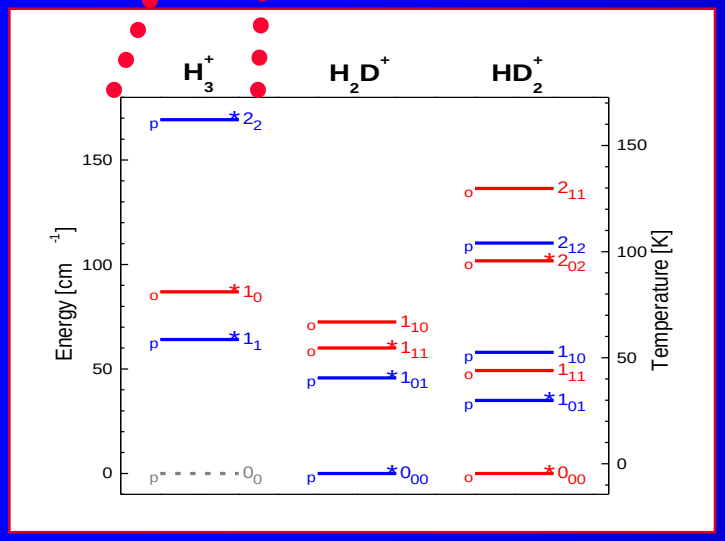

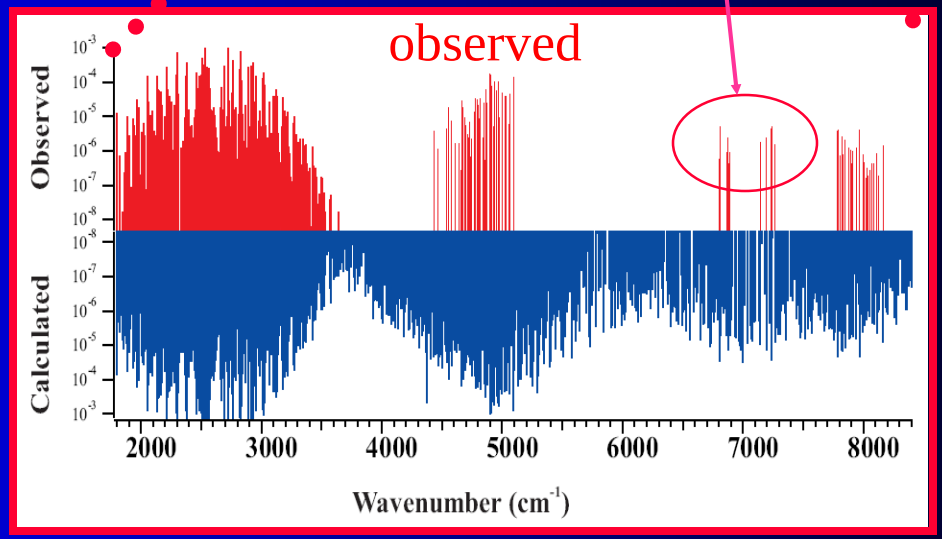

Stationary afterglow + Spectroscopic identification of recombining ions

$$\frac{d[H_3^+]}{dt} = -\alpha[H_3^+]n_e = -\alpha[H_3^+]^2$$

IR-CRDS

Laser absorption spectroscopy

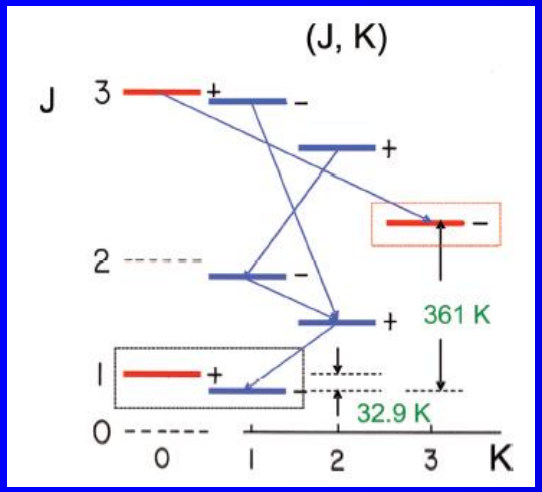

CRDS

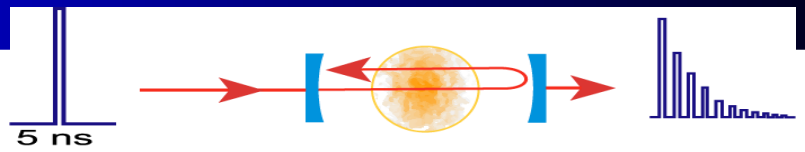

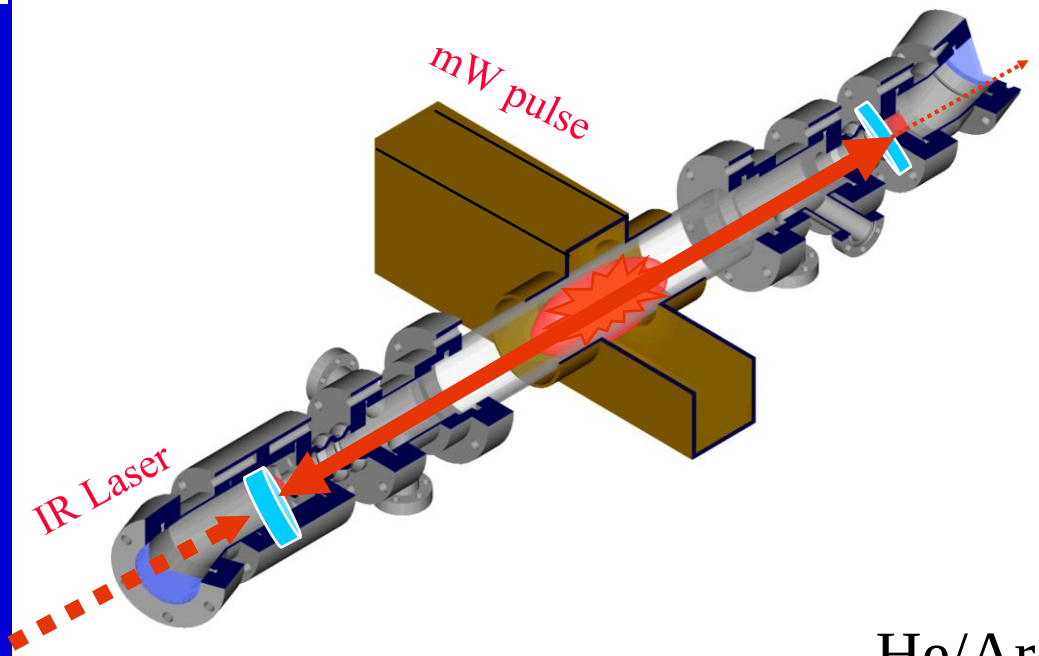

$He/Ar/H_2$

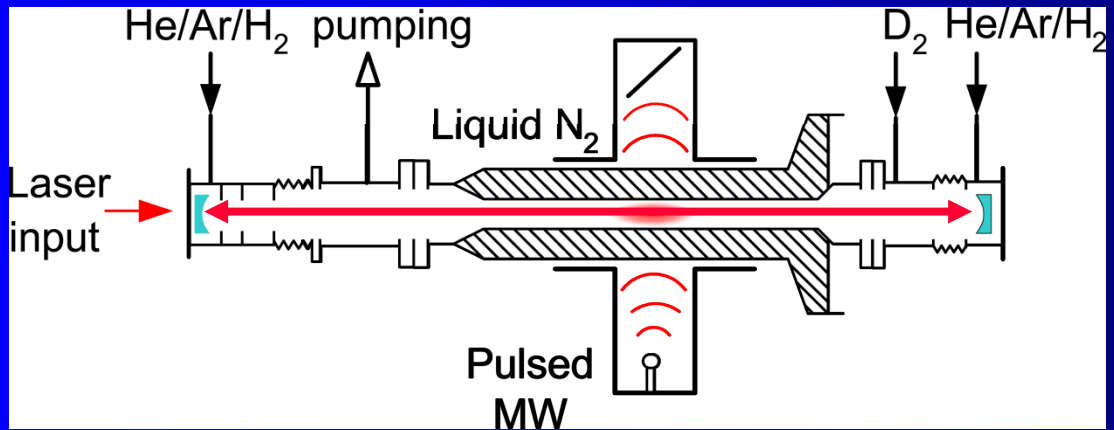

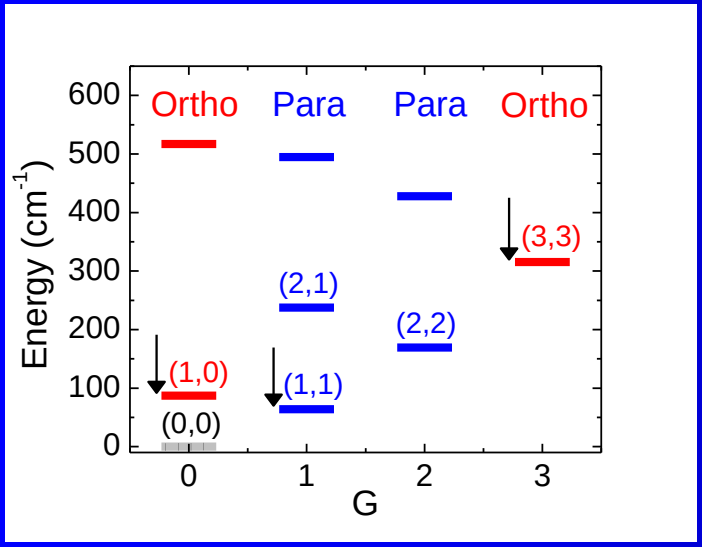
Ortho
Para
Para
Ortho
(3,3)
(2,1)
(2,2)
(1,0)
(1,1)
(0,0)
Energy (cm-1)
G

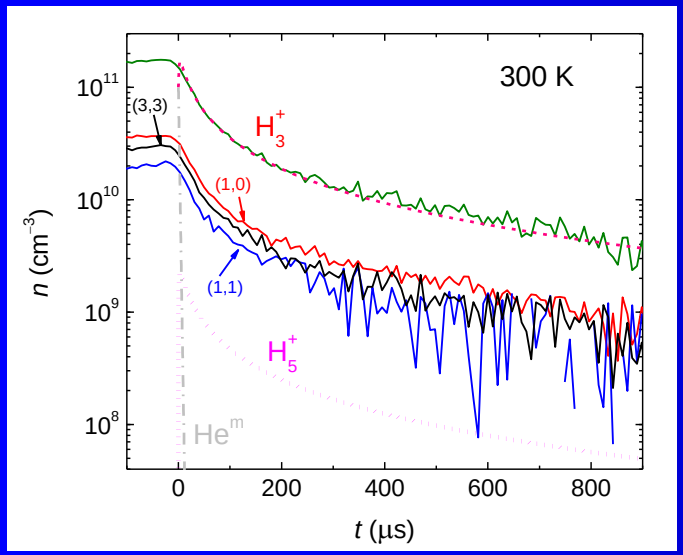
300 K
(3,3)
H3+
(1,0)
(1,1)
H5+
Hem
n (cm-3)
t (μs)

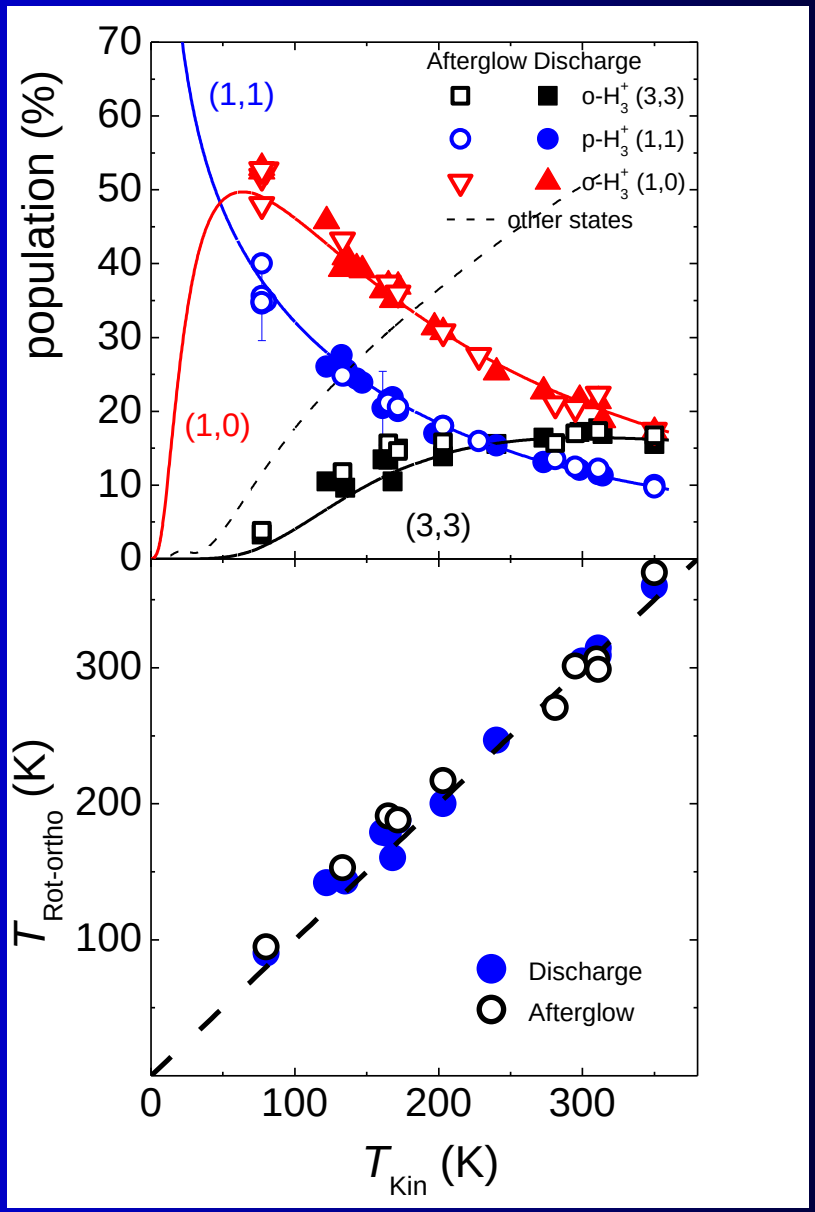
Afterglow Discharge
o-H3+ (3,3)
p-H3+ (1,1)
o-H3+ (1,0)
other states
(1,1)
(1,0)
(3,3)
population (%)
T Rot-ortho (K)
T Kin (K)
Discharge
Afterglow

Absorption studies

He/Ar/H_2/D_2

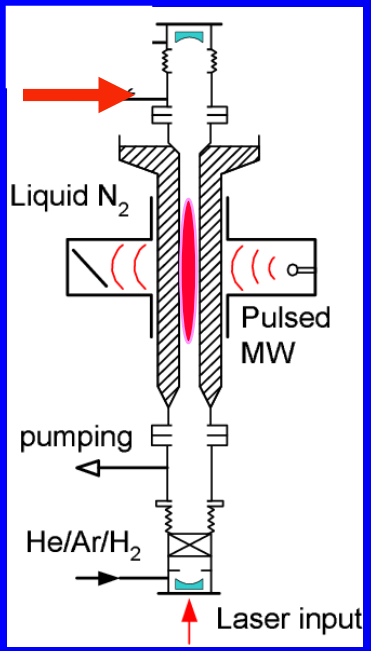

H_3^+

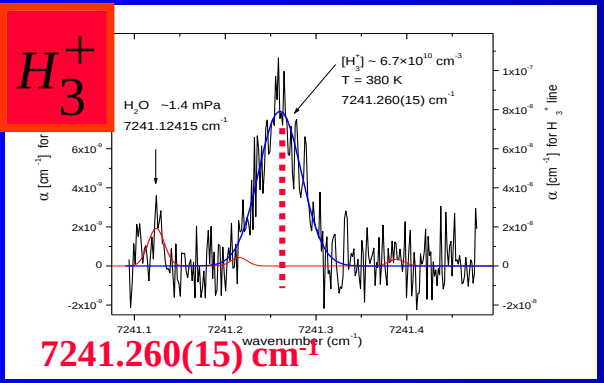

7241.260(15) cm^{-1}

H_2D^+ ($2\nu_2 + \nu_3 \leftarrow 0$)

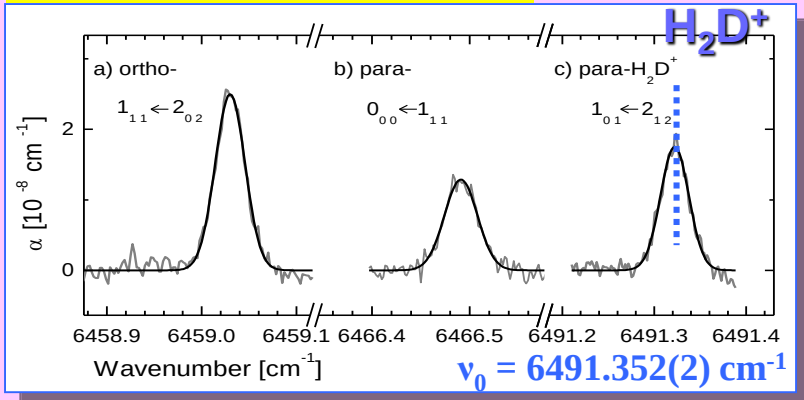

ν_0 = 6491.352(2) cm^{-1}

Combination band

D_2H^+ ($\nu_1 + 2\nu_3 \leftarrow 0$)

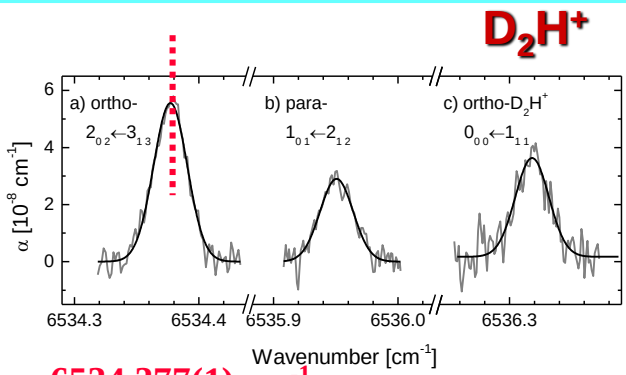

ν_0 = 6534.377(1) cm^{-1}

Combination band

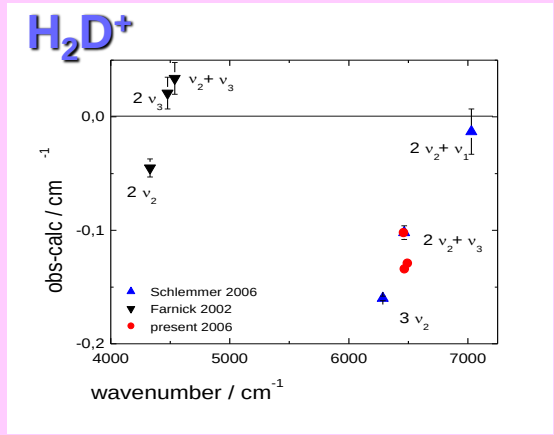

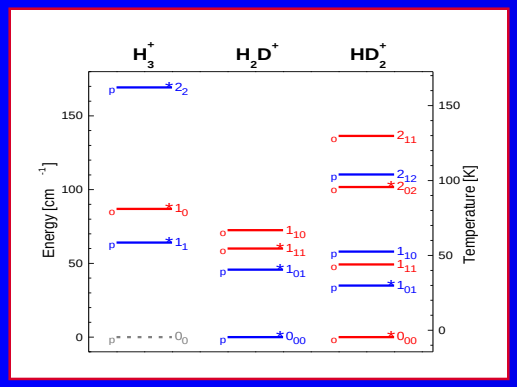

E'[K]	Wavenumber [cm^{-1}]		
	ν_{Exp}	ν_{Theor}	$\nu_{Theor} - \nu_{Exp}$
146.3	6534.377(1)	6534.374	0.003
50.2	6535.950(1)	6535.943	0.007
0	6536.319(2)	6536.301	0.018

D_3^+ ???

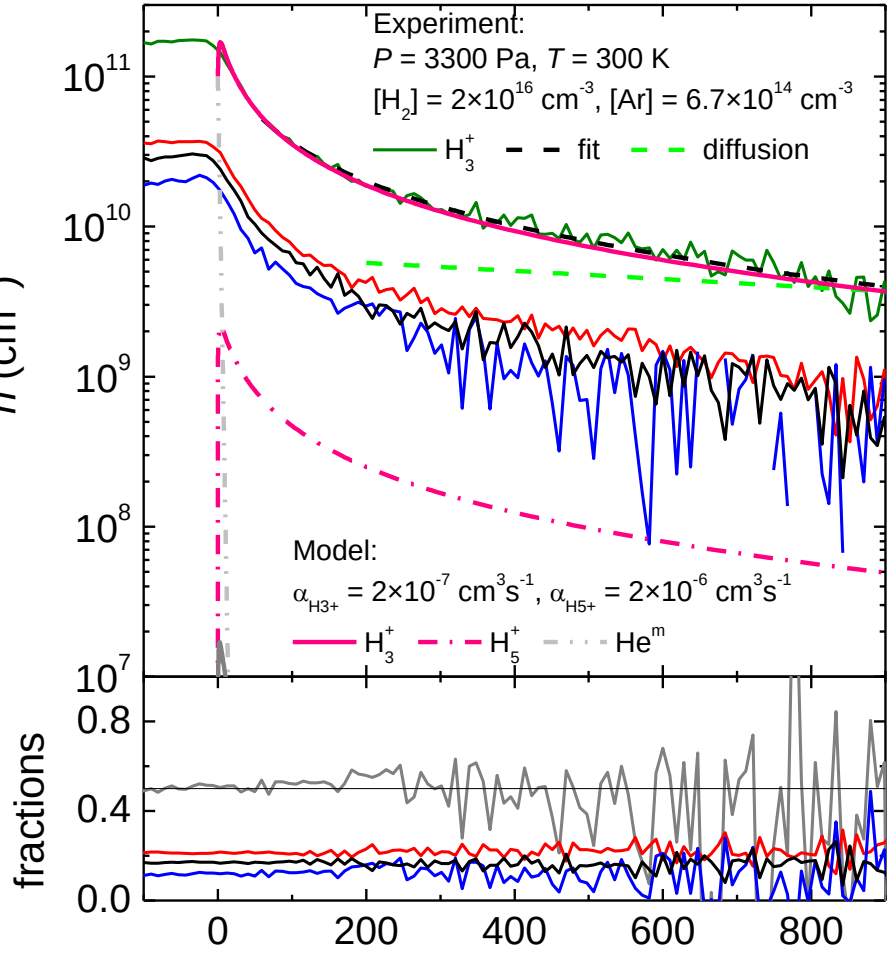

$$\frac{dn_e}{dt} = -[\alpha_1 n_1(t) + \alpha_2 n_2(t)] n_e$$

$$\Rightarrow \alpha_{eff}(t) = [\alpha_1 f_1(t) + \alpha_2 f_2(t)]$$

$$f_1 + f_2 = 1$$

Model + data. Pocatecni podminka: $n_e = He^m = [H_3^+]$.

Poznamka. Namerene τ difuznich ztrat 1.6 ms. Teoreticke τ pri danem tlaku je 1.8 ms (odpovida cca 4×10^{10} cm^{-3} koncentraci necistot (pri 2×10^{-9} cm^3s^{-1} rychlosti reakce H_3^+ s necistotami). Namerena koncentrace vody $[H_2O] = 5\times10^{10}$ cm^{-3} ($[He] = 8\times10^{17}$ cm^{-3}).

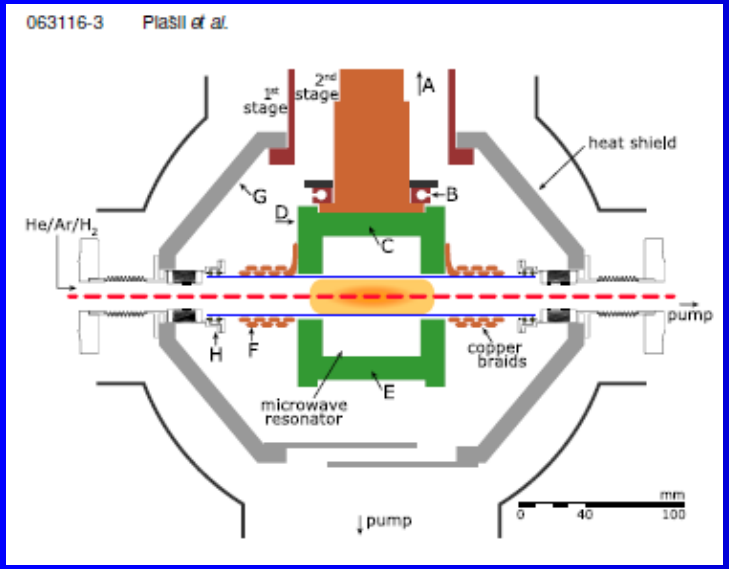

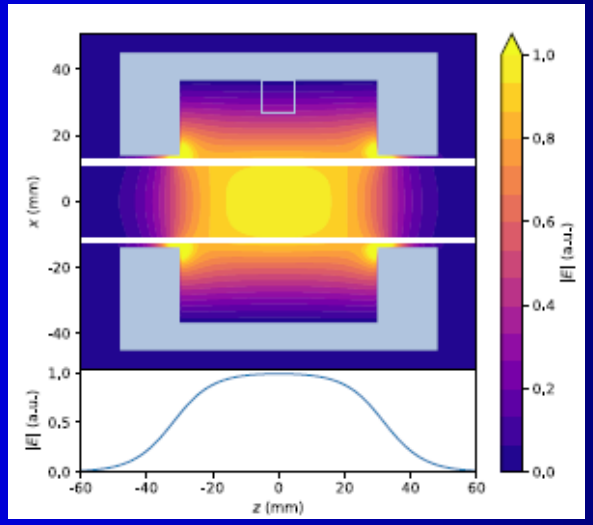

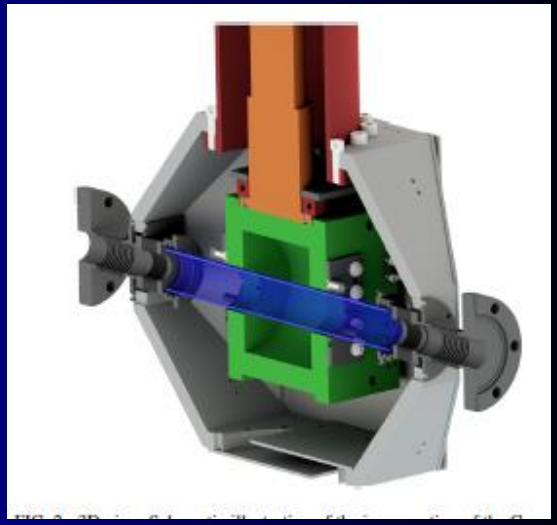

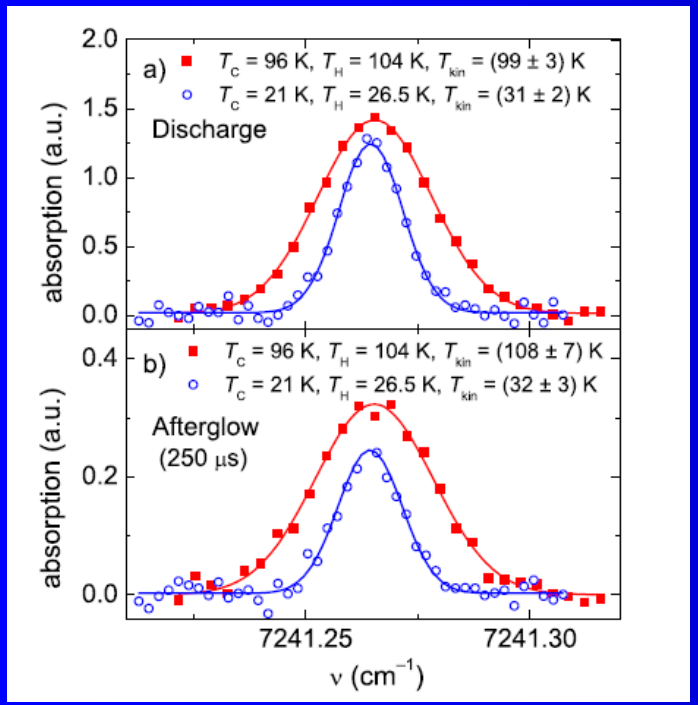

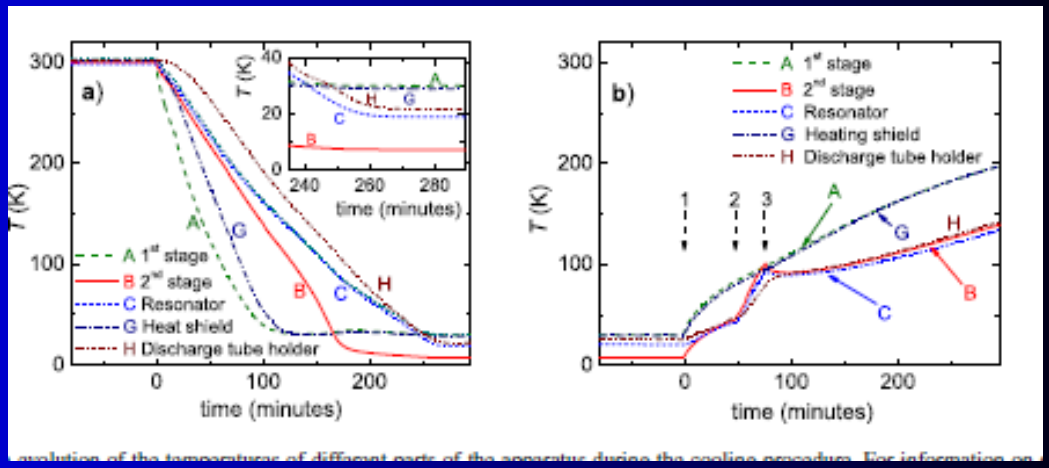

REVIEW OF SCIENTIFIC INSTRUMENTS **89**, 063116 (2018)

Stationary afterglow apparatus with CRDS for study of processes in plasmas from 300 K down to 30 K

R. Plašil,[1,a)] P. Dohnal,[1] Á. Kálosi,[1] Š. Roučka,[1] D. Shapko,[1] S. Rednyk,[1]
R. Johnsen,[2] and J. Glosík[1]

Recombination

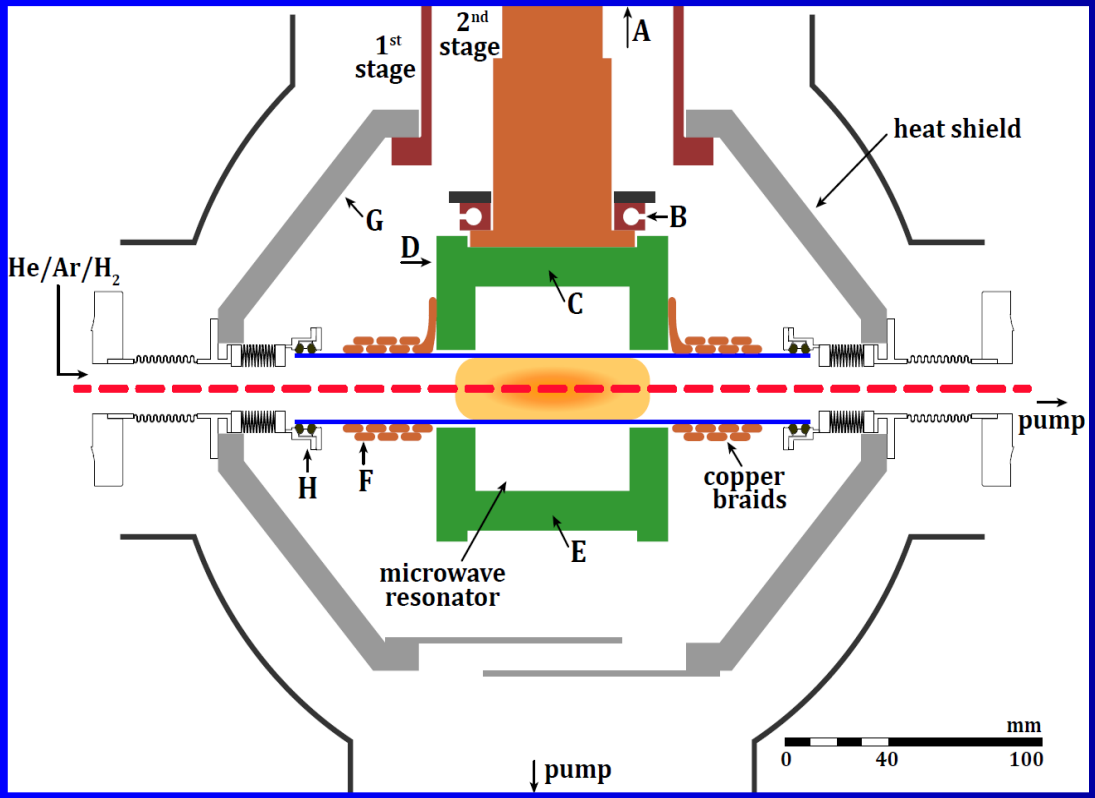

Recombination

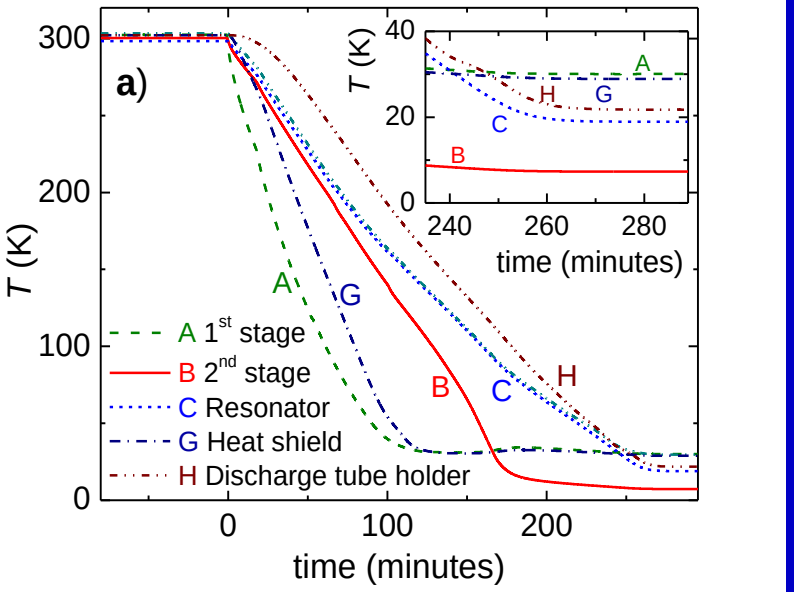

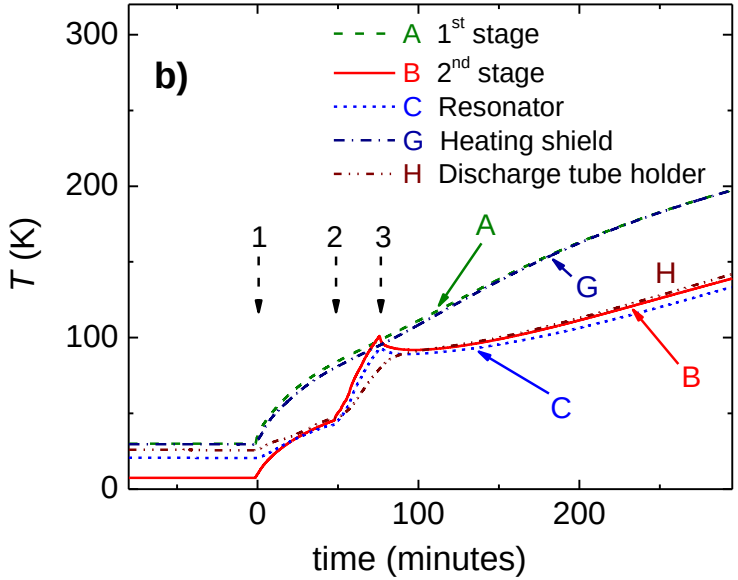

Recombination

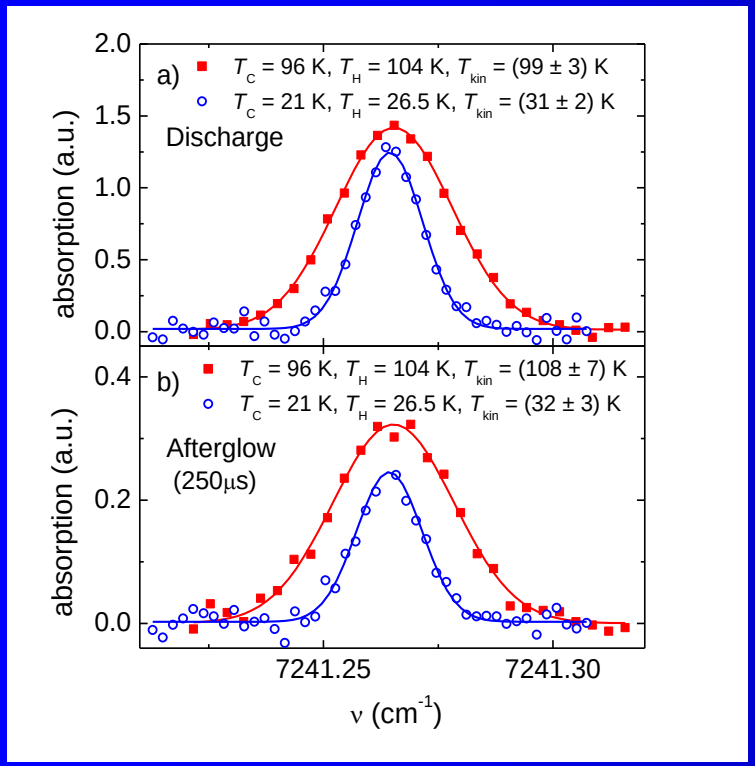

Examples of H_3^+ absorption line profiles

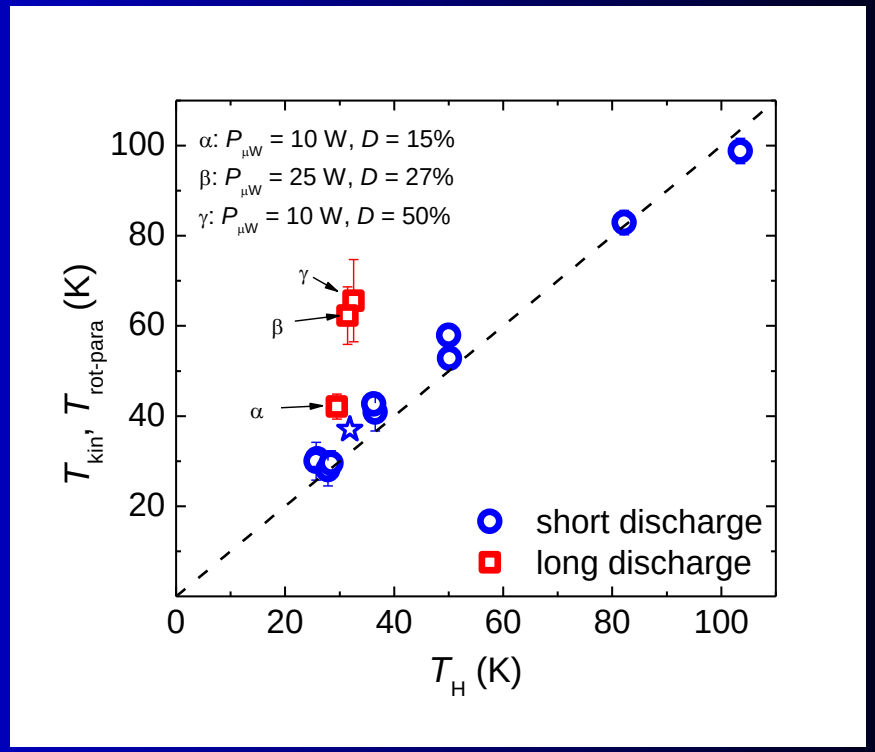

The dependence of the kinetic temperature (T_{kin}) of H_3^+ ions on the temperature T_H (temperature of the discharge tube holder.

Recombination

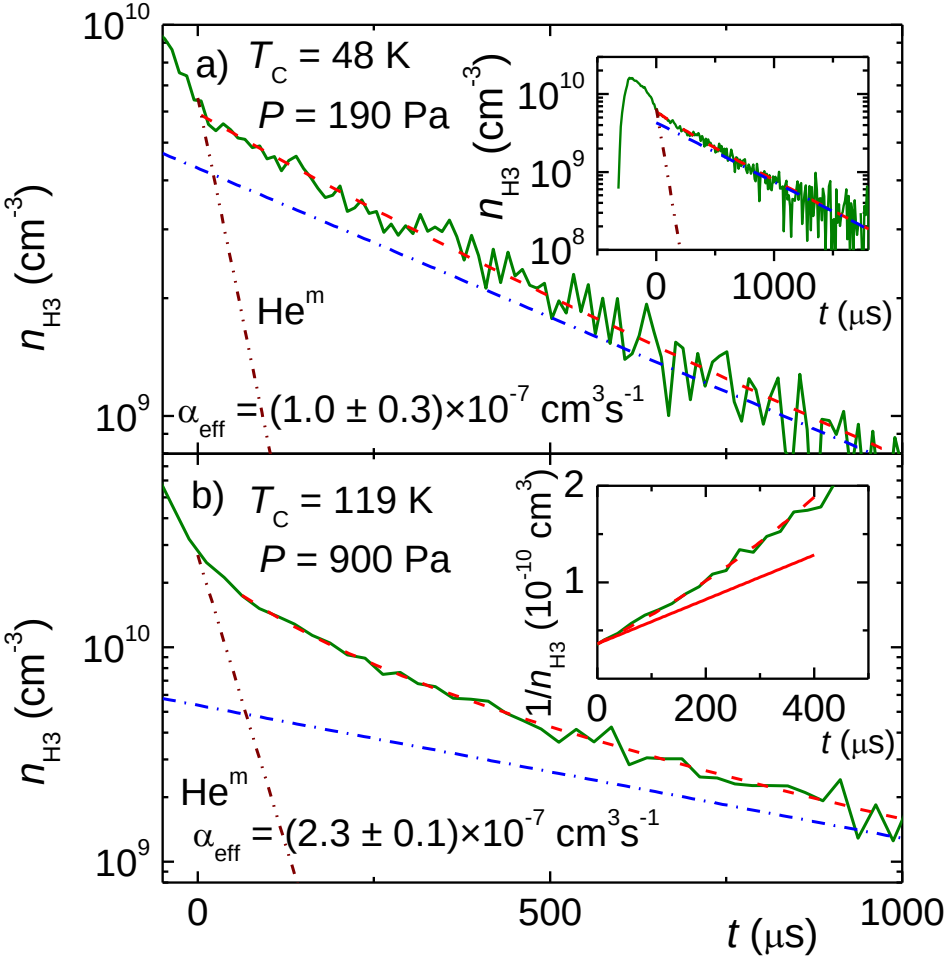

Time evolutions of the number densities of the H_3^+ ions measured at two different temperatures

The battle ship enters the stage

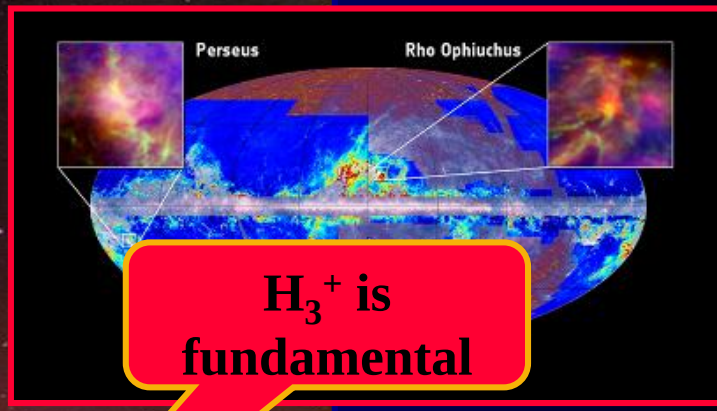

H_3^+ is fundamental

FALP

10-8

Πλασμα

AISA

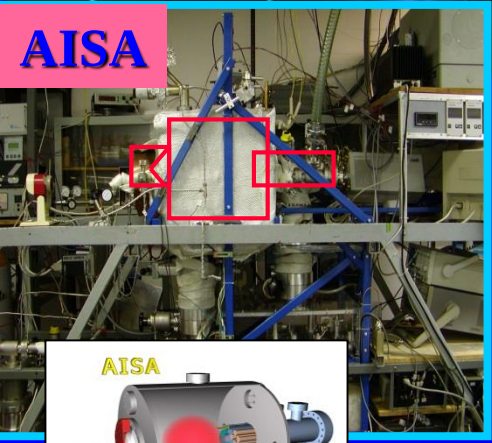

Cryo-FALP

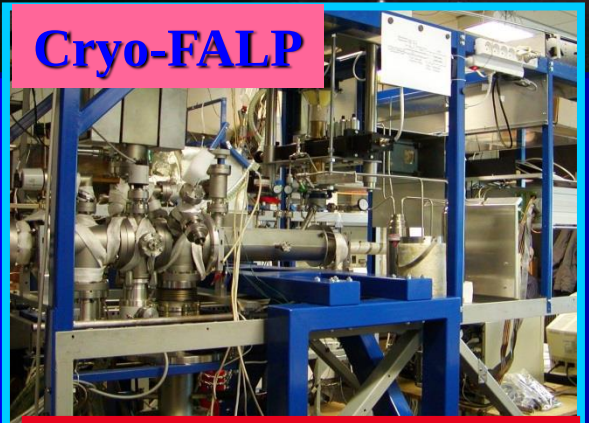

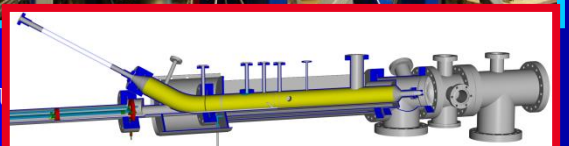

Cryo-NIR-CRDS

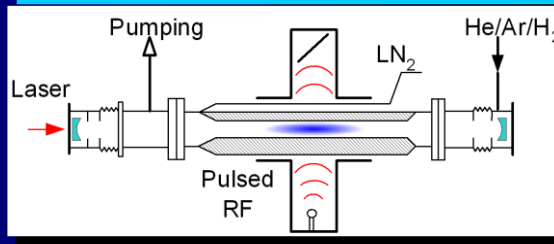

Different views
& different plasmas

H_3^+ and its interaction of with e^- is FUNDAMENTAL

If you understand hydrogen,
you understand all
that can be understood.
(*V. Weisskopf & G. Herzberg*).

$H_3^+ + e^-$

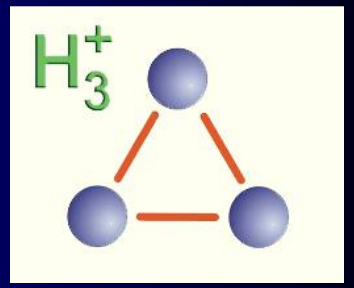

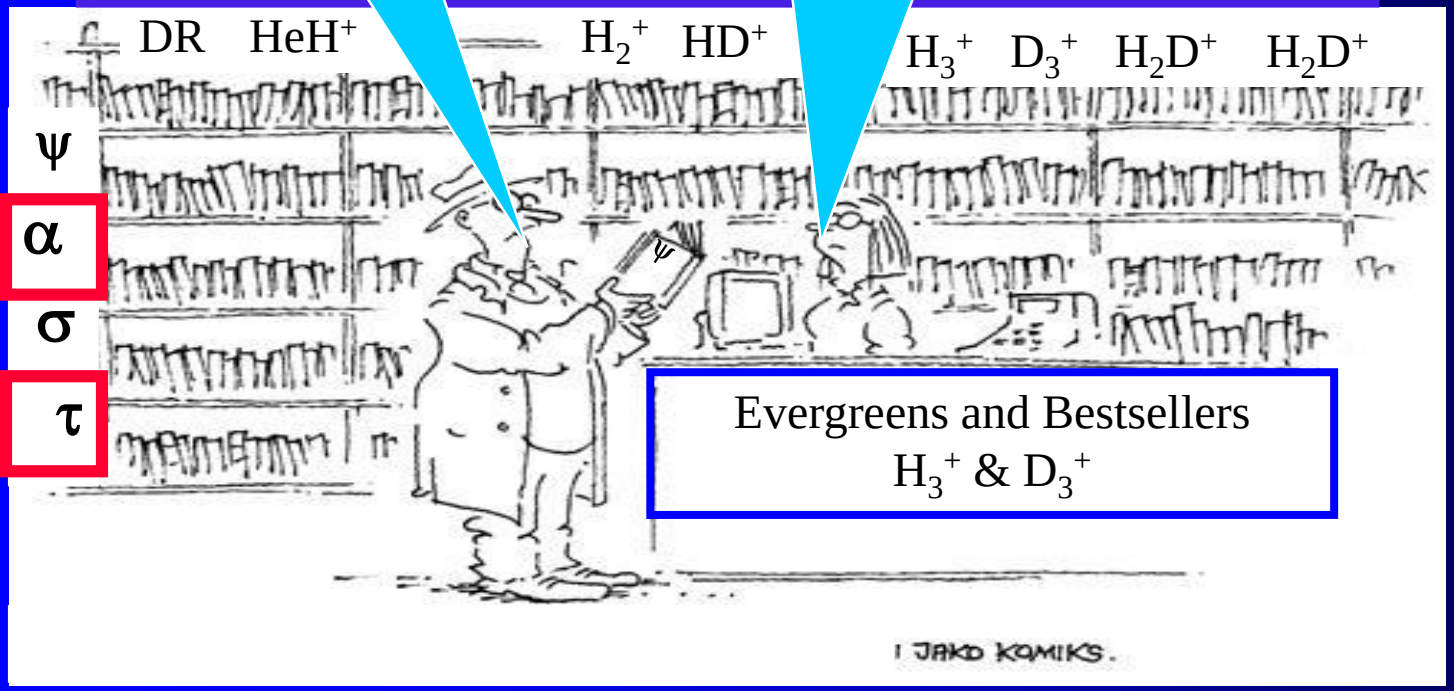

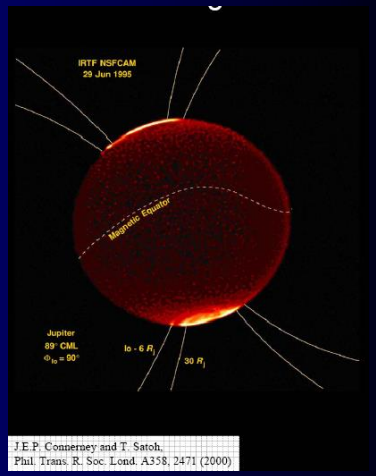

VT - AISA

$dn_i/dt=-\alpha n_i n_e$

$He/Ar/H_2$

$\alpha(T)$

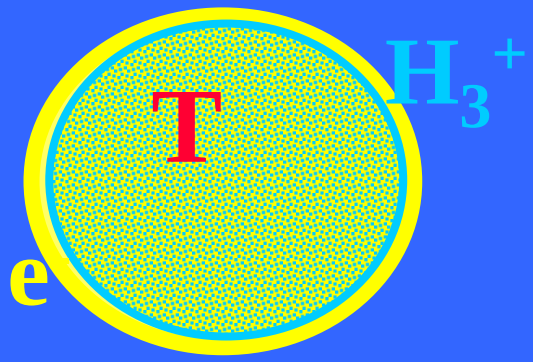

40 cm diameter
UHV - 10^{-9} Torr
External magnetron
2 Torr of $He/Ar/H_2$

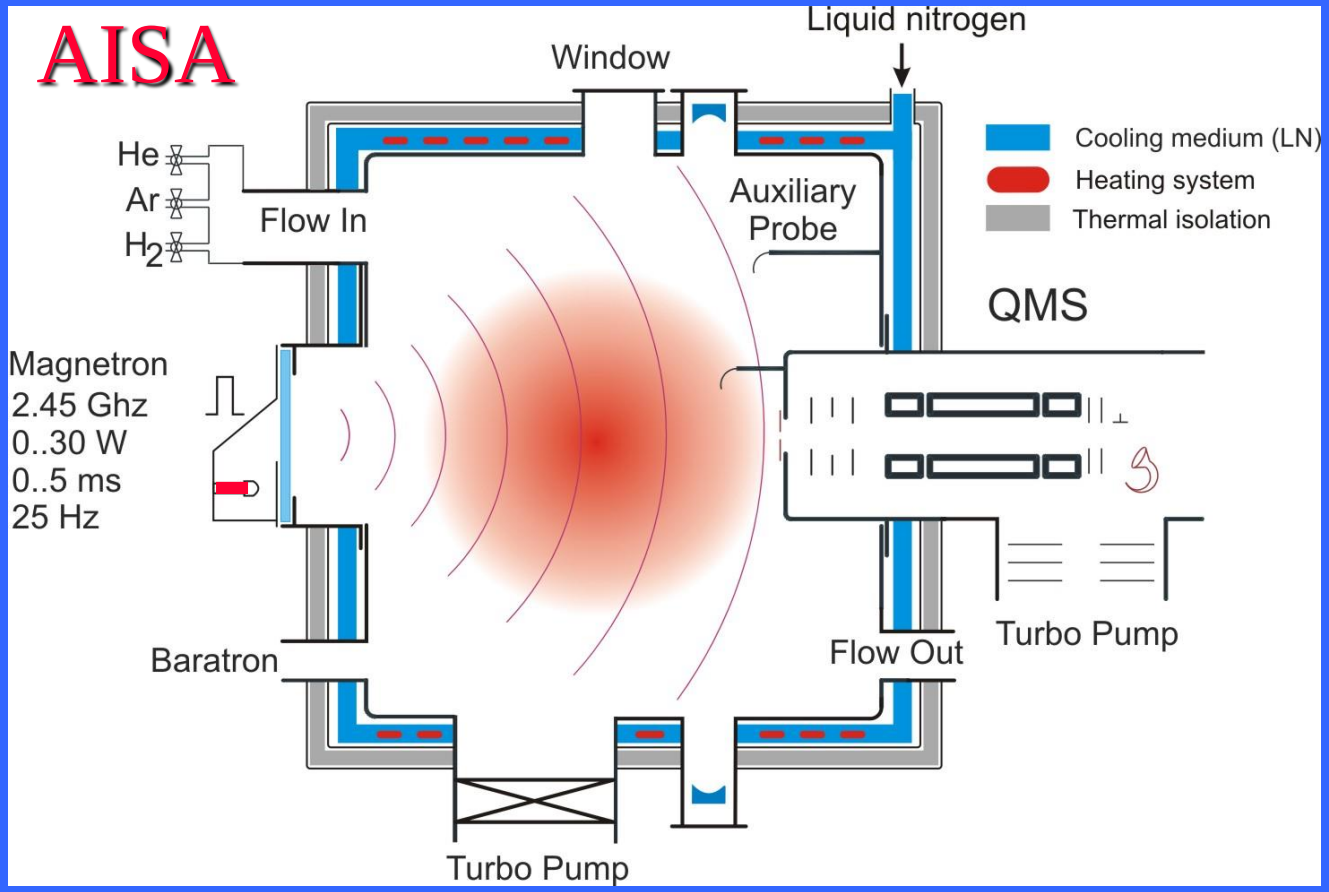

PULSED STATIONARY AFTERGLOW

20-100ms decay

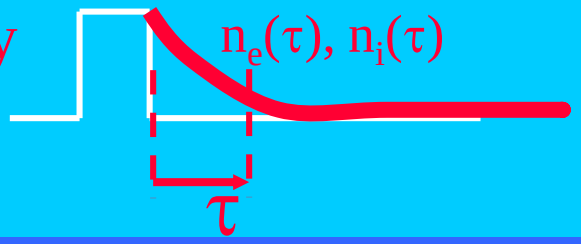

Formation of H_3^+ in He/Ar/H_2

99/1/<0.01% ($10^{17}/10^{14}/10^{11-14}$)

microwave discharge

He^+
He^m
e^-
Ar^+
Ar^m
H_2^+
H^+

He → He_2^+ → Ar → Ar^+ → H_2 → ArH^+, H_2^+ → H_2 → $H_3^+ + e^-$

Ar → Ar^+

$+e^-$(300K) → hν

HeH^+ +He+He

DECAY BY RECOMBINATION

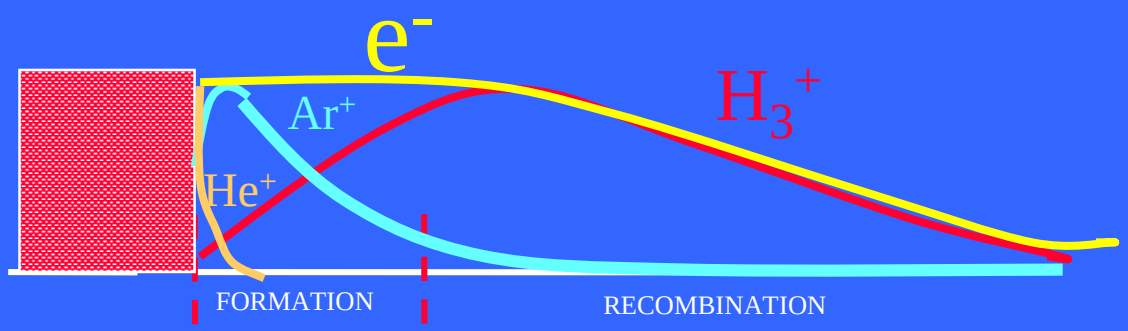

Time resolved mass spectra